Higher Order Galilean Invariant Lattice Boltzmann Method

Wahyu Perdana Yudistiawan

A Thesis Submitted to Nanyang Technological University

In Partial Fulfillment of The Requirement for The Degree of

Doctor of Philosophy

2013

Acknowledgement

Throughout my journey in Nanyang Technological University, I have learnt a lot and I really feel blessed for the great and amazing experiences in my graduate study which at last culminates in this thesis. Along the way I met with people whose help, support and suggestions were vital in the writing of this thesis, and I would like to express my most sincere acknowledgement and gratitude for their contribution in the past few years.

First and foremost, I would like to thank all my past and current supervisors that have been working tirelessly and patiently with me: Prof. Santosh Ansumali, Prof. Kwak Sang Kyu, and Prof. Lim Kok Hwa, for their dedication and effort, guidance, support and encouragement throughout my studies.

I would like to thank all my project collaborators: Iliya V. Karlin, Joycelyn Chng, Hu Enping, Irwan Ary Dharmawan, Dhiraj Patil, Xu Jiecheng, who have contributed in one way or another throughout my studies. I would also like to show an appreciation of gratitude to my past and current lab colleague members: Liu Chao, Chen Wen Wen, Huang Huancong, Tan Shiow Jin, Xi Hong Wei, SK Mahasin Alam, Li Xiang, Sultana Bedoura, Huang Lin, for their collegial support and friendship.

I would also like to thank my fellow friends in NTU localities who have provided me with

support and congeniality through the rain and shine of graduate studies: Katherine, Herlina, Yenni, Rully, Herry, Handarmin, Noel, Yudi, Bowo, Eveline, Trieska, Nancy, Chandra, Jordan, Nathan, Ricksen, Ivan, Michael, and to all the friends who have supported me throughout the years which I probably cannot mentioned by name one by one.

I am also grateful to the Nanyang Technological University for the research scholarship and the computational resources provided by the School of Chemical and Biomedical Engineering.

Last but not least, I would like to thank my parents, who give me immense support and encouragement in my pursuits and providing me with love and support through my life. This thesis is dedicated for you.

Abstract

With the increase of microfluidics applications in recent years, there has been more emphasis given to find alternative modeling method in the microflow regime where the classical Navier-Stokes model broke down. In this regime, the mean-free path of a particle is comparable to the characteristic size of the channel, giving the boundary interaction a major role to play. While methods such as molecular dynamics and Monte-Carlo are excellent for simulating transitional regime, the computational cost is too expensive to be used for any realistic simulation in near continuum sub-sonic regime.

In recent years, Lattice Boltzmann models are gaining traction as a robust method for simulations in the transitional microflow regime, filling the gap between the Navier-Stokes based solver and molecular dynamics. In this thesis, we present a systematic optimization of the standard Lattice Boltzmann (LB) models. The analytical study of $D2Q9$ model is elaborated for simple channel flow and the results are compared with slip flow solution by Cercignani giving a benchmark of LB performance. We then introduce a scheme to reduce the number of velocities of higher order models using renormalization method, projecting $D2Q16$ model back to a modified $D2Q9$ model while maintaining

the same analytical solution. In this manner, we manage to construct a modified $D2Q9$ model that capable of reproducing Knudsen layer in the velocity profile. Lastly, we introduce a novel scheme which gives additional degree of freedom for the same number of discrete velocities in three-dimension, in particular we discuss the application of the scheme on $D3Q27$ model. We show the existence of an off-lattice $D3Q27$ model with correct equilibrium to recover Galilean invariant form of Navier-Stokes equation, which exhibit better accuracy and excellent velocity profile that match the result from classical Grad 13-moments model.

Contents

List of Figures

List of Tables

Chapter 1

Introduction

1.1 Background and Motivation

The lattice Boltzmann (LB) method has emerged as an alternative tool to model a range of hydrodynamic applications [1, 2, 3, 4, 5, 6, 7, 8]. By now, it is understood that the LB model constitutes a well-defined hierarchy of approximations to the Boltzmann equation based on discrete velocity sets and is naturally equipped with relevant boundary conditions derived from the Maxwell-Boltzmann theory [9, 10, 11]. A lot of attention was given recently to the use of LB models for simulating gaseous flows in microdevices, where hydrodynamic approximation breaks down [9, 12, 13, 14, 15, 16, 17, 18]. Here, we can see the clear advantage of LB models from conventional CFD method for application in transitional regime, since Navier-Stokes equation based solver will not perform well, given that the fluid and boundary interaction now play a very significant role.

Although, lower order LB model is massively used in practice, recent works have indicated that higher order LB models perform much better for resolving complex phenomena such as Knudsen boundary layer [13], gaseous flow in small devices [19], thermal flows [20] and turbulence [21]. In the case of turbulence, better performance seems to be originating from the fact that the hydrodynamic limit of higher order LB models is Galilean invariant [21] (i.e. the approach is self-consistent and independent of the reference frame used). In order to recover the Galilean invariant hydrodynamics, it is crucial to have correct equilibrium of third order moments, at least up to the third order in the Mach number [21, 22, 23]. Here, the correct equilibrium means that it is the same as the one obtained from Maxwell–Boltzmann distribution.

The LB method can be viewed as a systematic approximation technique for solving the Boltzmann BGK equation with increasing accuracy [24, 25]. In Ref [11], it was shown that the LB method approximates the Boltzmann-BGK equation in terms of Hermite polynomials, similar to the Grad's moment method [26]. This idea was refined further in Ref [10, 12], which showed that it is possible to formulate the LB method in a thermodynamically consistent fashion [8, 27, 28, 29, 30, 31], in a way similar to the entropic formulation of the Grad's moment method [32]. However, the roots of the Hermite polynomials are irrational, and the corresponding discrete velocities cannot be fitted into a regular space-filling lattice. Recently, this problem was resolved by pointing out that a rational number approximations of the Hermite quadrature is possible for constructing computationally convenient on-lattice models [22, 23].

This route of working with the rational number approximation of the Hermite poly-

nomial is quite convenient for the turbulence modeling [21, 22, 23]. However, it might just add extra computational cost with less appreciable gain in mixture and/or microflow modeling. In the case of the mixture modeling, this happens because even for the lower order LB model (D2Q9 model) it is not always possible to match the spatial discretization with the discrete velocity set for all the components (see for example [33]). Similarly, for the microflow modeling the accuracy of the discretization in the velocity space is more crucial (see for example [34]). Thus unlike turbulence, for microflows better accuracy and efficient implementation for the space derivative is a secondary issue. For example it is well known that the Knudsen layer can be observed with the minimum of 16 velocity (which in 3-D implies 64 velocity) when the LB method is constructed via the route of Gauss-Hermite quadrature [13, 34]. It is interesting to note here that even this particular higher order LB model fails to reproduce both phenomena Knudsen minima and Knudsen layer [34]. In fact, numerical studies suggest that a very high order LB model is needed to reproduce the Knudsen minima correctly [34]. Thus, in order to model microflows, it will be quite useful to have a higher order LB model with a reduced velocity set (as compared to the Gauss-Hermite quadrature route).

1.2 Objectives

The objective of this thesis is to create an LB model of sixth order accuracy with minimal number of discrete velocities. We know that at one dimensional system Gauss-Hermite quadrature gives the best approximation for choosing discrete velocities for

LBM for a given number of discrete velocities (which corresponds to the degree of Hermite polynomial to be solved). However, at higher dimension, no such approximation exists. Current practice uses the tensor multiplication of the Hermite polynomial to create a quadrature that is too costly for computational purposes. For example, four discrete velocities in one dimension, will become 64 ($= 4^3$) discrete velocities in three dimension. Recently, *pruning*, a method to cut down the number of discrete velocities from a complete set of discrete velocities obtained from tensor multiplication, was introduced in Ref. [21]. This indicated that tensor multiplication might not be the correct way to obtain the least membered discrete velocity set for a given accuracy.

It is computationally much easier to deal with integers (or generally rational numbers) than with irrational numbers. The rational LB-system will be beneficial during numerical simulation, especially during the streaming process. However, such convenience comes with the price of accuracy. For the same level of accuracy, the number of discrete velocity required will be much more compared to its off-lattice counterpart. Indeed, convenience of on-lattice system can be advantageous, especially when streaming is easily dealt with. However, the convenience of on-lattice system will not be of much help in certain general setup condition (for example, in multiphase or multicomponent flow). In such cases, the number of discrete velocities will dominantly govern the efficiency of the code, rather than lattice nature of the model. We will show later on that it is possible to construct a novel 27-velocity LB model with better accuracy than standard 27-velocity LB model obtained from tensor multiplication of Hermite polynomial.

1.3 Scope and Organization of Thesis

The scope of this thesis are two-fold:

- Firstly, the construction of LB models. This construction is not limited to the Gauss-Hermite hierarchy, but also looking beyond the hierarchy to find velocity sets that can give better accuracy with less number of discrete velocities.

- Secondly, comparing the analytical results for the constructed LB models, as a proxy to the computational accuracy and performance.

This thesis is organized as follows: Chapter 2 reviewed kinetic theory and properties of Boltzmann equation. Chapter 3 deals with the analysis of classic $D2Q9$ model, the simplest model in standard hierarchy of Lattice Boltzmann Method and its stationary solution in unidirectional flow. Chapter 4 discuss the renormalization of $D2Q16$ to $D2Q9$ model and comparing the results from the two models. Chapter 5 elaborates the central discussion of the thesis, which is the Higher Order Galilean Invariant LBM, and its derivation. Finally, Chapter 6 discuss conclusion and possible future work.

Chapter 2

Kinetic Theory Revisited

This chapter is organised as follow: In section 2.1, a brief review on some basic notions of kinetic theory such as mean-free path, collision interval and Knudsen number will be given. In section 2.2, a brief discussion on Boltzmann equation will be given. A derivative of Boltzmann equation with simpler collision terms, Bhatnagar-Gross-Krook (BGK) model, will also be introduced in this section.

2.1 Elementary Kinetic Theory

Boltzmann equation is used to describe the kinetic theory of the dilute gases. One of the important assumptions made in the kinetic theory of rarefied gases, is that we can neglect collision of more than two bodies, as they are rarely occuring. Thus, in dilute gases, only binary collision is important. The mathematical limit in which this is a valid assumption and the Boltzmann equation holds is known as Grad-Boltzmann limit. This

is defined as the limit whereby the volume fraction goes to zero. In this limit, the gas is rarefied enough that the assumption of ideal gas holds, while at the same time the effect of collisions of the gas particles remains and observed at the macroscopic level as transport coefficients (viscosity, thermal conductivity, etc.).

2.1.1 Mean-free Path

The smallest length scale in molecular motion, mean-free path (l_{mfp}) is defined as the average distance travelled by a particle between two successive collisions. We can estimate this quantity by considering particles as hard spheres with diameter d.

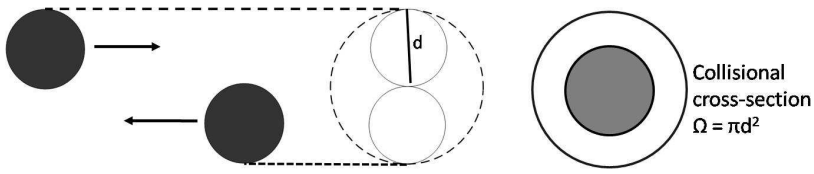

Figure 2.1: The concept of collision cross section

From Figure 2.1, it can be seen that the closest distance of approach between two spheres is diameter d. The cross sectional area of this effective sphere of radius d is termed as collision cross section, Ω given as:

$$\Omega = \pi d^2. \tag{2.1}$$

In order to compute the mean-free path, we consider a model system in which one particle of radius d is moving in a sea of stationary particles. The situation is depicted

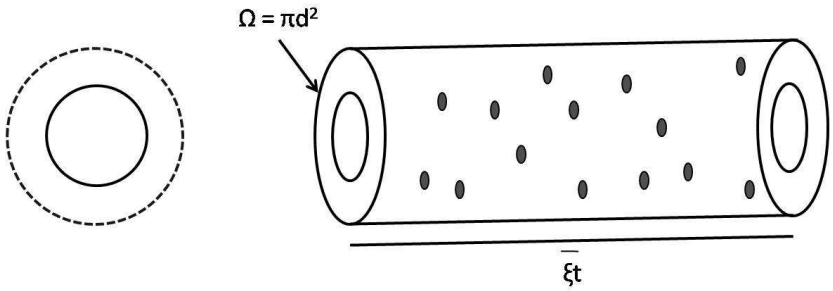

Figure 2.2: The concept of mean-free path

in Figure 2.2. In a time interval t, this particle sweeps a cylinder of cross sectional area Ω and length $\overline{\xi}$t. So mathematically,

$$l_{\mathrm{mfp}} \simeq \frac{1}{\rho_{\mathrm{n}} \pi d^2}, \tag{2.2}$$

where ρ_{n} is the number density of molecules per unit volume.

2.1.2 Collision Interval

The smallest time scale in molecular motion, collision interval (τ), is defined as the average time spent between two collisions [20]. It is represented as

$$\tau \simeq \frac{l_{\mathrm{mfp}}}{\overline{\xi}}, \tag{2.3}$$

where

$$\overline{\xi} = \sqrt{\frac{2k_{\mathrm{B}}T_0}{m}}, \tag{2.4}$$

is the mean molecular velocity. k_{B} is the Maxwell-Boltzmann constant; T_0 is the initial temperature in Kelvin; m is the molecular mass. For non-hard sphere molecules, these notions can still be applied with modification to account for the potential model used.

2.1.3 Knudsen Number

The Knudsen Number (Kn) is defined as the ratio of mean-free path l_{mfp} to the characteristic length L [20]. From Eq. (2.3), Kn can be defined as:

$$\mathrm{Kn} = \frac{l_{\mathrm{mfp}}}{L} = \frac{\tau\overline{\xi}}{L}. \tag{2.5}$$

2.2 The Boltzmann Equation

The Boltzmann equation describes the dynamics of molecular motion of particles in rare gases, which considers the process of advection and collision between them. The equation is expressed in terms of $f(\mathbf{x}, \mathbf{c}, t)$, the one-particle distribution function, where $f(\mathbf{x}, \mathbf{c}, t)d\mathbf{x}d\mathbf{c}$ is defined as the probability of finding a molecule with the velocity $\mathbf{c}$ at a location $\mathbf{x}$ at time t. The evolution of the distribution function $f(\mathbf{x}, \mathbf{c}, t)$ over time is determined by the following equation, known as Boltzmann equation [35]:

$$\frac{\partial f}{\partial t} + \mathbf{c} \cdot \frac{\partial f}{\partial \mathbf{x}} + \frac{\partial}{\partial \mathbf{c}} \cdot (\mathbf{X}\, f) = \mathcal{J}\,(f, f)\,, \tag{2.6}$$

where $\mathbf{X}$ represents the external force acting on each particle and $\mathcal{J}(f, f)$ is the collision integral, a term taking into account of the changes of distribution function as a result of the binary collision between a pair of particles. Mathematically we have:

$$\mathcal{J} = \int \mathcal{W} \left[f(\mathbf{c}_1) f(\mathbf{c}_2) - f(\mathbf{c}) f(\mathbf{c}') \right] d\mathbf{c}_1 d\mathbf{c}_2 d\mathbf{c}', \tag{2.7}$$

where $\mathcal{W}$ is the probability of a particular binary collision happening (where particles with initial velocity $\mathbf{c}$, $\mathbf{c}'$ change their particles to $\mathbf{c}_1$, $\mathbf{c}_2$). This probability will depend on the details of the intermolecular forces and potential model used. One important thing to note here, is that the current expression of Eq. (2.7) relies on *"stosszahlansatz"* (molecular chaos assumption), which assumes that the molecule entering a binary collision is not correlated in any way. This creates a distinction between pre- and post-collisional state, which break the time-reversal symmetry of the Newtonian mechanics and allows for entropy production. The H-theorem also follows from this consideration. It is able to explain the macroscopic irreversibility of a system consisting of a large number of particles through statistical description, and also it extends the concept of entropy and second law of thermodynamics to highly non-equilibrium conditions.

Since the total mass density, momentum density, and energy density are conserved during collisions, the role of collision is indeed only to redistribute the momentum and energy between particles. Hence this term indicates that the changes are due to the gain and loss of particles as they obtain or lose a particular velocity.

2.2.1 The Properties of Collision Operator

Locality

The collision term is local in the position space, and non-local in the velocity space [21]. Since Boltzmann kinetic theory consider particles as point particles and interacting via finite-range intermolecular forces, the collision will always be local in space. Thus, it is attractive for numerical implementations because the computation for the collision step only requires local variables (i.e. information from the same lattice points) and does not involve other neighboring lattices, which makes it simpler to implement.

Additive Invariants

During collision, the number of particles, total momentum and total energy are conserved. It can be represented mathematically:

$$\int \left(\chi + \zeta.\mathbf{c} + \lambda\mathbf{c}^2\right) \mathcal{J}(f,f)d\mathbf{c} = 0, \tag{2.8}$$

where χ and λ are arbitrary scalar constants and ζ is an arbitrary vector constant.

Zero Point of the Collision

The zero point of collision can be obtained from the solution to this equation:

$$\mathcal{J}(f,f) = 0, \tag{2.9}$$

which implies that

$$f(\mathbf{c}_1)f(\mathbf{c}_2) = f(\mathbf{c})f(\mathbf{c}^{'}). \tag{2.10}$$

It is the lowest-order approximation to the distribution function [20]. The probability distribution function shown earlier satisfies the condition Eq. (2.9).

$$f = \exp\left(\chi + \zeta.\mathbf{c} + \lambda\mathbf{c}^2\right). \tag{2.11}$$

Its solution will be

$$f^{eq}(\mathbf{c}, \rho, \mathbf{u}, \epsilon) = \rho\left(\frac{m}{2\pi k_{\mathrm{B}}T}\right)^{\frac{D}{2}} \exp\left(-\frac{m(\mathbf{c}-\mathbf{u})^2}{2k_{\mathrm{B}}T}\right). \tag{2.12}$$

which is the Maxwell-Boltzmann Distribution [35].

Local Entropy Production Inequality

$$\int \ln f\mathcal{J}(f, f)d\mathbf{c} \leq 0, \tag{2.13}$$

and the local entropy production inequality is

$$\sigma(x, t) = -k_{\mathrm{B}}\int \ln f\mathcal{J}(f, f)d\mathbf{c} \geq 0. \tag{2.14}$$

Eq. (2.13) displays the characteristic of irreversibility nature of Second Law of thermodynamics. As $\sigma(x, t) \geq 0$ which means entropy production term, σ is always positive.

This relation is known as Boltzmann H-theorem.

2.2.2 H-theorem and Entropy at Equilibrium

To understand the Boltzmann H-theorem, let us define the H-function as:

$$H = \int f \, \ln f \, d\mathbf{c} \tag{2.15}$$

The local H-theorem for distribution functions, independent of spatial position, states that the rate of change of the H-function is proportional to the entropy production σ [21]. Mathematically we have:

$$\frac{dH}{dt} = -\frac{\sigma}{k_{\mathrm{B}}} \tag{2.16}$$

Thus, the H-function decays monotonically along with σ. Since from (2.14) we have $\sigma \geq 0$, we are guaranteed a convergence to equilibrium distribution f^{eq} which will be achieved once $\sigma = 0$. A much more detailed discussion on this topic is available in the Ref. [36].

2.2.3 Bhatnagar-Gross-Krook Model

The Boltzmann collision integral is indeed rather complicated to be implemented directly. In 1954, Bhatnagar, Gross, and Krook proposed a simplification of the collision process into a relaxation with one homogeneous rate, while preserving the collision

integral's important properties which was discussed earlier [37]. It is very useful for numerical implementation, as the expression is elegantly simple. Mathematically we have,

$$\mathcal{J}_{BGK} = -\frac{1}{\tau}\left(f - f^{eq}\right). \tag{2.17}$$

In this case, the local entropy production inequality is satisfied:

$$\begin{aligned}
\sigma_{BGK} &= -k_{\mathrm{B}} \int \mathcal{J}_{BGK} \ln f d\mathbf{c} \\
&= \frac{k_{\mathrm{B}}}{\tau} \int (f - f^{eq}) \ln f d\mathbf{c} \\
&= \frac{k_{\mathrm{B}}}{\tau} \int (f - f^{eq}) \ln \frac{f}{f^{eq}} d\mathbf{c} \geq 0.
\end{aligned} \tag{2.18}$$

Chapter 3

Analysis of $D2Q9$ Lattice Model

3.1 Introduction

The emerging field of fluid dynamics at a micrometer scale becomes increasingly important due to fundamental engineering issues of micro-electromechanical systems [38]. Recently, much attention was attracted by the use of lattice Boltzmann (LB) models for simulation of microflows by a number of groups [9, 18, 15, 16, 12, 17, 14].

Agreement between LB and kinetic theory [9], hydrodynamics with slip boundary conditions [17], and molecular dynamics [14] was reported. However, most of these numerical works depend on simulation with finite accuracy while the crucial question whether or not the kinetic equations underpinning the LB method are valid physical models of microflow remains unanswered. Thus, the validity of LB models as physical models cannot be addressed unless a comparison to exact solutions is performed.

[1]Parts of this chapter were published in Physical Review E.

In this chapter, we analyze the $D2Q9$ LB model, which is the simplest in the hierarchy of standard LB models. This analysis also extends the results of Ref. [13] for the standard LB model. Specifically, we derived and provide details of the exact solution of the $D2Q9$ LB model for the flow between parallel shearing plates (Couette flow), and extend this solution to the presence of a forcing term in the kinetic equation which mimics a flow driven by a pressure drop (Poiseuille flow). We use these solutions in order to quantify the accuracy of the standard LB model as a slip flow model. This quantification is usually done by defining slip boundary condition in such a way that the velocity profile obtained from the Navier-Stokes equations with slip boundary condition matches with that obtained from a solution of kinetic equation for Poiseuille flow (see, for example, [36]). Specifically, in this formulation, for the slip boundary condition we have,

$$u_{\rm slip}|_{\rm wall} = A_1 {\rm Kn} \left(\frac{\partial u_x}{\partial \hat{n}} \right)_{\rm wall} - A_2 \, {\rm Kn}^2 \left(\frac{\partial^2 u_x}{\partial \hat{n}^2} \right)_{\rm wall}, \tag{3.1}$$

where $\hat{n}$ is normal defined inward, and coefficients A_1 and A_2 are found by using the velocity profile obtained from a solution (exact or approximate) of the Boltzmann equation. These coefficients provide a convenient way to compare accuracy of different approximations to the Boltzmann equation as many experimentally relevant quantities are directly dependent on these two coefficients. For example, in the Poiseuille flow, the minimum in the flow rate is observed at:

$$\frac{1}{{\rm Kn}_{\rm min}} = 2 \sqrt{3 \, A_2}, \tag{3.2}$$

and the reduced slip velocity at the wall u^* is:

$$u^* = \frac{u_{\text{slip}}}{u_{\text{centerline}}} = \frac{A_1\,\text{Kn} + 2\,A_2\,\text{Kn}^2}{\frac{1}{4} + A_1\,\text{Kn} + 2\,A_2\,\text{Kn}^2}, \tag{3.3}$$

where u_{slip} is the slip velocity at the wall and $u_{\text{centerline}}$ is the Poiseuille flow velocity at the centerline (i.e. the maximum) at a given Kn.

We show in the present work that

$$A_1 = 1,\ A_2 = \frac{2}{3}. \tag{3.4}$$

for the lattice Boltzmann model with nine velocities. These values can be compared with the available approximate solution of Boltzmann-BGK equation by Cercignani [36], which gives

$$A_1 = 0.8297,\ A_2 = 0.5108. \tag{3.5}$$

In Fig. 3.2, we compare the slip velocity obtained from exact solution of LB model, with that obtained from approximate solution of Boltzmann-BGK. Similarly, in Fig. 3.3, we compare the flow rate as a function of Knudsen number for these two approaches. From these two plots we see that the basic model of the LB hierarchy, the nonlinear $D2Q9$ model, can be quantified as the slip flow model for microflow simulation.

The outline of this chapter is as follows: In section 3.2, we remind the kinetic equation pertinent to the LB model with nine discrete velocities in two spatial dimensions, the $D2Q9$ model. We consider a general case which also includes a force term. In sec-

tion 3.3, we cast the kinetic equation in a form of a moment system for nine moments. The choice of the convenient moment representation helps in the course of finding the solution. In section 3.4, after describing the setup in which the fluid is confined between parallel moving plates, and is subject to the external force directed collinearly with the plates, we outline the strategy of finding the solution to the kinetic equation in the steady-state case. The explicit solutions obtained are analyzed in section 3.5, and compared with the slip flow solution by Cercignani from the linearized Boltzmann-BGK equation for the two limiting cases, Couette and Poiseuille flows. It is showed that the solution for the nine-velocity model agrees quantitatively with the Boltzmann-BGK case. It should be stressed that this solution assumes no tuning parameters or other optimization tricks. Another important access to the quality of a slip flow model is the behavior of the flow rate in the Poiseuille flow as a function of Knudsen number (so-called Knudsen minimum problem or Knudsen paradox, where the flow will not perpetually decrease as predicted by Navier-Stokes, but will eventually increase after some point). In section 3.6.1 we complete the solution by finding explicitly the higher-order moments. Finally, a discussion is given in section 3.7.

3.2 The $D2Q9$ Model

The discrete velocity set for $D2Q9$ model is given by:

$$\begin{aligned} c_x &= \sqrt{\frac{3k_{\mathrm{B}}T_0}{m}}\,\{0,1,0,-1,0,1,-1,-1,1\}, \\ c_y &= \sqrt{\frac{3k_{\mathrm{B}}T_0}{m}}\,\{0,0,1,0,-1,1,1,-1,-1\}, \end{aligned} \tag{3.6}$$

where T_0 is the reference temperature, k_B is the Boltzmann constant, m is the molecular mass. Here onwards c_{ix} and c_{iy} (the i-th component of c_x and c_y) will represent the i-th component of discrete velocity vector $\mathbf{c}_i \equiv (c_{ix}, c_{iy})$. The distribution function f (populations of the velocities $\mathbf{c}_i$, $i = 0, \ldots, 8$) will be represented by a vector,

$$f = \{f_0, f_1, f_2, f_3, f_4, f_5, f_6, f_7, f_8\}. \tag{3.7}$$

The entropy function of the $D2Q9$ model reads

$$H = \sum_{i=0}^{8} f_i \,\ln\left(\frac{f_i}{w_i}\right), \tag{3.8}$$

where the vector of weights w_i is

$$w = \frac{1}{36}\,\{16,4,4,4,4,1,1,1,1\}. \tag{3.9}$$

The local equilibrium distribution function, f^{eq}, is found upon minimizing H (3.8), subject to fixed density ρ and momentum j_α, $\alpha = x, y$,

$$\begin{aligned} \rho(f) &= \textstyle\sum_{i=0}^{8} f_i, \\ j_\alpha(f) &= \textstyle\sum_{i=0}^{8} c_{i\alpha} f_i. \end{aligned} \tag{3.10}$$

The result of this minimization problem reads [12]:

$$f_i^{\mathrm{eq}} = \rho w_i \prod_{\alpha=1}^{D} \left[\left(\frac{2c - \sqrt{3u_\alpha^2 + c^2}}{c} \right) \left(\frac{2u_\alpha + \sqrt{3u_\alpha^2 + c^2}}{c - u_\alpha} \right)^{c_{i\alpha}/c} \right], \tag{3.11}$$

where $c = \sqrt{\frac{3k_B T_0}{m}} = \sqrt{3} c_{\mathrm{s}}$, $c_{\mathrm{s}} = \sqrt{\frac{k_B T_0}{m}}$ is the speed of sound, $u_\alpha = j_\alpha / \rho$ is the fluid velocity, and $D = 2$ in the present case. Expanding Eq. (3.11) into powers of velocity to second order, we obtain the series expansion of the equilibrium which will be used throughout this study:

$$f_i^{\mathrm{eq}} = w_i \left[\rho + \frac{j_\alpha c_{i\alpha}}{c_{\mathrm{s}}^2} + \frac{j_\alpha j_\beta}{2\rho c_{\mathrm{s}}^4} \left(c_{i\alpha} c_{i\beta} - c_{\mathrm{s}}^2 \delta_{\alpha\beta} \right) \right]. \tag{3.12}$$

Using the Bhatnagar-Gross-Krook (BGK) collision model and applying a force term, the time evolution of f_i can be written as:

$$\partial_t f_i + c_{i\alpha} \partial_\alpha f_i - \mathcal{F}_i(\rho, \mathbf{g}, \mathbf{j}) = -\frac{1}{\tau} \left(f_i - f_i^{\mathrm{eq}} \right), \tag{3.13}$$

where $\mathbf{g} \equiv \{g_x, g_y\}$ is the acceleration vector, τ is the relaxation time which relate to

viscosity through $\nu = \tau c_{\rm s}^2$, and $c_{\rm s}$ is sound speed which is given by $c_{\rm s} = \sqrt{\frac{k_{\rm B}T_0}{m}}$.

A remark on the choice of the forcing term in the kinetic equation (3.13) is in order. In the discrete-velocity case, we do not have derivatives in the velocities, thus the familiar forcing term of the classical kinetic theory, viz. $g_\alpha(\partial f/\partial c_\alpha)$, is not applicable. In general, any forcing term is a valid approximation as long as its lower order moments coincide with the moments of $g_\alpha(\partial f/\partial c_\alpha)$ with at least second-order accuracy. For example, the forcing term [39]

$$\mathcal{F}_i^{(1)}(\rho, \mathbf{g}, \mathbf{j}) = g_\alpha \frac{(c_{i\alpha} - u_\alpha)}{c_{\rm s}^2} f_i^{\rm eq}, \tag{3.14}$$

is often used in the simulation due to its compact form. An alternate form of the force is also used in the literature [6],

$$\mathcal{F}_i^{(2)}(\rho, \mathbf{g}, \mathbf{j}) = w_i\, \rho \left(\frac{g_\alpha c_{i\alpha}}{c_s^2} + \frac{g_\beta j_\alpha + g_\alpha j_\beta}{2\rho c_s^4} \left(c_{i\alpha} c_{i\beta} - c_s^2 \delta_{\alpha\beta} \right) \right). \tag{3.15}$$

3.3 Moment Representation

In a sequel, we shall also need a different but equivalent representation of the kinetic equation (3.13) in terms of nine linearly independent linear combinations of the populations (moments). The three locally conserved moments (density and two components of the momentum density) have been already introduced above (see Eq. (3.10)). The remaining six independent moments are most conveniently chosen as fol-

lows: Three independent components of the pressure tensor, $P_{\alpha\beta}(f) = \sum_{i=0}^{8} f_i\, c_{i\alpha}\, c_{i\beta}$, which we choose as the diagonal elements, P_{xx} and P_{yy}, and the off-diagonal (shear) component, P_{xy}; two independent components, Q_{xyy} and Q_{yxx}, of the third-order moment tensor, $Q_{\alpha\beta\gamma}(f) = \sum_{i=0}^{8} f_i c_{\alpha i} c_{i\beta} c_{i\gamma}$, and a fourth-order moment, R_{xxyy}, where $R_{\alpha\beta\gamma\theta}(f) = \sum_{i=0}^{8} f_i c_{i\alpha} c_{i\beta} c_{i\gamma} c_{i\theta}$. Note that a different (but equivalent) choice of the moments was adopted originally in Ref. [13]. The set of nine moments just introduced is represented by a nine-dimensional vector $\mathcal{M}(f)$

$$\mathcal{M} = \{\rho, j_x, j_y, P_{xx}, P_{xy}, P_{yy}, Q_{yxx}, Q_{xyy}, R_{xxyy}\}, \tag{3.16}$$

which is compactly represented by a relation (from-populations-to-moments),

$$\mathcal{M} = \Psi \cdot f, \tag{3.17}$$

where Ψ is a 9×9 matrix:

$$\Psi = \{\mathit{1}, c_x, c_y, c_x c_x, c_x c_y, c_y c_y, c_x c_x c_y, c_x c_y c_y, c_x c_x c_y c_y\}, \tag{3.18}$$

with $\mathit{1} = \{1, 1, 1, 1, 1, 1, 1, 1, 1\}$. Any other moment can be expressed as a linear combinations of the set $\mathcal{M}$. It is easy to check using (3.12) that at the equilibrium,

$\mathcal{M}^{\rm eq} = \mathcal{M}(f^{\rm eq}(\rho, \mathbf{j}))$ where

$$\mathcal{M}^{\rm eq} = \left\{ \rho, j_x, j_y, \frac{j_x^2}{\rho} + \rho\, c_s^2, \frac{j_x\, j_y}{\rho}, \frac{j_y^2}{\rho} + \rho\, c_s^2, j_y\, c_s^2 + \frac{j_x^2\, j_y}{\rho^2}, j_x\, c_s^2 + \frac{j_y^2\, j_x}{\rho^2}, \frac{j^2}{\rho}\, c_{\rm s}^2 + \rho\, c_{\rm s}^4 \right\}. \tag{3.19}$$

Elsewhere below, the non-equilibrium value of any moment, $\mathcal{M} - \mathcal{M}^{\rm eq}$ will be denoted as $\mathcal{M}^{\rm neq}$. Furthermore, the moments of any valid forcing vector $\mathcal{F}$ are of the form,

$$\mathcal{M}(\mathcal{F}) = \{0, \rho\, g_x, \rho\, g_y, \phi_1(\mathcal{F}), \phi_2(\mathcal{F}), \phi_3(\mathcal{F}), \phi_4(\mathcal{F}), \phi_5(\mathcal{F}), \phi_6(\mathcal{F})\}. \tag{3.20}$$

For the two types of forcing considered here, Eqs. (3.14) and (3.15) the moments are provided in Appendix A.

Applying (3.17) to (3.13), we obtain the time evolution equations for the moments. Specifically, for the locally conserved fields, we have:

$$\begin{aligned} \partial_t \rho + \partial_x j_x + \partial_y j_y &= 0, \\ \partial_t j_x + \partial_x P_{xx} + \partial_y P_{xy} - \rho g_x &= 0, \\ \partial_t j_y + \partial_x P_{xy} + \partial_y P_{yy} - \rho g_y &= 0. \end{aligned} \tag{3.21}$$

For the components of the pressure tensor, we have:

$$\begin{aligned} \partial_t P_{xx} + 3c_{\rm s}^2\, \partial_x j_x + \partial_y Q_{yxx} - \phi_1 &= -\frac{1}{\tau}\left(P_{xx} - \frac{j_x^2}{\rho} - \rho c_{\rm s}^2 \right), \\ \partial_t P_{xy} + \partial_x Q_{yxx} + \partial_y Q_{xyy} - \phi_2 &= -\frac{1}{\tau}\left(P_{xy} - \frac{j_x j_y}{\rho} \right), \\ \partial_t P_{yy} + \partial_x Q_{xyy} + 3c_{\rm s}^2\, \partial_y j_y - \phi_3 &= -\frac{1}{\tau}\left(P_{yy} - \frac{j_y^2}{\rho} - \rho c_{\rm s}^2 \right). \end{aligned} \tag{3.22}$$

Finally, for the rest of the higher-order moments, we have:

$$\begin{aligned}
\partial_t Q_{yxx} + 3c_s^2\,\partial_x P_{xy} + \partial_y R_{xxyy} - \phi_4 &= -\frac{1}{\tau}\left(Q_{yxx} - j_y\,c_s^2 - j_y\frac{j_x^2}{\rho^2}\right),\\
\partial_t Q_{xyy} + \partial_x R_{xxyy} + 3c_s^2\,\partial_y P_{xy} - \phi_5 &= -\frac{1}{\tau}\left(Q_{xyy} - j_x\,c_s^2 - j_x\frac{j_y^2}{\rho^2}\right),\\
\partial_t R_{xxyy} + 3c_s^2\,\partial_x Q_{xyy} + 3c_s^2\,\partial_y Q_{yxx} - \phi_6 &= -\frac{1}{\tau}\left(R_{xxyy} - \frac{j^2}{\rho}\,c_s^2 - \rho\,c_s^4\right).
\end{aligned} \tag{3.23}$$

The moment system (3.21), (3.22) and (3.23) for nine moments is equivalent to the original kinetic equation. In the course of finding the solution to a generalized unidirectional flow (see next section) both the moment and the population representations will be used.

3.4 Unidirectional Flow: Stationary Solution

3.4.1 Setup Description and Outline of Solution

We consider the fluid to be enclosed by two parallel plates in x-direction and separated by a distance of L. The bottom plate at $y = -L/2$ moves with the velocity U_1 and the top plate at $y = L/2$ moves with the velocity U_2. Unidirectional forcing in x direction is also added ($\mathbf{g} = \{g, 0\}$). We aim at finding the steady state solution to the kinetic equation of section 3.2 (or, equivalently, of the moment system of section 3.3) in this setup. Let us outline the solution strategy which consists of three steps.

- Step 1. Integration of the steady state moment system. This is done under two assumptions: (i). The flow is unidirectional. All the fields only vary with respect

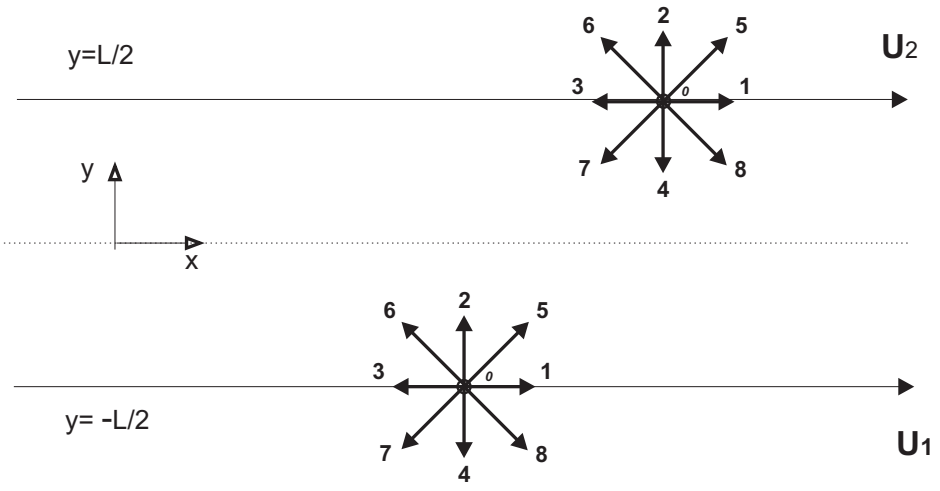

Figure 3.1: Channel geometry where the fluid is enclosed in the y-direction by two parallel plates with forcing only applied in the x-direction. Discrete velocities of the D2Q9 model at the bottom and the top plates are indicated to explain boundary conditions.

to the y-coordinate. (ii). No mass flow through the walls. As the result, we find the inner solution for all the moments. This inner solution is a parametric family which depends on four yet undetermined constants of integration.

- Step 2. Inner solution for the populations. In this step, we invert the map from the population space to the moments space, and use a representation of the populations in terms of moments. This representation is similar to the Grad's distribution function albeit in the present context it is exact representation. Using the result of Step 1, we find the inner solution for the populations. The latter depends on the same integration constants as introduced above. This step is required in order to apply the boundary conditions at the next Step 3.

- Step 3. Matching the boundary condition for the populations with the inner solution. Accordingly, we apply the diffusively reflecting wall boundary condition

at the top and bottom plates and match it with the inner solution for the populations. Thereby, the integration constants will be unambiguously determined, and the solution for the moments can be found. The complete solution for Couette and Poiseuille flow setup will be explicitly given. Note that in this part, solving for j_x is prioritized and some related moments are solved as well. A separate section is dedicated to discuss the remaining moments.

3.4.2 Step 1. Inner Solution to the Stationary Moment System

Assuming that the flow is in the steady-state and is unidirectional (all the fields only vary with respect to the y-coordinate due to the nature of the setup which is infinite in the x-direction), the stationary moment system reads (with some rearrangement of the order of the equations which will prove useful below):

$$\partial_y j_y = 0, \tag{3.24}$$

$$\begin{aligned} \partial_y P_{yy} &= 0, \\ 3c_\mathrm{s}^2\,\partial_y j_y - \phi_3 &= -\frac{1}{\tau}\left(P_{yy} - \frac{j_y^2}{\rho} - \rho c_\mathrm{s}^2\right), \end{aligned} \tag{3.25}$$

$$
\begin{aligned}
\partial_y P_{xy} - \rho g &= 0, \\
\partial_y Q_{xyy} - \phi_2 &= -\frac{1}{\tau}\left(P_{xy} - \frac{j_x j_y}{\rho}\right), \\
3c_{\mathrm{s}}^2\,\partial_y P_{xy} - \phi_5 &= -\frac{1}{\tau}\left(Q_{xyy} - j_x\,c_{\mathrm{s}}^2\right),
\end{aligned}
\tag{3.26}
$$

$$
\begin{aligned}
\partial_y Q_{yxx} - \phi_1 &= -\frac{1}{\tau}\left(P_{xx} - \frac{j_x^2}{\rho} - \rho c_{\mathrm{s}}^2\right), \\
\partial_y R_{xxyy} - \phi_4 &= -\frac{1}{\tau}\left(Q_{yxx} - j_y\,c_{\mathrm{s}}^2\right), \\
3c_{\mathrm{s}}^2\,\partial_y Q_{yxx} - \phi_6 &= -\frac{1}{\tau}\left(R_{xxyy} - \frac{j_x^2 + j_y^2}{\rho}\,c_{\mathrm{s}}^2 - \rho\,c_{\mathrm{s}}^4\right).
\end{aligned}
\tag{3.27}
$$

From (3.24) and the no-flux condition at the walls, $j_y|_{\mathrm{wall}} = 0$, we obtain that the transverse momentum flux is vanishing,

$$
j_y = 0. \tag{3.28}
$$

Substituting $j_y = 0$ into the rest of the moment equations, we arrive at three decoupled sets of equations. Using (A.10) and (A.11), we see that for both type of forcings, we have

$$
\phi_2 = \phi_3 = \phi_4 = 0;\ \phi_5 = \rho\,c_s^2\,g. \tag{3.29}
$$

In particular, we have unidirectional pressure gradient, i.e. $g_x = g$ and $g_y = 0$.

Let us now integrate the resulting moment system. From the first set (3.25), we

find

$$\begin{aligned} P_{yy} &= \rho c_{\mathrm{s}}^2, \\ \rho &= \text{const}, \end{aligned} \tag{3.30}$$

that is, the density is a constant. From the second set (3.26), we find,

$$\begin{aligned} P_{xy}(y) &= \rho g y + k_1, \\ Q_{xyy}(y) &= c_s^2 \, \left(j_x(y) - 2 \, \rho \, g \, \tau \right), \\ j_x(y) &= -\frac{\rho g}{2\tau c_{\mathrm{s}}^2} y^2 - \frac{k_1}{\tau c_{\mathrm{s}}^2} y + \left(\frac{k_2}{c_{\mathrm{s}}^2} + 2\rho g \tau \right), \end{aligned} \tag{3.31}$$

where k_1 and k_2 are yet undetermined constants of integration. This result shows that the macroscopic velocity profile is insensitive to the choice of the particular form of the forcing.

Finally, the third set (3.27), can be simplified in terms of two auxiliary functions:

$$\begin{aligned} X_1 &= R_{xxyy}^{\mathrm{neq}} + \sqrt{3} \, c_s \, Q_{yxx}^{\mathrm{neq}}, \\ X_2 &= R_{xxyy}^{\mathrm{neq}} - \sqrt{3} \, c_s \, Q_{yxx}^{\mathrm{neq}}. \end{aligned} \tag{3.32}$$

The non-equilibrium part of the normal stress can be written as follows:

$$\mathcal{N}^{\mathrm{neq}} = \frac{X_1 + X_2}{6 \, c_s^2} - \frac{\tau}{3 \, c_s^2} \left(\phi_6 - 3 \, c_s^2 \, \phi_1 \right), \tag{3.33}$$

while X_1 and X_2 satisfy

$$\begin{aligned}
\partial_y \left\{ X_1 \, \exp\left(\frac{y}{\tau \sqrt{3}\, c_s} \right) \right\} &= \exp\left(\frac{y}{\tau \sqrt{3}\, c_s} \right) \left\{ \frac{\phi_6}{\sqrt{3}\, c_s} - \partial_y \, R^{\rm eq}_{xxyy} \right\}, \\
\partial_y \left\{ X_2 \, \exp\left(-\frac{y}{\tau \sqrt{3}\, c_s} \right) \right\} &= -\exp\left(-\frac{y}{\tau \sqrt{3}\, c_s} \right) \left\{ \frac{\phi_6}{\sqrt{3}\, c_s} + \partial_y \, R^{\rm eq}_{xxyy} \right\},
\end{aligned} \tag{3.34}$$

which, upon integration, gives

$$\begin{aligned}
X_1(y) &= X_1(y_1) \, \exp\left(\frac{(y_1 - y)}{\tau \sqrt{3}\, c_s} \right) + \int_{s=y_1}^{s=y} ds \, \exp\left(\frac{s - y}{\tau \sqrt{3}\, c_s} \right) \left\{ \frac{\phi_6(j_x(s))}{\sqrt{3}\, c_s} + \frac{2}{\tau} \, u_x(s) \, P_{xy}(s) \right\}, \\
X_2(y) &= X_2(y_2) \, \exp\left(\frac{-(y_2 - y)}{\tau \sqrt{3}\, c_s} \right) - \int_{s=y_2}^{s=y} ds \, \exp\left(\frac{(y - s)}{\tau \sqrt{3}\, c_s} \right) \left\{ \frac{\phi_6(j_x(s))}{\sqrt{3}\, c_s} - \frac{2}{\tau} \, u_x(s) \, P_{xy}(s) \right\}.
\end{aligned} \tag{3.35}$$

Here y_1 and y_2 are two fixed points, at which the values of X_1 and X_2 have to be provided, and we have used the fact that (3.26) can be rewritten as

$$\partial_y j_x = -\frac{P_{xy}}{\tau \, c_s^2}. \tag{3.36}$$

Using integration by parts, Eq. (3.35) can be simplified as

$$\begin{aligned}
X_1(y) &= \exp\left(\frac{y_1 - y}{\tau \sqrt{3}\, c_s} \right) \{ X_1(y_1) - \Theta_1(y_1) \} + \Theta_1(y), \\
X_2(y) &= \exp\left(-\frac{y_2 - y}{\tau \sqrt{3}\, c_s} \right) \{ X_2(y_2) - \Theta_2(y_2) \} + \Theta_2(y),
\end{aligned} \tag{3.37}$$

where

$$\Theta_1 = \frac{6}{\rho}\,P_{xy}^2 + (2\,u_x - 18\,\tau\,g)\,\left(\sqrt{3}\,c_s\,P_{xy} - \tau\,3\,c_s^2\rho\,g\right) + \tau\phi_6 - \tau^2\,\sqrt{3}\,c_s\,\partial_y\phi_6$$
$$+ \tau^3\,3\,c_s^2\,\partial_y^2\phi_6 - 3\,\sqrt{3}\,\tau^4\,c_s^3\,\partial_y^3\phi_6 + 9\,\tau^5\,c_s^4\,\partial_y^4\phi_6 - 9\sqrt{3}\,\tau^6\,c_s^5\,\partial_s^5\phi_6 + 27\,\tau^7\,c_s^6\,\partial_y^6\phi_6,$$
$$\Theta_2 = \frac{6}{\rho}\,P_{xy}^2 - (2\,u_x - 18\,\tau\,g)\,\left(\sqrt{3}\,c_s\,P_{xy} + \tau\,3\,c_s^2\rho\,g\right) + \tau\phi_6 + \tau^2\,\sqrt{3}\,c_s\,\partial_y\phi_6$$
$$+ \tau^3\,3\,c_s^2\,\partial_y^2\phi_6 + 3\,\sqrt{3}\,\tau^4\,c_s^3\,\partial_y^3\phi_6 + 9\,\tau^5\,c_s^4\,\partial_y^4\phi_6 + 9\sqrt{3}\,\tau^6\,c_s^5\,\partial_y^5\phi_6 + 27\,\tau^7\,c_s^6\,\partial_y^6\phi_6,$$

(3.38)

and we have used the fact that for all the forcing schemes under consideration, ϕ_6 is at most a sixth-order polynomial in y. Thus, the expression Θ_1 and Θ_2 are not approximated, but exactly truncated because of the knowledge about ϕ_6.

In summary, equations (3.28), (3.30), (3.31), (3.37) and (3.33) provide the general inner solution for the stationary moment system, and it depends on four integration constants, k_1, k_2, and value of X_1 and X_2 at some specified points y_1 and y_2, respectively. To determine these, we need to specify boundary conditions at the walls. Note that this is precisely where the LB hierarchy differs from the method of moments. It is well known that for moment methods, such as Grad's systems, it is not possible to provide self-consistent boundary conditions for the moments. In our case, this is possible because the boundary conditions for the LB kinetic equations are formulated in terms of populations rather than in terms of moments. For that, we need to invert the linear relation between the moments and the populations, which is done in the next section.

3.4.3 Step 2. Population Representation of the Inner Solution

Let us consider the following basis of the nine-dimensional space:

$$e = \{1, c_x, c_y, (c_x c_x - c_s^2 1), c_x c_y, (c_y c_y - c_s^2 1), (c_x c_x c_y - c_s^2 c_y), (c_x c_y c_y - c_s^2 c_x), (c_x c_x - c_s^2 1)(c_y c_y - c_s^2 1)\}. \tag{3.39}$$

The basis (3.39) is orthogonal with respect to the scalar product $\langle x, y\rangle = \sum_{i=0}^{8} w_i x_i y_i$. We represent the population vector f in the basis (3.39),

$$f = \sum_{k=0}^{8} w_k e_k \varphi_k, \tag{3.40}$$

where expansion coefficients φ_k are found by taking the inner product of f with the basis elements e_k. Thus, the populations can be written in a Grad-like form (from-moments-to-populations representation),

$$f_i = w_i \left[\rho + \frac{j_\alpha c_{i\alpha}}{c_\mathrm{s}^2} + \frac{\mathcal{G}^{(2)}}{2c_\mathrm{s}^4} + \frac{\mathcal{G}^{(3)}}{6c_\mathrm{s}^6} + \frac{\mathcal{G}^{(4)}}{4c_\mathrm{s}^8} \right], \tag{3.41}$$

where

$$\begin{aligned}
\mathcal{G}^{(2)} &= \left(P_{\alpha\beta} - \rho c_\mathrm{s}^2\, \delta_{\alpha\beta}\right)\left(c_{i\alpha}c_{i\beta} - c_\mathrm{s}^2\, \delta_{\alpha\beta}\right), \\
\mathcal{G}^{(3)} &= \left(Q_{\alpha\beta\gamma} - j_\alpha c_\mathrm{s}^2 \delta_{\beta\gamma} - j_\beta c_\mathrm{s}^2 \delta_{\alpha\gamma} - j_\gamma c_\mathrm{s}^2 \delta_{\alpha\beta}\right)\left(c_{i\alpha}c_{i\beta}c_{i\gamma} - c_\mathrm{s}^2(c_{i\alpha}\delta_{\beta\gamma} + c_{i\beta}\delta_{\alpha\gamma} + c_{i\gamma}\delta_{\alpha\beta})\right), \\
\mathcal{G}^{(4)} &= \left(R_{xxyy} - P\, c_\mathrm{s}^2 + \rho c_\mathrm{s}^4\right)\left(c_{ix}^2 - c_\mathrm{s}^2\right)\left(c_{iy}^2 - c_\mathrm{s}^2\right).
\end{aligned} \tag{3.42}$$

Note that $P = P_{\alpha\alpha} = P_{xx} + P_{yy}$. The explicit form of the individual populations f_i can be found in Appendix A.1.

Upon substituting the solution for the moments obtained in section 3.4.2 into equations (3.41) and (3.42), we obtain the inner solution in terms of populations. Note that populations obtained in this way depend on the same four integration constants previously introduced. Thus, the result of this section enables to impose the boundary conditions which is done in the next section.

3.4.4 Step 3. From Boundary Condition to Explicit Solution

Diffusive Wall Boundary Condition

Boundary condition for discrete velocity models are formulated in terms of populations (distribution function). Thus, in order to apply the boundary conditions, it is convenient to come back from the moment representation to the representation in terms of the distribution using (3.41). For the present system, we apply the classical Maxwell's diffusive wall boundary condition. In this condition, particles that reach the wall are redistributed in a way consistent with the mass-balance and normal-flux conditions:

$$f_i\,|_{\mathbf{c}_i\cdot\mathbf{n}>0} = \frac{\sum_{\mathbf{c}_i\cdot\mathbf{n}<0} |(\mathbf{c}_i\cdot\mathbf{n})| f_i}{\sum_{\mathbf{c}_i\cdot\mathbf{n}<0} |(\mathbf{c}_i\cdot\mathbf{n})| f_i^{\mathrm{eq}}(\rho,\mathbf{U}_{\mathrm{wall}})}\, f_i^{\mathrm{eq}}(\rho,\mathbf{U}_{\mathrm{wall}}), \tag{3.43}$$

where $\mathbf{n}$ is the inner normal at the wall, and $\mathbf{U}_{\mathrm{wall}}$ is the wall velocity. Equation (3.43) means that the redistribution of the particles that reach the wall will be according to the equilibrium distribution of the population that leaves the wall. Note that, the

dependence on the density entering the wall equilibrium distribution $f_i^{\rm eq}(\rho, \mathbf{U}_{\rm wall})$ is immaterial in (3.43), it cancels out both in the numerator and the denominator because the density dependence factors out. In order to avoid confusion, we shall rewrite (3.43) using a nominal value $\rho = 1$:

$$f_i\,|_{\mathbf{c}_i\cdot\mathbf{n}>0} = \frac{\sum_{\mathbf{c}_i\cdot\mathbf{n}<0}|(\mathbf{c}_i\cdot\mathbf{n})|f_i}{\sum_{\mathbf{c}_i\cdot\mathbf{n}<0}|(\mathbf{c}_i\cdot\mathbf{n})|f_i^{\rm eq}(1,\mathbf{U}_{\rm wall})}\,f_i^{\rm eq}(1,\mathbf{U}_{\rm wall}), \tag{3.44}$$

Let us proceed with evaluating the left hand side of (3.44) for the present case.

First, using the formula for the equilibrium (3.12), and taking into account that $\mathbf{U}_{\rm wall} = \{U_{\rm wall}, 0\}$ where $U_{\rm wall} = U_1$ for lower plate and $U_{\rm wall} = U_2$ for upper plate, we obtain the equilibrium of the populations leaving the walls:

$$f_i^{\rm eq}(1, U_{\rm wall}) = w_i\left(1 + \frac{c_{ix}\,U_{\rm wall}}{c_{\rm s}^2} + \frac{(c_{ix}\,U_{\rm wall})^2}{2c_{\rm s}^4} - \frac{U_{\rm wall}^2}{2c_{\rm s}^2}\right). \tag{3.45}$$

Second, noticing that $|(\mathbf{c}_i\cdot\mathbf{n})| = c = \sqrt{3}c_{\rm s}$ for all i satisfying $\mathbf{c}_i\cdot\mathbf{n} < 0$, the denominator in (3.44) is evaluated using the equilibrium (3.45) and the auxiliary identities collected in Appendix A.2, Eq. (A.5):

$$\sum_{\mathbf{c}_i\cdot\mathbf{n}<0}|(\mathbf{c}_i\cdot\mathbf{n})|f_i^{\rm eq}(1, U_{\rm wall}) = \frac{c}{6}. \tag{3.46}$$

Equation (3.46) is valid for both the top and the bottom plates since the identities in (A.5) are the same for either case of $c_{iy} < 0$ or $c_{iy} > 0$. Third and final, using identities given in Appendix A.3, we evaluate the nominator in equation (3.44) (the total flux of

impinging populations):

$$\sum_{\mathbf{c}_i\cdot\mathbf{n}<0} |(\mathbf{c}_i\cdot\mathbf{n})| f_i = c \sum_{\mathbf{c}_i\cdot\mathbf{n}<0} w_i \left[\rho + \frac{j_\alpha c_{i\alpha}}{c_\mathrm{s}^2} + \frac{\mathcal{G}^{(2)}}{2c_\mathrm{s}^4} + \frac{\mathcal{G}^{(3)}}{6c_\mathrm{s}^6} + \frac{\mathcal{G}^{(4)}}{4c_\mathrm{s}^8}\right] = \frac{c\rho}{6}. \tag{3.47}$$

Here ρ is the density of the fluid found above (that is, $\rho = \text{const}$).

Combining together the results (3.45), (3.46) and (3.47), we find the diffusive wall boundary conditions in the present setup:

$$f_i\,|_{\mathbf{c}_i\cdot\mathbf{n}>0} = \rho f_i^{\mathrm{eq}}(1, U_{\mathrm{wall}}) f_i^{\mathrm{eq}}(\rho, U_{\mathrm{wall}}). \tag{3.48}$$

Thus, in the present steady-state flow, the boundary condition amounts to setting the outgoing populations at the wall equilibrium. For the purpose of what will follow, we shall write equation (3.48) for each individual population explicitly: At $y = -L/2$ (bottom wall)

$$\begin{aligned}
f_2|_{y=-L/2} &= \frac{4}{36}\,\rho\left(1 - \frac{1}{2c_\mathrm{s}^2}\,{U_1}^2\right), \\
f_5|_{y=-L/2} &= \frac{1}{36}\,\rho\left(1 + \frac{\sqrt{3}}{c_\mathrm{s}}\,U_1 + \frac{1}{c_\mathrm{s}^2}\,{U_1}^2\right), \\
f_6|_{y=-L/2} &= \frac{1}{36}\,\rho\left(1 - \frac{\sqrt{3}}{c_\mathrm{s}}\,U_1 + \frac{1}{c_\mathrm{s}^2}\,{U_1}^2\right),
\end{aligned} \tag{3.49}$$

and at $y = L/2$ (top wall):

$$
\begin{aligned}
f_4|_{y=L/2} &= \frac{4}{36}\rho \left(1 - \frac{1}{2c_\mathrm{s}^2}\, {U_2}^2\right), \\
f_7|_{y=L/2} &= \frac{1}{36}\rho \left(1 - \frac{\sqrt{3}}{c_\mathrm{s}}\, U_2 + \frac{1}{c_\mathrm{s}^2}\, {U_2}^2\right), \\
f_8|_{y=L/2} &= \frac{1}{36}\rho \left(1 + \frac{\sqrt{3}}{c_\mathrm{s}}\, U_2 + \frac{1}{c_\mathrm{s}^2}\, {U_2}^2\right).
\end{aligned}
\tag{3.50}
$$

In the next section we match the inner solution for the populations with the boundary condition.

Evaluation of k_1 and k_2

In the first step of the matching procedure, we evaluate the two integration constants k_1 and k_2. This will be sufficient for finding the closed-form velocity profile and the shear stress, and thus to quantify the slip model.

Functions $Q_{xyy}(y; k_1, k_2)$ and $P_{xy}(y; k_1, k_2)$ are given by the inner solution, Eq. (3.31). Substituting these into boundary condition Eq.(A.4), we arrive at two linear algebraic equations for the two unknowns, k_1 and k_2. After some algebra, we find

$$
\begin{aligned}
k_1 &= -\frac{\rho\nu}{(2\,\mathrm{Kn} + 1)} \frac{(U_2 - U_1)}{L}, \\
k_2 &= \rho c_\mathrm{s}^2 \frac{(U_1 + U_2)}{2} + \frac{\rho c_\mathrm{s}^2\, g}{2\nu} (4\,\mathrm{Kn} + 1) \left(\frac{L}{2}\right)^2.
\end{aligned}
\tag{3.51}
$$

Here we have introduced the Knudsen number

$$
\mathrm{Kn} = \frac{\sqrt{3}\tau c_\mathrm{s}}{L}. \tag{3.52}
$$

With (3.51), equations (3.31) give us closed-form expressions for the velocity profile, shear stress, and the xyy-component of the third-order moments tensor. This information is sufficient in order to compare the present $D2Q9$ model with other known results of kinetic theory. Therefore, we shall do this in the next section, and will complete the solution for the rest of the higher-order moments (which requires evaluation of the two remaining integration constants) in section 3.6.1.

3.5 Slip Model

3.5.1 Velocity profile

Using (3.51) in (3.31), and with some rearrangement of the terms, we find the solution for the x-component of the velocity $u_x = j_x/\rho$:

$$u_x = \frac{gL^2}{2\nu}\left[-\left(\frac{y}{L}-\frac{1}{2}\right)\left(\frac{y}{L}+\frac{1}{2}\right)+\mathrm{Kn}+\frac{4}{3}\,\mathrm{Kn}^2\right]+\frac{(U_2-U_1)}{(2\,\mathrm{Kn}+1)}\,\frac{y}{L}+\frac{(U_1+U_2)}{2}, \tag{3.53}$$

while for the off-diagonal component of the pressure tensor, we have

$$P_{xy} = \rho g y - \frac{\rho\nu}{(2\,\mathrm{Kn}+1)}\frac{(U_2-U_1)}{L}. \tag{3.54}$$

It is instructive to consider the two limiting cases of the general expressions (3.53) and (3.54). For a purely shear driven flow (Couette flow), we set $g = 0$. Then formulas

(3.53) and (3.54) recover the solution already derived in our previous Letter [13]. On the other hand, in the case of Poiseuille flow, we set $U_1 = U_2 = U$ to obtain in (3.53) the familiar parabolic velocity profile with an additional slip correction terms of the order Kn and Kn^2. The latter indicates that the $D2Q9$ model amount to the second-order slip velocity model to be discussed in the next section.

3.5.2 Second-order Slip Velocity

In order to characterize the $D2Q9$ as a slip velocity model, let us introduce the slip velocity at the walls:

$$u_{\mathrm{slip}}\big|_{y=\mp L/2} = u_x\big|_{y=\mp L/2} - U_{\mathrm{wall}}\big|_{y=\mp L/2}\,. \tag{3.55}$$

From (3.53) we have:

$$u_{\mathrm{slip}}\big|_{y=\pm L/2} = \frac{gL^2}{2\nu}\left(\mathrm{Kn} + \frac{4}{3}\,\mathrm{Kn}^2\right) \mp \frac{(U_2 - U_1)\,\mathrm{Kn}}{2\,\mathrm{Kn} + 1}. \tag{3.56}$$

The slip velocity model is usually characterized by a relation between the slip velocity and the second and the first derivatives of the velocity in the direction normal to the wall. In order to present our results in this form, let us define the reduced y-coordinate $\hat{y} = \frac{y}{L}$. Let us also define $\hat{n}$ as the normal of the wall, such that:

$$\hat{n}\big|_{y=\mp L/2} = \pm\hat{y}. \tag{3.57}$$

With this, we can write the slip velocity as follows:

$$u_{\text{slip}}|_{\text{wall}} = \text{Kn}\left(\frac{\partial u_x}{\partial \hat{n}}\right)_{\text{wall}} - \frac{2}{3}\,\text{Kn}^2\left(\frac{\partial^2 u_x}{\partial \hat{n}^2}\right)_{\text{wall}}. \tag{3.58}$$

Note that the results are the same for the top and the bottom walls. The quality of the slip velocity model (3.58) can be accessed through a comparison with a slip velocity solution of the Boltzmann-BGK kinetic equation by Cercignani [36]. The result of Cercignani can be written using the notation adopted here as

$$u_{\text{slip}}|_{\text{wall}} = 0.8297\,\text{Kn}\left(\frac{\partial u_x}{\partial \hat{n}}\right)_{\text{wall}} - 0.5108\,\text{Kn}^2\left(\frac{\partial^2 u_x}{\partial \hat{n}^2}\right)_{\text{wall}}. \tag{3.59}$$

It is clear that the result of the $D2Q9$ model (3.58) is reasonably close to the full Boltzmann-BGK result (3.59). It should be stressed that our solution assumed no tuning parameter or other optimization techniques. In order to make the comparison even more transparent, let us consider the special case of the Poiseuille flow (for simplicity, we set $U_1 = U_2 = 0$). In this case, our solution yields the following slip:

$$u_{\text{slip}}|_{\text{wall}} = \frac{gL^2}{2\nu}\left(\text{Kn} + \frac{4}{3}\,\text{Kn}^2\right), \tag{3.60}$$

whereas the result of Cercignani reads:

$$u_{\text{slip}}|_{\text{wall}} = \frac{gL^2}{2\nu}\left(0.8297\,\text{Kn} + 1.0216\,\text{Kn}^2\right). \tag{3.61}$$

The reduced form of the two results for the slip are compared in Fig. 3.2.

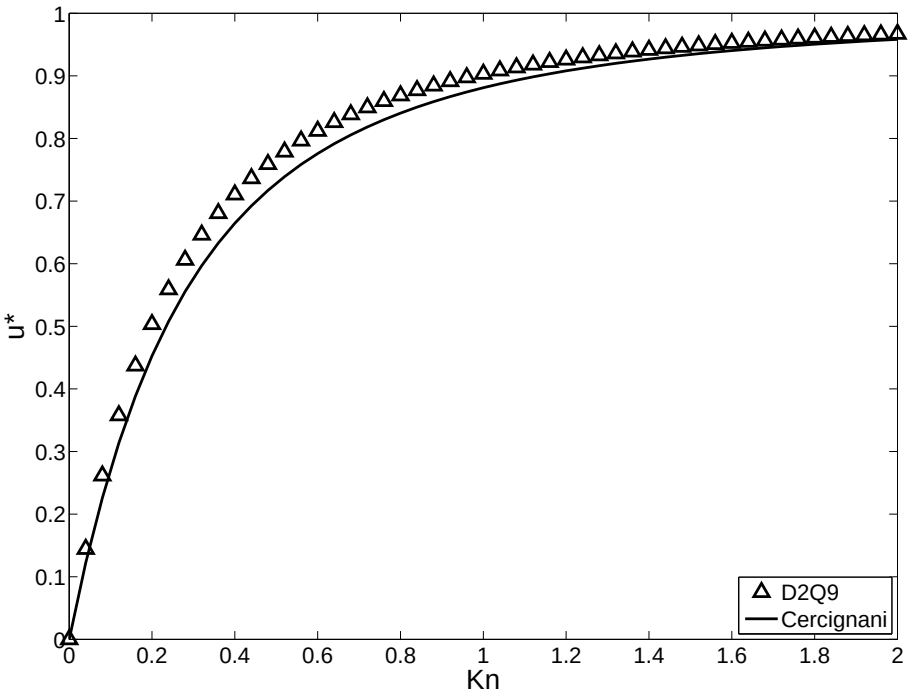

Figure 3.2: Slip velocity (u^*) profile for $D2Q9$ model as a function of Knudsen numbers for the Poiseuille flow. Slip velocity from Cercignani's solution for Boltzmann-BGK kinetic equation is given here as a comparison.

3.5.3 Flow Rate

Another important characteristics of the slip models is the ability to predicting a non-monotonic dependence of the mass flow rate in the Poiseuille flow on the Knudsen number (so-called Knudsen minimum problem). The flow rate Q is defined as

$$Q = \int_{y=-L/2}^{y=L/2} u_x \, dy. \tag{3.62}$$

Assuming Poiseuille flow condition $U_1 = U_2 = 0$ in the general solution (3.53), and taking into account the relation between the Knudsen number and shear viscosity,

$$\nu = \mathrm{Kn}\frac{c_\mathrm{s} L}{\sqrt{3}}, \tag{3.63}$$

we find the flow rate for the current model as follows:

$$Q = \frac{\sqrt{3} g L^2}{2\, c_\mathrm{s}} \left(\frac{1}{6\,\mathrm{Kn}} + 1 + \frac{4}{3}\,\mathrm{Kn} \right). \tag{3.64}$$

In the continuum limit ($\mathrm{Kn} \to 0$), the solution asymptotically approaches the Navier-Stokes solution,

$$Q_\mathrm{NS} = \frac{\sqrt{3} g L^2}{12\, c_\mathrm{s}} \frac{1}{\mathrm{Kn}}. \tag{3.65}$$

The flow rate (3.64) has the minimum located at Kn_min, where

$$\frac{1}{\mathrm{Kn}_\mathrm{min}} = 2\sqrt{2} \approx 2.82843. \tag{3.66}$$

In the case of Cercignani's slip model, we have:

$$Q = \frac{\sqrt{3} g L^2}{2\, c_\mathrm{s}} \left(\frac{1}{6\,\mathrm{Kn}} + 0.8297 + 1.0216\,\mathrm{Kn} \right), \tag{3.67}$$

and the minimum is located at Kn_min, where

$$\frac{1}{\mathrm{Kn}_\mathrm{min}} \approx 2.47580. \tag{3.68}$$

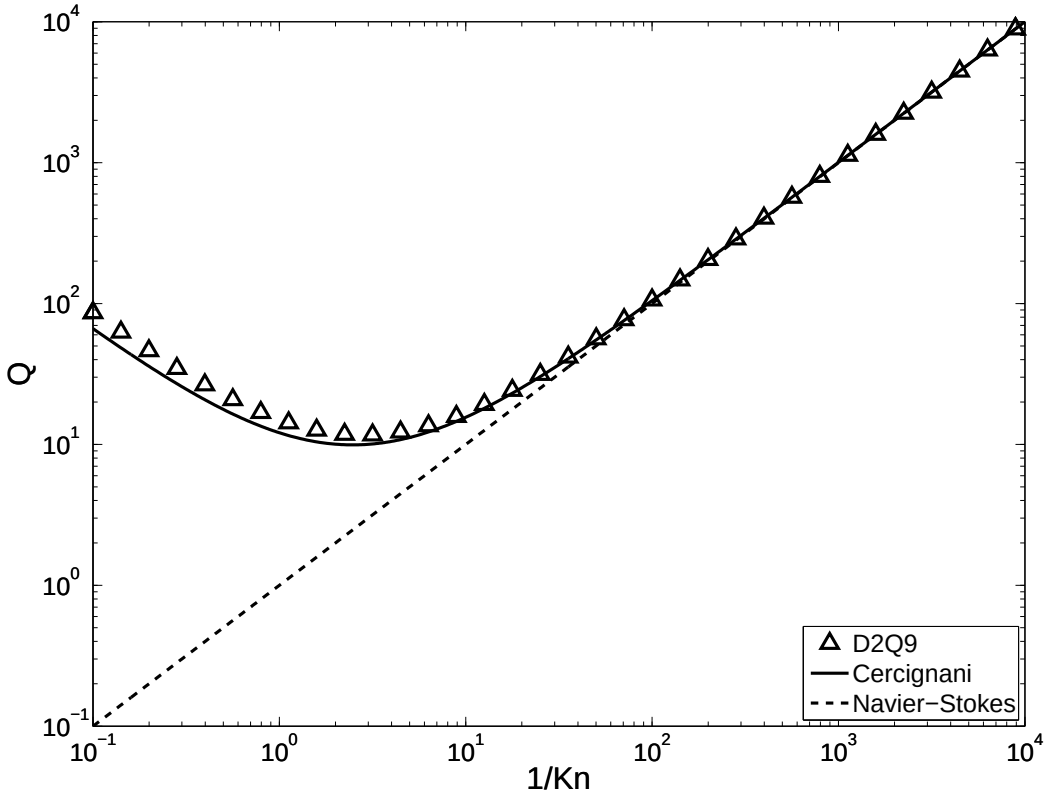

Figure 3.3: Flowrate versus reciprocal of Knudsen number in log-log scale. The flowrate Q is normalized such that $Q_{\mathrm{NS}} = \frac{1}{\mathrm{Kn}}$.

From Fig. 3.3, it is clear that both the $D2Q9$ model and the slip-flow approximation based on the Boltzmann-BGK kinetic equation give a reasonably close result for the flow rate.

3.6 Higher Order Moments

3.6.1 Shear Stress

The shear stress in the present model is purely Newtonian and satisfies a relation:

$$P_{xy} = -\rho\,\nu\,\frac{\partial u_x}{\partial y}, \tag{3.69}$$

which can be checked by using (3.53) and (3.54). However, what is non-trivial is the velocity gradient itself. The Navier-Stokes equation with no-slip boundary condition predicts that the velocity gradient is independent of the Knudsen number. However, we know from the numerical solutions of the linearized Bolztmann equation and DSMC simulations that this is not the case. The present model is able to predict this behavior qualitatively. This agreement is qualitative only due to the absence of kinetic boundary layer (Knudsen layer) in the $D2Q9$ model [13]. A comparison is possible by introducing a non-dimensional velocity gradient W at the center-line as

$$W = 1 - (U_2 - U_1)\,\frac{\partial u_x}{\partial (y/L)}\bigg|_{y=0}, \tag{3.70}$$

which can be evaluated for the present model using (3.53),

$$W = \frac{2\,\mathrm{Kn}}{(2\,\mathrm{Kn} + 1)}. \tag{3.71}$$

In Tab. 3.1, the $D2Q9$ model is compared against data for the linearized Boltzmann-BGK equation [40]. It can be seen from Table 3.1 that in the slip-flow regime error with respect to the Boltzmann-BGK equation is around 20%, while for the transitional flow it is around 30%.

Table 3.1: Deviation of non-dimensional velocity gradient from Navier-Stokes value for the $D2Q9$ model and the Boltzmann-BGK kinetic equation.

Kn	$D2Q9$	Boltzmann-BGK	% Error from Boltzmann-BGK value
0.06124	0.10911	0.09134	19.45
0.12247	0.19675	0.1648	19.89
0.17496	0.25922	0.2136	21.36
0.24495	0.32881	0.2664	23.43
0.30619	0.37979	0.3041	24.89
0.61327	0.55051	0.4290	28.32
0.81649	0.62020	0.4821	28.64
1.22474	0.71010	0.5556	27.81

3.6.2 Third and Fourth Order Moments

In the present model, none of the third order moments (which are related to the energy flux) have independent dynamics. They are slaved by the dynamics of the lower-order moments. This is not surprising as the dynamics considered here is essentially isothermal. In particular, from (3.31) we have already seen that one of third order moments, Q_{xyy}:

$$Q_{xyy} = c_s^2 \, (j_x - 2\rho \, g \, \tau), \tag{3.72}$$

that is, the longitudinal energy flux Q_{xyy}^{neq} reads,

$$Q_{xyy}^{\mathrm{neq}} = -2 \, c_s^2 \, \rho \, g \, \tau. \tag{3.73}$$

On the other hand, for the transversal energy flux, we have while using (3.27),

$$Q_{yxx}^{\mathrm{neq}} = -\tau\, \partial_y R_{xxyy}. \tag{3.74}$$

Furthermore, using (3.33),

$$R_{xxyy}^{\mathrm{neq}} = 3\, c_s^2\, \mathcal{N}^{\mathrm{neq}} + \tau\, \left(\phi_6 - 3\, c_s^2\, \phi_1\right), \tag{3.75}$$

which means that the transversal energy flux is completely determined from the knowledge of the non-equilibrium part of the normal stress difference. Notice that this relationship is equivalent to an algebraic relations offered by (3.32) and (3.33). In the next section, we shall find the explicit expression for the normal stress difference.

3.6.3 Normal Stress Difference

Above, we have evaluated the integration constants k_1 and k_2 which was sufficient to find the velocity and the shear stress in the general unidirectional setup. The remaining two integration constants, k_3 and k_4, are required in order to find the remaining higher-order moments of the solution. This is the subject of the present section.

Combining (3.37) with (A.4), we have

$$\begin{aligned} X_1(y) &= \exp\left(-\frac{\frac{1}{2}+\frac{y}{L}}{\mathrm{Kn}}\right)\, \left\{-\rho\, c_s^2\, (u_x^2 - U_1^2)_{y=-L/2} - \Theta_1(y=-L/2)\right\} + \Theta_1(y), \\ X_2(y) &= \exp\left(-\frac{\frac{1}{2}-\frac{y}{L}}{\mathrm{Kn}}\right)\, \left\{-\rho\, c_s^2\, (u_x^2 - U_2^2)_{y=L/2} - \Theta_2(y=L/2)\right\} + \Theta_2(y). \end{aligned} \tag{3.76}$$

This general expression can be simplified for special flow situations. In particular, for the Couette flow, we set $g = 0$ to get

$$\begin{aligned}\Theta_1(y) &= 2\,\rho\,c_s^2\,\left(\frac{\mathrm{Kn}^2\;(U_2-U_1)^2}{(2\,\mathrm{Kn}+1)^2}\right) + 2\,\sqrt{3}\,c_s\;u_x(y)\,P_{xy},\\ \Theta_2(y) &= 2\,\rho\,c_s^2\,\left(\frac{\mathrm{Kn}^2\;(U_2-U_1)^2}{(2\,\mathrm{Kn}+1)^2}\right) - 2\,\sqrt{3}\,c_s\;u_x(y)\,P_{xy}.\end{aligned} \tag{3.77}$$

Using Eq. (3.54) and Eq. (3.53) in the latter expression, it can be shown that

$$\begin{aligned}\Theta_1(-L/2) &= \rho\,c_s^2\,\left(\frac{\mathrm{Kn}^2\;(U_2-U_1)^2}{(2\,\mathrm{Kn}+1)^2}\right) - \rho\,c_s^2\,(u_x^2-U_1^2)_{y=-L/2},\\ \Theta_2(L/2) &= \rho\,c_s^2\,\left(\frac{\mathrm{Kn}^2\;(U_2-U_1)^2}{(2\,\mathrm{Kn}+1)^2}\right) - \rho\,c_s^2\,(u_x^2-U_2^2)_{y=L/2}.\end{aligned} \tag{3.78}$$

Thus,

$$\begin{aligned}X_1(y) &= \rho\,c_s^2\;\left(\frac{\mathrm{Kn}^2\,(U_2-U_1)^2}{(2\mathrm{Kn}+1)^2}\right)\left\{2-\exp\left(-\frac{\frac{1}{2}+\frac{y}{L}}{\mathrm{Kn}}\right)\right\} + 2\,\sqrt{3}\,c_s\,P_{xy}\,u_x(y),\\ X_2(y) &= \rho\,c_s^2\;\left(\frac{\mathrm{Kn}^2\,(U_2-U_1)^2}{(2\mathrm{Kn}+1)^2}\right)\left\{2-\exp\left(-\frac{\frac{1}{2}-\frac{y}{L}}{\mathrm{Kn}}\right)\right\} - 2\,\sqrt{3}\,c_s\,P_{xy}\,u_x(y).\end{aligned} \tag{3.79}$$

which is equivalent to the following non-equilibrium normal stress difference:

$$\mathcal{N}^{\mathrm{neq}} = \rho\left(\frac{U_2-U_1}{L}\right)^2\frac{\nu^2}{c_s^2\,(1+2\mathrm{Kn})^2}\left[2-e^{-\frac{1}{2\mathrm{Kn}}}\cosh\left(\frac{y}{\mathrm{Kn}\,L}\right)\right]. \tag{3.80}$$

The result (3.80) was already reported in [13], and we do not dwell on it here. As it was explained above, all the remaining higher-order moments are expressed using the non-equilibrium normal stress (3.80). In particular, the non-equilibrium transversal

energy flux $q_y^{\rm neq} = Q_{yxx}^{\rm neq}$ reads:

$$q_y^{\rm neq} = Q_{yxx}^{\rm neq} = \rho \left(\frac{U_2 - U_1}{L}\right)^2 \frac{\sqrt{3}\,\nu^2}{c_s\,(1+2{\rm Kn})^2} \left[e^{-\frac{1}{2{\rm Kn}}}\,\sinh\left(\frac{y}{{\rm Kn}\,L}\right) - 2y\right] + P_{xy}\,(U_1+U_2). \tag{3.81}$$

For the pressure-driven flow (Poiseuille flow), the normal stress difference is evaluated in the same way. In this case, combining Eq. (3.37) with Eq. (A.4), we have

$$\begin{aligned} X_1(y) &= \exp\left(-\frac{\frac{1}{2}+\frac{y}{L}}{\rm Kn}\right)\left\{-\rho\,g^2\,L^2\,\left(\frac{3}{4}+2\,{\rm Kn}+\frac{4}{3}\,{\rm Kn}^2\right) - \Theta_1(y=-L/2)\right\} + \Theta_1(y), \\ X_2(y) &= \exp\left(-\frac{\frac{1}{2}-\frac{y}{L}}{\rm Kn}\right)\left\{-\rho\,g^2\,L^2\,\left(\frac{3}{4}+2\,{\rm Kn}+\frac{4}{3}\,{\rm Kn}^2\right) - \Theta_2(y=L/2)\right\} + \Theta_2(y). \end{aligned} \tag{3.82}$$

Let us now discuss the effect of the choice of the forcing term. For the first type of the forcing, Eqs. (3.14) and (A.10), we have the following relationship:

$$\begin{aligned} \Theta_1(y)+\Theta_2(y) = {} & \frac{3\rho g^4}{4c_s^4{\rm Kn}^2L^2}\,y^6 + \frac{3\rho g^4}{16c_s^4{\rm Kn}^2}\,(-3-12{\rm Kn}+104{\rm Kn}^2)\,y^4 + \\ & \frac{\rho g^2L^2}{3}(-3-12{\rm Kn}+80{\rm Kn}^2) + 16\rho g^2y^2 - \frac{3\rho g^4L^4}{256c_s^4}\left(\frac{1}{{\rm Kn}^2}+\frac{12}{\rm Kn}\right) + \\ & \frac{\rho g^4L^2}{64c_s^4{\rm Kn}^2}\left(9+72{\rm Kn}-192{\rm Kn}^2-1344{\rm Kn}^3+15232{\rm Kn}^4\right)y^2 + \\ & \frac{\rho g^4L^4}{2304c_s^4}(-1080-20340{\rm Kn}^2-105984{\rm Kn}^3+1092608{\rm Kn}^4), \end{aligned} \tag{3.83}$$

$$\Theta_1(y) - \Theta_2(y) = \frac{9\rho g^4}{2c_s^4 \mathrm{Kn} L}\, y^5 + \left(\frac{6\rho g^2}{\mathrm{Kn}\, L} + \frac{3\rho g^4 L}{4c_s^4 \mathrm{Kn}}\left(-3 - 12\mathrm{Kn} + 104\mathrm{Kn}^2\right)\right) y^3 + \frac{\rho g^4 L^3}{32 c_s^4 \mathrm{Kn}}(9 + 72\mathrm{Kn} - 192\mathrm{Kn}^2 - 1344\mathrm{Kn}^3 + 15232\mathrm{Kn}^4) y + \frac{3\rho g^2 L}{2\mathrm{Kn}}(-1 - 4\mathrm{Kn} + 16\mathrm{Kn}^2) y. \tag{3.84}$$

Thus we have,

$$\Theta_1(-L/2) = \Theta_2(L/2) = \rho\, g^2\, L^2\, \mathrm{Kn}\left(4 + \frac{40}{3}\,\mathrm{Kn}\right) + \frac{\rho\, g^4\, L^4}{36 c_s^4}\,\mathrm{Kn}\left(27 + 513\,\mathrm{Kn} + 3456\,\mathrm{Kn}^2 + 8536\,\mathrm{Kn}^3\right). \tag{3.85}$$

For second type of forcing (Eqs. (3.15) and (A.11)), we have:

$$\begin{aligned}
\Theta_1(y) &= 6\,\rho\, g^2\, y^2 + \sqrt{3}\, c_s\, \rho\, g\, L\, \left(2\, u_x(y) - 18\,\tau\, g\right)\left(\frac{y}{L} - \mathrm{Kn}\right) + \\
&\quad \rho\, g^2\, L^2\left[-\left(\frac{y}{L} - \frac{1}{2}\right)\left(\frac{y}{L} + \frac{1}{2}\right) + \mathrm{Kn} - \frac{2}{3}\,\mathrm{Kn}^2 + 2\,\mathrm{Kn}\,\frac{y}{L}\right], \\
\Theta_2(y) &= 6\,\rho\, g^2\, y^2 - \sqrt{3}\, c_s\, \rho\, g\, L\, \left(2\, u_x(y) - 18\,\tau\, g\right)\left(\frac{y}{L} + \mathrm{Kn}\right) + \\
&\quad \rho\, g^2\, L^2\left[-\left(\frac{y}{L} - \frac{1}{2}\right)\left(\frac{y}{L} + \frac{1}{2}\right) + \mathrm{Kn} - \frac{2}{3}\,\mathrm{Kn}^2 - 2\,\mathrm{Kn}\,\frac{y}{L}\right].
\end{aligned} \tag{3.86}$$

Therefore,

$$\Theta_1(-L/2) = \Theta_2(L/2) = \rho\, g^2\, L^2\, \mathrm{Kn}\left(4 + \frac{40}{3}\,\mathrm{Kn}\right). \tag{3.87}$$

As we have already mentioned, both suggestions for the forcing term result in the same expression for the velocity profile, shear stress and the longitudinal energy flux. The difference occurs only in the higher-order moments such as the normal stress dif-

ference. In order to compare the three cases, we introduce the Mach number Ma as the ratio of the average velocity to the speed of sound,

$$\mathrm{Ma} = \frac{u_x^{\mathrm{avg}}}{c_s}, \tag{3.88}$$

where:

$$u_x^{\mathrm{avg}} = \frac{1}{L}\int_{y=-L/2}^{y=L/2} u_x\, dy = \frac{gL^2}{2\nu}\left(\frac{1}{6} + \mathrm{Kn} + \frac{4}{3}\,\mathrm{Kn}^2\right). \tag{3.89}$$

Thus,

$$\mathrm{Ma} = \frac{gL^2}{2\nu\, c_s}\left(\frac{1}{6} + \mathrm{Kn} + \frac{4}{3}\,\mathrm{Kn}^2\right). \tag{3.90}$$

In Fig. 3.4 and Fig. 3.5, the normal stress difference at the centerline (that is, the maximum of the normal stress difference) is shown as a function of Knudsen number for two different values of Mach number. From Figs. 3.4 and 3.5, we see that the firs and the second forcing schemes agree with each other at least up to $\mathrm{Kn} < 0.5$ for low Mach number, as expected. The third and the simplest forcing scheme is likely to be applicable only in the hydrodynamic regime.

3.7 Discussion

In this study, we quantified the standard and very popular lattice Boltzmann model with nine discrete velocities (the $D2Q9$ model) for the simulation beyond the Navier-Stokes hydrodynamics. The exact solution to the generic unidirectional flow under an external force between moving parallel plates is given in this Chapter. It is noted that

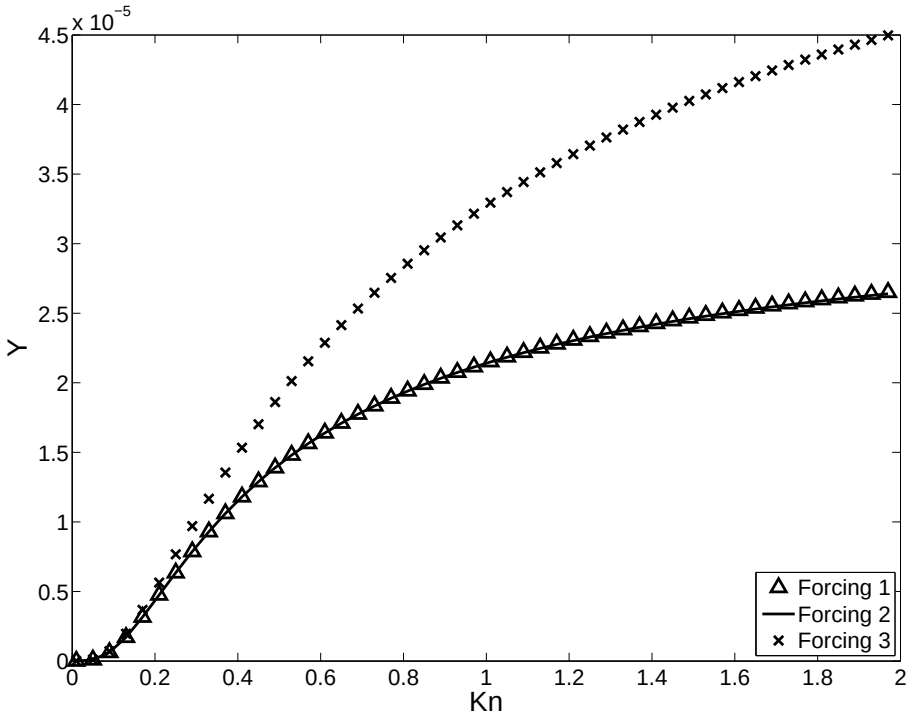

Figure 3.4: Comparison of the centerline non-equilibrium normal stress difference ($Y = \mathcal{N}^{\mathrm{neq}}\big|_{y=0}$) versus Knudsen number at Ma = 0.01 for various force terms. Forcing 1: Eq. (3.14); Forcing 2: Eq. (3.15).

the performance of $D2Q9$ model is rather limited since it does not describe the Knudsen layer for the velocity profile, and thus only qualifies as a slip-flow approximation.

In order to assess its quality, we made a comparison with the well-known slip-flow approximation of the Boltzmann-BGK kinetic equation in the Poiseuille flow. The comparison shows that the slip-flow $D2Q9$ is reasonably close to the slip-flow solution of the Boltzmann-BGK equation. Thus, due to its high computational efficiency, the $D2Q9$ model can be used for semi-quantitative analysis in engineering applications.

It should be noted that the excellent result is not only due to the use of the BGK collision model, but also the choice of the boundary condition. The diffusive wall boundary

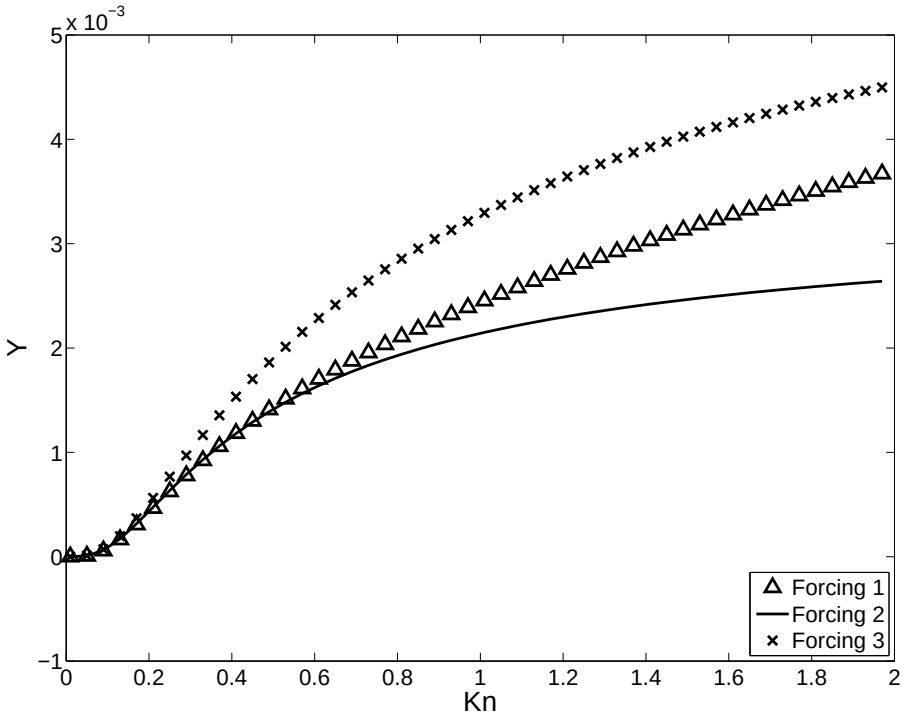

Figure 3.5: Comparison of the centerline non-equilibrium normal stress difference ($Y = \mathcal{N}^{\mathrm{neq}}\big|_{y=0}$) versus Knudsen number at Ma = 0.1. Notation as in Fig. 3.4.

condition is used here because it is derived from the kinetic theory of gases, unlike other commonly used approaches [9]. Note also that the analytical results presented here are pertinent to the discrete-velocity model (3.13) while the temporal and spatial variables are still continuous and not yet discretized.

Various discretization procedures for (3.13) have been already suggested in the literature, see, for example, [41, 17]. Discretization of the boundary conditions should provide a useful benchmark for various discretization schemes of the kinetic equation (3.13), and especially for the implementation of the boundary conditions. It has been demonstrated already that, under an appropriate discretization, the numerical solution

to the Couette flow converges to the analytical result [13].

We have also analyzed the effect of various force implementations on the higher-order moments and have found that the most popular models of the force agree with each other in a range of Knudsen number for low Mach number flows.

In the next Chapter, we would attempt to address the absence of Knudsen layer in $D2Q9$ model by borrowing some elements from $D2Q16$ model. As the next set of approximation in the Gauss-Hermite hierarchy, $D2Q16$ model gives a better approximation to the kinetic equation but comes with a higher computational cost. An alternative is proposed in the next Chapter, where we reduce the known $D2Q16$ model to fit into the $D2Q9$ velocity set while conserving the dynamics of the moment system the same. This will translate into the introduction of additional terms to the standard $D2Q9$ model, which will induce a representation of Knudsen layer in the velocity model.

Chapter 4

Renormalization of Lattice Boltzmann Method

4.1 Introduction

It is well understood by now that standard Lattice Boltzmann (LB) models form a well-defined hierarchy approximating classical kinetic theory, which characterized by a set of discrete velocities given by Hermite polynomials of the order N, where $N \geq 3$ [9, 11, 10]. In this sense, higher N will constitute a better approximation for realistic application, but at the same time will also introduce an increasingly difficult computational problem. A general method of reducing the numbers of velocities has been introduced recently in Ref. [10], which allows us to reduce the size of velocity sets without compromising on accuracy and physics. The methodology is based on a sim-

[1] A working manuscript in preparation

ple modification to the BGK assumption of uniform temporal decay. In the proposed method, a set of higher order moments is separated and assumed to relax at a faster rate than the rest of the moments. Here, we can think of the evolution of higher order moments to first reach some pseudo-equilibrium state, before eventually relaxing further to the equilibrium.

In this particular Chapter, we are taking the example of $D2Q16$ model which is relaxed in two steps: First to the moment system of $D2Q9$, followed by the relaxation to equilibrium (normal BGK terms). Thus, we are selecting 7 moments (16 minus 9) that do not appear in the $D2Q9$ construction and classify them as the set of higher order moments that fastly relaxing to the $D2Q9$ system. By doing so, we obtain a modified $D2Q9$ moment chain which has the same dynamics as the $D2Q16$. Consequently, this methodology allows a simulation using the velocity set from $D2Q9$ system while obtaining the result of higher LB model (in this case $D2Q16$).

In section 4.2 a brief introduction to the $D2Q16$ model is presented. In section 4.3, method to renormalize $D2Q16$ to a more compact $D2Q9$-like form is elaborated and the resultant expression is given in an explicit formula. In section 4.4 the formal stationary solution for the case of unidirectional flow is presented, whereas the diffusive boundary conditions are given in section 4.5 and used to obtained the explicit solution for flow between parallel plates. These results are analyzed further in the sections 4.6 (shear stress), 4.7 (flow rate) and 4.8 (higher moments).

4.2 $D2Q16$ Lattice Model

In two-dimension, one can construct a set of discrete velocity model by considering the zeroes of the fourth-order Hermite polynomials [10]. The two-dimensional set of discrete velocities obtained using Gauss-Hermite quadrature are:

$$\begin{aligned} \frac{c_x}{c_s} &= \{a, -a, b, -b, a, -a, b, -b, a, -a, b, -b, a, -a, b, -b\}, \\ \frac{c_y}{c_s} &= \{a, a, a, a, -a, -a, -a, -a, b, b, b, b, -b, -b, -b, -b\}, \end{aligned} \tag{4.1}$$

where $c_{\mathrm{s}} = \sqrt{\frac{k_{\mathrm{B}} T_0}{m}}$ and the corresponding weights are:

$$W = \left\{w_a^2, w_a^2, w_a\, w_b, w_a\, w_b, w_a^2, w_a^2, w_a\, w_b, w_a\, w_b, w_a\, w_b, w_a\, w_b, w_b^2, w_b^2, w_a\, w_b, w_a\, w_b, w_b^2, w_b^2\right\}, \tag{4.2}$$

where:

$$\begin{aligned} a &= \sqrt{3 - \sqrt{6}}, & w_a &= \frac{1}{4\, a^2}, \\ b &= \sqrt{3 + \sqrt{6}}, & w_b &= \frac{1}{4\, b^2}. \end{aligned} \tag{4.3}$$

Typically for a set of discrete velocities one can define either population representation or moment representation. For D2Q16 velocity model, we have the following sixteen independent moments $\mathcal{M}_{16}(f)$ as basis

$$\mathcal{M}_{16}(f) = \{\rho, j_x, j_y, P_{xx}, P_{xy}, P_{yy}, Q_{xxx}, Q_{yxx}, Q_{xyy}, Q_{yyy}, R_{xxxy}, R_{xxyy}, R_{yyyx}, L_{xxxyy}, L_{yyyxx}, \psi\}, \tag{4.4}$$

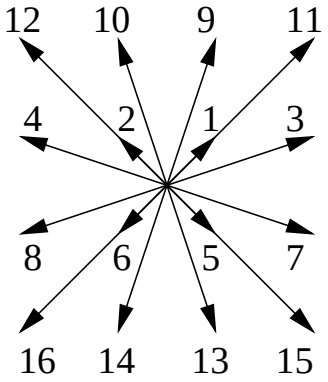

Figure 4.1: 16 velocity lattice model.

defined by the relation (from-populations-to-moments),

$$\mathcal{M}_{16} = \Psi_{16} \cdot f, \tag{4.5}$$

where Ψ_{16} is a 16×16 matrix:

$$\begin{aligned} \Psi_{16} = \{&1, c_x, c_y, c_x c_x, c_x c_y, c_y c_y, c_x c_x c_x, c_y c_x c_x, c_x c_y c_y, c_y c_y c_y, \\ &c_x c_x c_x c_y, c_x c_x c_y c_y, c_y c_y c_y c_x, c_x^3 c_y^2, c_x^2 c_y^3, c_x^3 c_y^3\}. \end{aligned} \tag{4.6}$$

Any other moment can be expressed as a linear combinations of the set $\mathcal{M}$. It is worthwhile to note that the nine independent moments relevant to $D2Q9$ model form a subset of the sixteen moments considered in the present work. In the present work, we are interested in projecting the $D2Q16$ model on $D2Q9$ model. The basic idea is to reduce the model in such a way that only a subset of 16 (relevant to $D2Q9$ model) appear as basic variables. In order to do so, we decompose the set of moments in three

subclasses. The first one are usual conserved ones

$$M_{\rm con}(f) = \{\rho, j_x, j_y\}\,, \tag{4.7}$$

which are included in the slow ones (the set of moments relevant to the $D2Q9$ model) :

$$M_{\rm Slow}(f) = \{\rho, j_x, j_y, P_{xx}, P_{xy}, P_{yy}, Q_{yxx}, Q_{xyy}, R_{xxyy}\}\,. \tag{4.8}$$

We then classify the rest of the moments as fast ones:

$$M_{\rm Fast}(f) = \{Q_{xxx}, Q_{yyy}, R_{xxxy}, R_{yyyx}, L_{xxxyy}, L_{yyyxx}, \psi\}\,. \tag{4.9}$$

For this model the H-function (in all dimensions) is:

$$H_{\{w_i,\mathbf{C}_i\}} = \sum_{i=1}^{\rm n_d} f_i \ln\left(\frac{f_i}{W_i}\right), \tag{4.10}$$

and the equilibrium is found by minimizing the H-function under the constraints of Eq.(4.7).

The formal solution can be written as:

$$f_i^{\rm eq} = W_i\,\mathcal{A}\,X^{\frac{c_{ix}}{c_s}}\,Y^{\frac{c_{iy}}{c_s}}, \tag{4.11}$$

where $\mathcal{A}$, X and Y are corresponding Lagrange multipliers. A series solution, second

order in accuracy, of this equilibrium is

$$\tilde{f}_i^{(2)} = W_i \left[1 + \frac{\mathbf{u}\cdot\mathbf{C}_i}{c_s^2} + \frac{1}{2}\left(\frac{\mathbf{u}\cdot\mathbf{C}_i}{c_s^2}\right)^2 - \frac{1}{2\,c_s^2}\mathbf{u}^2 \right]. \tag{4.12}$$

It can be proved that at the equilibrium, $\mathcal{M}^{\rm eq} \equiv \mathcal{M}(\tilde{f}^{(2)})$ is:

$$\mathcal{M}^{\rm eq} = \left\{ \rho, j_x, j_y, \frac{j_x^2}{\rho} + \rho\, c_s^2, \frac{j_x\, j_y}{\rho}, \frac{j_y^2}{\rho} + \rho\, c_s^2, 3j_x\, c_s^2, j_y\, c_s^2, j_x\, c_s^2, 3j_y\, c_s^2, \frac{j^2}{\rho}\, c_{\rm s}^2 + \rho\, c_{\rm s}^4 \right\}. \tag{4.13}$$

Once we have defined the equilibrium and H-function, we can write the kinetic equation. We will follow typical apporach of discrete kinetic theory that forcing is completly representable in terms of conserved variables. Finally, we write a generalization of the BGK model in terms of auxiliary population $f^\star(f)$ as

$$\partial_t f + c_\alpha\, \partial_\alpha f + \mathcal{F}(\rho, \mathbf{j}) = -\frac{1}{\tau}\left(f^\star - f^{eq}\right) - \frac{1}{\eta\,\tau}\left(f - f^\star\right), \tag{4.14}$$

where τ is the usual relaxation time of the BGK model, related with the viscosity and η is another smallness parameter (less than unity, with value unity corresponding to BGK model) giving the ratio of relaxation time of fast and slow moments. Further more, we have defined an auxiliary population f^* as

$$f^{\star} = W_i\Bigg(\rho + \frac{j_\alpha\, c_\alpha}{c_s^2} + \frac{(P_{\alpha\beta} - \rho c_s^2\delta_{\alpha\beta})(c_\alpha c_\beta - c_s^2\delta_{\alpha\beta})}{2c_s^4} + \\ \frac{(Q_{xyy} - j_x c_s^2)(c_x c_y^2 - c_x c_s^2) + (Q_{yxx} - j_y c_s^2)(c_y c_x^2 - c_y c_s^2)}{2c_s^6} + \\ \frac{(R_{xxyy} - (P_{xx} + P_{yy})c_s^2 + \rho c_s^4)(c_x^2 - c_s^2)(c_y^2 - c_s^2)}{4c_s^8}\Bigg). \tag{4.15}$$

Note here that the weights and velocities involved are that of 16 velocity model.

The auxiliary population $f^{\star}$ is chosen such that $M_{\text{Slow}}(f^{\star}) = M_{\text{Slow}}(f)$. It can be checked easily that:

$$M_{\text{Fast}}(f^{\star}) = \left\{3\, c_s^2\, j_x, 3\, c_s^2\, j_y, 3\, c_s^2\, P_{xy}, 3\, c_s^2\, P_{xy}, 3\, c_s^2\, Q_{xyy}, 3\, c_s^2\, Q_{yxx}, 9\, c_s^4\, P_{xy}\right\}. \tag{4.16}$$

Later, the fast moments are projected to the slow moments, allowing the relaxation of the fast moments dominated by the slow moments relaxation behavior. In other words, one can say that the fast moments are slaved by the dynamics of slow one. Furthermore, the moments of any valid forcing vector $\mathcal{F}$ are of the form,

$$\mathcal{M}(\mathcal{F}) = \{0, \rho\, g_x, \rho\, g_y, \phi_1(\mathcal{F}), \phi_2(\mathcal{F}), \phi_3(\mathcal{F}), \phi_7(\mathcal{F}), \phi_4(\mathcal{F}), \phi_5(\mathcal{F}), \phi_8(\mathcal{F}), \phi_9(\mathcal{F}), \\ \phi_6(\mathcal{F}), \phi_{10}(\mathcal{F}), \phi_{11}(\mathcal{F}), \phi_{12}(\mathcal{F}), \phi_{13}(\mathcal{F})\}. \tag{4.17}$$

where $\mathbf{g} \equiv \{g_x, g_y\}$ is the acceleration vector.

4.3 Reduction in terms of $D2Q9$ model

In this section, we will show that it is possible to write the kinetic equation Eq.(4.14), in a form similar to $D2Q9$ model. The goal is to create a model which can be solved by lattice Boltzmann scheme used to solve $D2Q9$ model. In order to do so, firstly we will write the moment system of $D2Q16$ model and then use a Chapman-Enskog like expansion [42] to simplify it.

4.3.1 Renormalization of D2Q16 Velocity Model

In this subsection, we will elaborate details of the work done in [43] to greater detail in generalized fashion. The renormalization steps are similar to Chapman-Enskog method:

- Step 1. We would like to visualize $D2Q9$ model as a subset of $D2Q16$ model where a few fast moments are slaved to quasi-equilibrium manifold. In order to do so, first we decompose the moments into set of fast moments and slow moments. The BGK model is then modified to introduce a hierarchy of time-scale.

- Step 2. The distribution function f is then expanded in power of some smallness parameter, in such a way that only lowest term in the expansion of f corresponds to the set of slow moments. Any other terms in the expansion of f will not contribute to slow moments.

To achieve this, first we write the Chapman-Enskog like expansion [42] of distribution function f and time derivative as:

$$\begin{aligned} f &= f^{(0)} + \eta f^{(1)} + \eta^2 f^{(2)} + \cdots \\ \partial_t &= \partial_t^{(0)} + \eta \partial_t^{(1)} + \eta^2 \partial_t^{(2)} + \cdots , \end{aligned} \tag{4.18}$$

and we are defining $f^{(i)}$ in such a way that:

$$\begin{aligned} &M_{\text{Slow}}(f^{(i)}) = M_{\text{Slow}}(f) && \text{for } i = 0, \\ &M_{\text{Slow}}(f^{(i)}) = 0 && \text{for any } i > 0. \end{aligned} \tag{4.19}$$

assuming that $\tau = \mathcal{O}(1)$, we start off with the coefficient of the lowest power of η (i.e. $\frac{1}{\eta}$) in the expansion in (4.14). We have:

$$f^{(0)} = f^{\star}. \tag{4.20}$$

At the next step of the expansion, substituting f^* to the equation gives us:

$$\partial_t^{(0)} f^* + c_\alpha \, \partial_\alpha f^* + \mathcal{F} = -\frac{1}{\tau} \left(f^* - f^{eq} \right) - f^{(1)}. \tag{4.21}$$

From this, we recover the $D2Q9$ moment chain system

$$
\begin{aligned}
\partial_t^{(0)}\rho + \partial_\alpha j_\alpha &= 0,\\
\partial_t^{(0)} j_\alpha + \partial_\beta P_{\alpha\beta} - \rho g_\alpha &= 0,\\
\partial_t^{(0)} P_{xx} + \partial_x\left(3c_{\mathrm{s}}^2\, j_x\right) + \partial_y Q_{yxx} - \phi_1 &= -\frac{1}{\tau}\left(P_{xx} - \frac{j_x^2}{\rho} - \rho c_{\mathrm{s}}^2\right),\\
\partial_t^{(0)} P_{xy} + \partial_x Q_{yxx} + \partial_y Q_{xyy} - \phi_2 &= -\frac{1}{\tau}\left(P_{xy} - \frac{j_x j_y}{\rho}\right),\\
\partial_t^{(0)} P_{yy} + \partial_x Q_{xyy} + \partial_y\left(3c_{\mathrm{s}}^2\, j_y\right) - \phi_3 &= -\frac{1}{\tau}\left(P_{yy} - \frac{j_y^2}{\rho} - \rho c_{\mathrm{s}}^2\right).\\
\partial_t^{(0)} Q_{yxx} + \partial_x\left(3c_{\mathrm{s}}^2\, P_{xy}\right) + \partial_y R_{xxyy} - \phi_4 &= -\frac{1}{\tau}\left(Q_{yxx} - j_y\, c_{\mathrm{s}}^2 - j_y\frac{j_x^2}{\rho^2}\right),\\
\partial_t^{(0)} Q_{xyy} + \partial_x R_{xxyy} + \partial_y\left(3c_{\mathrm{s}}^2\, P_{xy}\right) - \phi_5 &= -\frac{1}{\tau}\left(Q_{xyy} - j_x\, c_{\mathrm{s}}^2 - j_x\frac{j_y^2}{\rho^2}\right),\\
\partial_t^{(0)} R_{xxyy} + \partial_x\left(3c_{\mathrm{s}}^2\, Q_{xyy}\right) + \partial_y\left(3c_{\mathrm{s}}^2\, Q_{xxy}\right) - \phi_6 &= -\frac{1}{\tau}\left(R_{xxyy} - \frac{j^2}{\rho}\, c_{\mathrm{s}}^2 - \rho\, c_{\mathrm{s}}^4\right),
\end{aligned}
\tag{4.22}
$$

as solvability condition.

Using equation (4.21), the evolution equation for fast moments can be written as:

$$
\begin{aligned}
3c_s^2\partial_t^{(0)} j_x + \partial_x\left(6c_s^2 P_{xx} - 3c_s^4\rho\right) + 3c_s^2\partial_y P_{xy} - \phi_7 &= -Q^{(1)}_{xxx},\\
3c_s^2\partial_t^{(0)} j_y + 3c_s^2\partial_x P_{xy} + \partial_y\left(6c_s^2 P_{yy} - 3c_s^4\rho\right) - \phi_8 &= -Q^{(1)}_{yyy},\\
3c_s^2\partial_t^{(0)} P_{xy} + \partial_x\left(6c_s^2 Q_{yxx} - 3c_s^4 j_y\right) + 3c_s^2\partial_y Q_{xyy} - \phi_9 &= -\frac{3c_s^2}{\tau}\left(P_{xy} - \frac{j_x j_y}{\rho}\right) - R^{(1)}_{xxxy},\\
3c_s^2\partial_t^{(0)} P_{xy} + 3c_s^2\partial_x Q_{yxx} + 3c_s^2\partial_y\left(6c_s^2 Q_{xyy} - 3c_s^4 j_x\right) - \phi_{10} &= -\frac{3c_s^2}{\tau}\left(P_{xy} - \frac{j_x j_y}{\rho}\right) - R^{(1)}_{yyyx},\\
3c_s^2\partial_t^{(0)} Q_{xyy} + \partial_x\left(6c_s^2 R_{xxyy} - 3c_s^4 P_{yy}\right) + 9c_s^4\partial_x P_{xy} - \phi_{11} &= -\frac{3c_s^2}{\tau}\left(Q_{xyy} - j_x c_s^2\right) - L^{(1)}_{xxxyy},\\
3c_s^2\partial_t^{(0)} Q_{yxx} + 9c_s^4\partial_x P_{xy} + \partial_y\left(6c_s^2 R_{xxyy} - 3c_s^4 P_{xx}\right) - \phi_{12} &= -\frac{3c_s^2}{\tau}\left(Q_{yxx} - j_y c_s^2\right) - L^{(1)}_{yyyxx},\\
\partial_t^{(0)} P_{xy} + \partial_x\left(2Q_{yxx} - c_s^2 j_y\right) + \partial_y\left(2Q_{xyy} - c_s^2 j_x\right) - \frac{\phi_{13}}{9c_s^4} &= -\frac{1}{\tau}\left(P_{xy} - \frac{j_x j_y}{\rho}\right) - \frac{\psi^{(1)}}{9c_s^4},
\end{aligned}
\tag{4.23}
$$

which by using the solvability condition (Eq.(4.22)), will give us:

$$
\begin{aligned}
M^{(1)}_{\text{Fast}} = 3c_s^2\Big\{ &\partial_x\left(\rho\, c_s^2 - P_{xx}\right), \partial_y\left(\rho\, c_s^2 - P_{yy}\right), \partial_x\left(j_y\, c_s^2 - Q_{yxx}\right),\\
&\partial_y\left(j_x\, c_s^2 - Q_{xyy}\right), \partial_x\left(P_{yy}\, c_s^2 - R_{xxyy}\right), \partial_y\left(P_{xx}\, c_s^2 - R_{xxyy}\right),\\
&3c_s^2\partial_x\left(j_y\, c_s^2 - Q_{yxx}\right) + 3c_s^2\partial_y\left(j_x\, c_s^2 - Q_{xyy}\right)\Big\}.
\end{aligned}
\tag{4.24}
$$

Note that all the forcing term cancel off in the expansion.

At the next order of smallness parameter, we have:

$$\partial_t^{(0)} f^{(1)} + \partial_t^{(1)} f^* + c_\alpha \, \partial_\alpha f^{(1)} = -f^{(2)}, \tag{4.25}$$

and the solvability condition thus read:

$$\begin{aligned}
\partial_t^{(1)} \rho &= 0, \\
\partial_t^{(1)} j_x &= 0, \\
\partial_t^{(1)} j_y &= 0, \\
\partial_t^{(1)} P_{xy} &= 0, \\
\partial_t^{(1)} P_{xx} + \partial_x Q_{xxx}^{(1)} &= 0, \\
\partial_t^{(1)} P_{yy} + \partial_y Q_{yyy}^{(1)} &= 0, \\
\partial_t^{(1)} Q_{xyy} + \partial_y R_{yyyx}^{(1)} &= 0, \\
\partial_t^{(1)} Q_{yxx} + \partial_x R_{xxxy}^{(1)} &= 0, \\
\partial_t^{(1)} \psi + \partial_x L_{xxxyy}^{(1)} + \partial_y L_{yyyxx}^{(1)} &= 0.
\end{aligned} \tag{4.26}$$

4.3.2 Renormalized form

Eq.(4.22) and Eq. (4.26) allows us to write down the renormalized $D2Q9$ model equation. For conserved moments we have

$$\begin{aligned}
\partial_t \rho + \partial_x j_x + \partial_y j_y &= 0, \\
\partial_t j_x + \partial_x P_{xx} + \partial_y P_{xy} - \rho g_x &= 0, \\
\partial_t j_y + \partial_x P_{xy} + \partial_y P_{yy} - \rho g_y &= 0.
\end{aligned} \tag{4.27}$$

For the components of the pressure tensor, we have

$$\begin{aligned}
\partial_t P_{xx} + \partial_x \left(3c_{\mathrm{s}}^2\, j_x\right) + \partial_y Q_{yxx} - \phi_1 &= -\frac{1}{\tau}\left(P_{xx} - \frac{j_x^2}{\rho} - \rho c_{\mathrm{s}}^2\right) - \partial_x\, Q^{(1)}_{xxx}, \\
\partial_t P_{xy} + \partial_x Q_{yxx} + \partial_y Q_{xyy} - \phi_2 &= -\frac{1}{\tau}\left(P_{xy} - \frac{j_x j_y}{\rho}\right), \\
\partial_t P_{yy} + \partial_x Q_{xyy} + \partial_y \left(3c_{\mathrm{s}}^2\, j_y\right) - \phi_3 &= -\frac{1}{\tau}\left(P_{yy} - \frac{j_y^2}{\rho} - \rho c_{\mathrm{s}}^2\right) - \partial_y\, Q^{(1)}_{yyy}.
\end{aligned} \tag{4.28}$$

Finally, for the rest of the higher-order moments, we have:

$$\begin{aligned}
\partial_t Q_{yxx} + \partial_x \left(3c_{\mathrm{s}}^2\, P_{xy}\right) + \partial_y R_{xxyy} - \phi_4 &= -\frac{1}{\tau}\left(Q_{yxx} - j_y\, c_{\mathrm{s}}^2 - j_y \frac{j_x^2}{\rho^2}\right) - \partial_x R^{(1)}_{xxxy}, \\
\partial_t Q_{xyy} + \partial_x R_{xxyy} + \partial_y \left(3c_{\mathrm{s}}^2\, P_{xy}\right) - \phi_5 &= -\frac{1}{\tau}\left(Q_{xyy} - j_x\, c_{\mathrm{s}}^2 - j_x \frac{j_y^2}{\rho^2}\right) - \partial_y R^{(1)}_{yyyx}, \\
\partial_t R_{xxyy} + \partial_x \left(3c_{\mathrm{s}}^2\, Q_{xyy}\right) + \partial_y \left(3c_{\mathrm{s}}^2\, Q_{xxy}\right) - \phi_6 &= -\frac{1}{\tau}\left(R_{xxyy} - \frac{j^2}{\rho}\, c_{\mathrm{s}}^2 - \rho\, c_{\mathrm{s}}^4\right) - \partial_x L^{(1)}_{xxxyy} - \partial_y L^{(1)}_{yyyxx}.
\end{aligned} \tag{4.29}$$

where:

$$
\begin{aligned}
Q^{(1)}_{xxx} &= 3\,c_s^2\tau\eta\partial_x(c_s^2\rho - P_{xx}),\\
Q^{(1)}_{yyy} &= 3\,c_s^2\tau\eta\partial_y(c_s^2\rho - P_{yy}),\\
R^{(1)}_{xxxy} &= 3\,c_s^2\tau\eta\partial_x(c_s^2 j_y - Q_{yxx}),\\
R^{(1)}_{yyyx} &= 3\,c_s^2\tau\eta\partial_y(c_s^2 j_x - Q_{xyy}),\\
L^{(1)}_{xxxyy} &= 3\,c_s^2\tau\eta\partial_x(c_s^2 P_{yy} - R_{xxyy}),\\
L^{(1)}_{yyyxx} &= 3\,c_s^2\tau\eta\partial_y(c_s^2 P_{xx} - R_{xxyy}).
\end{aligned}
\tag{4.30}
$$

The moment system (4.27), (4.28) and (4.29) for nine moments is equivalent to the original kinetic equation in nine velocity model. It is therefore logical to transform the moments back to population balance in nine velocity model.

4.3.3 Population Representation in D2Q9 Velocity Model

We write the distribution function for $D2Q9$ velocity model as:

$$
f^{\{9\}} = \{f_0^{\{9\}}, f_1^{\{9\}}, f_2^{\{9\}}, f_3^{\{9\}}, f_4^{\{9\}}, f_5^{\{9\}}, f_6^{\{9\}}, f_7^{\{9\}}, f_8^{\{9\}}\}. \tag{4.31}
$$

The discrete velocity set for the $D2Q9$ model is given by:

$$\begin{aligned} c_x^{\{9\}} &= \sqrt{\frac{3k_{\mathrm{B}}T_0}{m}}\,\{0,1,0,-1,0,1,-1,-1,1\}, \\ c_y^{\{9\}} &= \sqrt{\frac{3k_{\mathrm{B}}T_0}{m}}\,\{0,0,1,0,-1,1,1,-1,-1\}, \end{aligned} \tag{4.32}$$

while the vector of weights $w_i^{\{9\}}$ is

$$w^{\{9\}} = \frac{1}{36}\,\{16,4,4,4,4,1,1,1,1\}. \tag{4.33}$$

we have:

$$\begin{aligned} f_i^{\{9\}} = w_i^{\{9\}}\Bigg(\rho + \frac{j_\alpha\, c_\alpha^{\{9\}}}{c_s^2} + \frac{(P_{\alpha\beta} - \rho c_s^2\delta_{\alpha\beta})(c_\alpha^{\{9\}}c_\beta^{\{9\}} - c_s^2\delta_{\alpha\beta})}{2c_s^4} + \\ \frac{(Q_{xyy} - j_x c_s^2)(c_x^{\{9\}}{c_y^{\{9\}}}^2 - c_x^{\{9\}}c_s^2) + (Q_{yxx} - j_y c_s^2)(c_y^{\{9\}}{c_x^{\{9\}}}^2 - c_y^{\{9\}}c_s^2)}{2c_s^6} + \\ \frac{(R_{xxyy} - (P_{xx}+P_{yy})c_s^2 + \rho c_s^4)({c_x^{\{9\}}}^2 - c_s^2)({c_y^{\{9\}}}^2 - c_s^2)}{4c_s^8}\Bigg), \end{aligned} \tag{4.34}$$

and we write corrected evolution equation as:

$$\partial_t f_i^{\{9\}} + \partial_\alpha\left(f_i^{\{9\}} c_{i\,\alpha}^{\{9\}}\right) - \frac{1}{\tau}\left(f_i^{\{9\}} - {f^{eq}}_i^{\{9\}}\right) = 3c_s^2\tau\eta\left(\partial_x^2\left(\mathcal{S}_{ij}^{(x)} f_j\right) + \partial_y^2\left(\mathcal{S}_{ij}^{(y)} f_j\right)\right), \tag{4.35}$$

where the correction matrices is given by:

$$\begin{aligned}
\mathcal{S}_{ij}^{(x)} &= w_i^{\{9\}} w_j^{\{9\}}\, {c_{ix}^{\{9\}}}^2 ({c_{jx}^{\{9\}}}^2 - c_s^2) \left(\frac{1}{2c_s^4} + \frac{c_{iy}^{\{9\}} c_{jy}^{\{9\}}}{2c_s^6} + \frac{{c_{iy}^{\{9\}}}^2 {c_{jy}^{\{9\}}}^2}{4c_s^8} \right), \\
\mathcal{S}_{ij}^{(y)} &= w_i^{\{9\}} w_j^{\{9\}}\, {c_{iy}^{\{9\}}}^2 ({c_{jy}^{\{9\}}}^2 - c_s^2) \left(\frac{1}{2c_s^4} + \frac{c_{ix}^{\{9\}} c_{jx}^{\{9\}}}{2c_s^6} + \frac{{c_{ix}^{\{9\}}}^2 {c_{jx}^{\{9\}}}^2}{4c_s^8} \right).
\end{aligned} \tag{4.36}$$

In the course of finding the solution to a generalized unidirectional flow (see next section) both the moment and the population representations will be used.

4.4 Unidirectional Flow: Stationary Solution

4.4.1 Setup Description and Outline of Solution

We consider the fluid to be enclosed by two parallel plates in x-direction and separated by a distance of L. The bottom plate at $y = -L/2$ moves with the velocity U_1 and the top plate at $y = L/2$ moves with the velocity U_2. Unidirectional forcing in x direction is also added ($\mathbf{g} = \{g, 0\}$). We aim at finding the steady state solution to the kinetic equation of the renormalized model in this setup.

Let us outline the solution strategy which consists of three steps.

- Step 1. Integration of the steady state moment system. This is done under two assumptions: (i). The flow is unidirectional. All the fields only vary with respect to the y-coordinate. (ii). No mass flow through the walls. As the result, we find the inner solution for all the moments. This inner solution is a parametric family

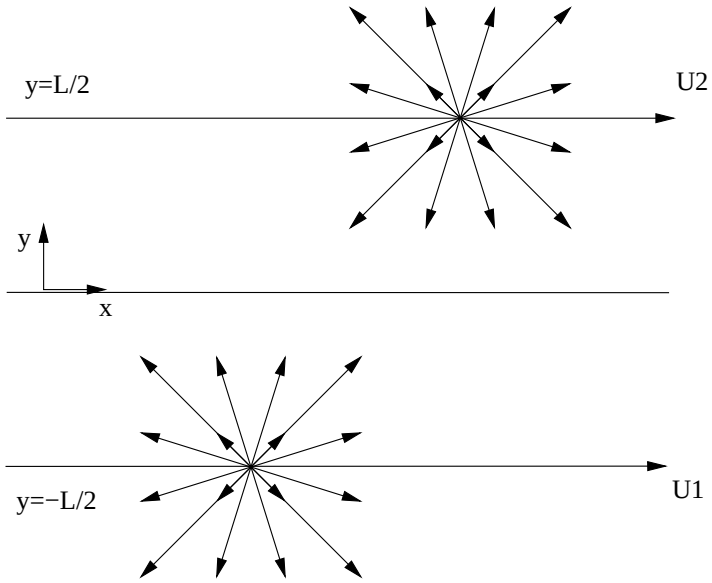

Figure 4.2: Channel geometry. Discrete velocities of the D2Q16 model at the bottom and the top plates are indicated to explain boundary conditions

which depends on four yet undetermined constants of integration.

- Step 2. Inner solution for the populations. In this step, we invert the map from the population space to the moments space, and use a representation of the populations in terms of moments. This representation is similar to the Grad's distribution function albeit in the present context it is exact representation. Using the result of Step 1, we find the inner solution for the populations. The latter depends on the same integration constants as introduced above. This step is required in order to apply the boundary conditions at the next Step 3.

- Step 3. Matching the boundary condition for the populations with the inner solution. Accordingly, we apply the diffusively reflecting wall boundary condition at the top and bottom plates and match it with the inner solution for the popula-

tions. Thereby, the integration constants will be unambiguously determined, and the solution for the moments can be found. The complete solution for Couette and Poiseuille flow setup will be explicitly given. Note that in this part, solving for j_x is prioritized and some related moments are solved as well. A separate section is dedicated to discuss the remaining moments.

Assuming that the flow is in the steady-state and is unidirectional (all the fields depend only on the y-coordinate due to the nature of the setup which is infinite in the x-direction), the stationary moment system reads (with some rearrangement of the order of the equations which will prove useful below):

$$\partial_y j_y = 0, \tag{4.37}$$

$$\begin{aligned} \partial_y P_{yy} &= 0, \\ \partial_y \left[3c_{\mathrm{s}}^2\, j_y + 3\, c_s^2 \tau\eta \partial_y (c_s^2 \rho - P_{yy})\right] - \phi_3 &= -\frac{1}{\tau}\left(P_{yy} - \frac{j_y^2}{\rho} - \rho c_{\mathrm{s}}^2\right), \end{aligned} \tag{4.38}$$

$$\begin{aligned} \partial_y P_{xy} - \rho g &= 0, \\ \partial_y Q_{xyy} - \phi_2 &= -\frac{1}{\tau}\left(P_{xy} - \frac{j_x j_y}{\rho}\right), \\ \partial_y \left(3c_{\mathrm{s}}^2\, P_{xy} + 3\, c_s^2 \tau\eta \partial_y (c_s^2 j_x - Q_{xyy})\right) - \phi_5 &= -\frac{1}{\tau}\left(Q_{xyy} - j_x\, c_{\mathrm{s}}^2\right), \end{aligned} \tag{4.39}$$

$$
\begin{aligned}
\partial_y Q_{yxx} - \phi_1 &= -\frac{1}{\tau}\left(P_{xx} - \frac{j_x^2}{\rho} - \rho c_{\mathrm{s}}^2\right), \\
\partial_y R_{xxyy} - \phi_4 &= -\frac{1}{\tau}\left(Q_{yxx} - j_y\, c_{\mathrm{s}}^2\right), \\
\partial_y\left(3c_{\mathrm{s}}^2\, Q_{xxy} + 3\, c_s^2 \tau\eta \partial_y(c_s^2\rho - P_{yy} - \psi)\right) - \phi_6 &= -\frac{1}{\tau}\left(R_{xxyy} - \frac{j_x^2 + j_y^2}{\rho}\, c_{\mathrm{s}}^2 - \rho\, c_{\mathrm{s}}^4\right).
\end{aligned}
\tag{4.40}
$$

From (4.37) and the no-flux condition at the walls, $j_y|_{\mathrm{wall}} = 0$, we obtain that the transverse momentum flux is vanishing,

$$
j_y = 0. \tag{4.41}
$$

Substituting $j_y = 0$ into the rest of the moment equations, we arrive at three decoupled sets of equations. We have

$$
\phi_2 = \phi_3 = \phi_4 = 0;\ \ \phi_5 = \rho\, c_s^2\, g. \tag{4.42}
$$

Let us now integrate the resulting moment system. From the first set (4.38), we find

$$
\begin{aligned}
P_{yy} &= \rho_0 c_s^2, \\
3\, c_s^2 \tau\eta \partial_y^2 \rho &= -\frac{1}{\tau}\left(\rho_0 - \rho\right),
\end{aligned}
\tag{4.43}
$$

where ρ_0 is some constant. From this set we can solve for density as:

$$\rho = \rho_0 + A_1 \cosh\left(\frac{y}{\tau\sqrt{3\eta}\,c_s}\right) + A_2 \sinh\left(\frac{y}{\tau\sqrt{3\eta}\,c_s}\right). \tag{4.44}$$

By solving (4.39), we have:

$$\begin{aligned} P_{xy}(y) &= \rho g y + k_1, \\ Q_{xyy}(y) &= -\frac{\rho g}{2\tau} y^2 - \frac{k_1}{\tau} y + k_2, \\ j_x(y)\, c_s^2 - Q_{xyy} &= 3\, c_s^2 \tau^2 \eta \partial_y^2 \left(c_s^2 j_x - Q_{xyy}\right) + 2\,\rho\, g\, \tau\, c_s^2, \end{aligned} \tag{4.45}$$

where k_1 and k_2 are yet undetermined constants of integration. This result shows that the macroscopic velocity profile is insensitive to the choice of the particular form of the forcing. From this set we can solve for momentum as

$$j_x = \frac{1}{c_s^2}\left[Q_{xyy} + A_3 \cosh\left(\frac{y}{\tau\sqrt{3\eta}\,c_s}\right) + A_4 \sinh\left(\frac{y}{\tau\sqrt{3\eta}\,c_s}\right)\right] + 2\,\rho\, g\, \tau, \tag{4.46}$$

with the integration constants determined by solving the boundary condition in the next section.

4.5 Exact Boundary Condition for moment system

Boundary condition for discrete velocity models are formulated in terms of populations (distribution function). Thus, in order to apply the boundary conditions, it is convenient to come back from the moment representation to population distribution. For the

present system, we apply the classical Maxwell's diffusive wall boundary condition. In this condition, the particle that reaches the wall are redistributed in a way consistent with the mass-balance and normal-flux conditions:

$$f_i\,|_{\mathbf{c}_i\cdot\mathbf{n}>0} = \frac{\sum_{\mathbf{c}_i\cdot\mathbf{n}<0}|(\mathbf{c}_i\cdot\mathbf{n})|f_i}{\sum_{\mathbf{c}_i\cdot\mathbf{n}<0}|(\mathbf{c}_i\cdot\mathbf{n})|f_i^{\mathrm{eq}}(\rho,\mathbf{U}_{\mathrm{wall}})}\,f_i^{\mathrm{eq}}(\rho,\mathbf{U}_{\mathrm{wall}}), \tag{4.47}$$

where $\mathbf{n}$ is the inner normal at the wall, and $\mathbf{U}_{\mathrm{wall}}$ is the wall velocity. Equation (4.47) means that the redistribution of the particles that reach the wall will be according to the equilibrium distribution of the population that leaves the wall. Let us evaluate the right hand side of (4.47) for the present case.

We can compute equilibrium flux for one dimensional flows as:

$$\sum_{c_{iy}>0}|c_{iy}|\,f_i^{\mathrm{eq}}(1,V,0) = \sum_{c_{iy}<0}|c_{iy}|\,f_i^{\mathrm{eq}}(1,V,0) = \frac{a+b}{4\,a\,b}c_s. \tag{4.48}$$

Further we also have relation on flux for unidirectional flow ($j_y = 0$) itself as:

$$\sum_{c_{iy}>0}|c_{iy}|\,f_i = \sum_{c_{iy}<0}|c_{iy}|\,f_i = \frac{2\,(a+b)\,P_{yy} + \sqrt{6}\,(b-a)\,(\rho\,c_s^2 - P_{yy})}{8\,a\,b\,c_s}. \tag{4.49}$$

This simplifies the diffusive boundary condition as:

At $y = L/2$,

$$f_i = f_i^{\mathrm{eq}}(1, U_1, 0) \times \frac{2\,(a+b)\,P_{yy}\Big|_{y=L/2} + \sqrt{6}\,(b-a)\,(\rho\,c_s^2 - P_{yy})\Big|_{y=L/2}}{2\,(a+b)\,c_s^2} \qquad \text{if } c_{iy} < 0, \tag{4.50}$$

while at $y = -L/2$

$$f_i = f_i^{\mathrm{eq}}(1, U_2, 0) \times \frac{2\,(a+b)\,P_{yy}\Big|_{y=-L/2} + \sqrt{6}\,(b-a)\,(\rho\,c_s^2 - P_{yy})|_{y=-L/2}}{2\,(a+b)\,c_s^2} \qquad \text{if } c_{iy} > 0. \tag{4.51}$$

4.5.1 Density Profile

So at the boundary $y = \pm L/2$, we have:

$$\left(P_{yy} - \rho c_s^2\right)\Big|_{y=\pm L/2} = \pm \frac{2}{(b-a)\,\sqrt{6} c_s}\, Q_{yyy}\Big|_{y=\pm L/2}. \tag{4.52}$$

But, we have the fact that P_{yy} is a constant from (4.43), and since Q_{yyy}^{eq} is zero, and using Eq.(4.30), we have:

$$\partial_y\,\rho\Big|_{y=L/2} = -\partial_y\,\rho\Big|_{y=-L/2}. \tag{4.53}$$

Substituting the solution of ρ from (4.44), we have that A_2 is zero. So:

$$\rho = A_1 \cosh\left(\frac{y}{\sqrt{3\,\eta}\,c_s\,\tau}\right) + \rho_0, \tag{4.54}$$

and

$$Q_{yyy} = -A_1\, c_s^2\, \sqrt{3\,\eta\, c_s^2}\, \sinh\!\left(\frac{y}{\sqrt{3\,\eta}\, c_s\, \tau}\right). \tag{4.55}$$

and thus the final result will read

$$\rho = \rho_0, \qquad Q_{yyy} = 0, \qquad P_{yy} = 0. \tag{4.56}$$

This simplifies of diffusive boundary condition (Eq.(4.47)) as:

$$f_i\,|_{\mathbf{c}_i\cdot\mathbf{n}>0} = f_i^{\mathrm{eq}}(\rho, \mathbf{U}_{\mathrm{wall}}). \tag{4.57}$$

Thus, in the present steady-state flow, the boundary condition amounts to setting the outgoing populations at the wall equilibrium.

We divide the population into two categories, namely inner population (f^{i}) and outer population (f^{o}). Population inside the domain will follow equation (4.14), and thus we call them inner population. While at the boundary condition, part of the population will follow equation (4.57), which is called outer population. Thus, it will be convenient to split the population into two half-set ($c_y > 0$ and $c_y < 0$). At the boundary, half of the contribution will be from inner population and half will be from outer population.

Let us define, for any moments $\mathcal{M}$:

$$\mathcal{M} = \mathcal{M}^{+} + \mathcal{M}^{-}, \tag{4.58}$$

where

$$\mathcal{M}^{+} = \mathcal{M}(f^{+}) = \sum_{c_{iy}>0} \Psi f_i \qquad , \qquad \mathcal{M}^{-} = \mathcal{M}(f^{-}) = \sum_{c_{iy}<0} \Psi f_i. \tag{4.59}$$

Thus we have the inner population as:

$$\begin{aligned} f_i = \; W_i \Bigg(& \rho\mathcal{H}^{(0)} + \frac{j_\alpha}{c_s}\,\mathcal{H}^{(1)}_\alpha + \left(\frac{P_{\alpha\beta} - \rho c_s^2\delta_{\alpha\beta}}{2c_s^2}\right)\bar{\mathcal{H}}^{(2)}_{\alpha\beta} + \\ & \left(\frac{Q_{\alpha\beta\gamma} - (c_\alpha\delta_{\beta\gamma} + c_\beta\delta_{\alpha\gamma} + c_\gamma\delta_{\beta\alpha})\,c_s^2}{2\sqrt{6}\,c_s^3}\right)\bar{\mathcal{H}}^{(3)}_{\alpha\beta\gamma} + \\ & \left(\frac{R_{xxyy} - (P_{xx}+P_{yy})c_s^2 + \rho c_s^4}{2c_s^4}\right)\mathcal{H}^{(4)}_{xxyy} + \\ & \left(\frac{R_{xyyy} - 3c_s^2P_{xy}}{\sqrt{6}c_s^4}\right)\mathcal{H}^{(4)}_{xyyy} + \left(\frac{R_{yxxx} - 3c_s^2P_{xy}}{\sqrt{6}c_s^4}\right)\mathcal{H}^{(4)}_{yxxx} + \\ & \left(\frac{L_{xxxyy} - 3c_s^2Q_{xyy} - c_s^2Q_{xxx} + 3c_s^4j_x}{\sqrt{12}c_s^5}\right)\mathcal{H}^{(5)}_{x} + \\ & \left(\frac{L_{xxxyy} - 3c_s^2Q_{yxx} - c_s^2Q_{yyy} + 3c_s^4j_y}{\sqrt{12}c_s^5}\right)\mathcal{H}^{(5)}_{y} + \\ & \left(\frac{\psi - 3c_s^2(R_{xxxy} + R_{yyyx}) + 9c_s^4P_{xy}}{6c_s^6}\right)\mathcal{H}^{(6)}\Bigg). \end{aligned} \tag{4.60}$$

So, by evaluating the moment from the inner population, we can write:

$$\mathcal{M}^{+\mathrm{i}} = \mathcal{M}(f^{+\mathrm{i}}) = \sum_{c_{iy}>0} \Psi f_i \qquad , \qquad \mathcal{M}^{-\mathrm{i}} = \mathcal{M}(f^{-\mathrm{i}}) = \sum_{c_{iy}<0} \Psi f_i. \tag{4.61}$$

Similarly, at the boundary condition (outer population), we can write:

$$\mathcal{M}^{\mathrm{o}} = \mathcal{M}^{+\mathrm{o}} + \mathcal{M}^{-\mathrm{o}}, \tag{4.62}$$

$$\mathcal{M}^{+\mathrm{o}} = \sum_{c_{iy}>0} \Psi f_i^{eq}(\rho, U_{\mathrm{wall}}) \qquad , \qquad \mathcal{M}^{-\mathrm{o}} = \sum_{c_{iy}<0} \Psi f_i^{eq}(\rho, U_{\mathrm{wall}}). \tag{4.63}$$

Taking into account (4.57), at the boundary we have:

$$\mathcal{M}\Big|_{y=L/2} = \mathcal{M}^{-\mathrm{o}} + \mathcal{M}^{+\mathrm{i}} \qquad , \qquad \mathcal{M}\Big|_{y=-L/2} = \mathcal{M}^{+\mathrm{o}} + \mathcal{M}^{-\mathrm{i}}. \tag{4.64}$$

Thus, full boundary condition reads:

$$\rho\Big|_{y=\pm L/2} = \rho\Big|_{y=\pm L/2} \pm \frac{a+b}{4\,a\,b}\frac{j_y}{c_s}\Big|_{y=\pm L/2} \mp \frac{(\sqrt{3}-1)(a+b)}{4}\frac{Q_{yyy}-3c_s^2 j_y}{6c_s^3}\Big|_{y=\pm L/2}, \tag{4.65}$$

$$\begin{aligned} j_x\Big|_{y=\pm L/2} &= \frac{j_x+\rho U_{\mathrm{wall}}}{2}\Big|_{y=\pm L/2} \pm \frac{a+b}{4\,a\,b}\frac{P_{xy}}{c_s}\Big|_{y=\pm L/2} \mp \frac{(\sqrt{3}-1)(a+b)}{4}\frac{R_{xyyy}-3c_s^2 P_{xy}}{6c_s^3}\Big|_{y=\pm L/2}, \\ j_y\Big|_{y=\pm L/2} &= \frac{j_y}{2}\Big|_{y=\pm L/2} \mp \frac{(\sqrt{3}-3)(a+b)}{12}\frac{P_{yy}-\rho c_s^2}{2c_s}\Big|_{y=\pm L/2}, \end{aligned} \tag{4.66}$$

$$
\begin{aligned}
P_{xx}\Big|_{y=\pm L/2} &= \frac{P_{xx}+\rho(c_s^2+U_{\rm wall}^2)}{2}\Big|_{y=\pm L/2} \pm \frac{\mu}{6\sqrt{2}}\frac{Q_{yxx}-j_y c_s^2}{2\,c_s}\Big|_{y=\pm L/2} \mp \\
&\qquad \frac{(\sqrt{3}-1)\mu}{8}\frac{L_{yyyxx}-Q_{yxx}c_s^2}{2\,c_s^3}\Big|_{y=\pm L/2}, \\
P_{xy}\Big|_{y=\pm L/2} &= \frac{P_{xy}}{2}\Big|_{y=\pm L/2} \pm \frac{\mu}{4\,a\,b}\,(j_x-U_{\rm wall})c_s\Big|_{y=\pm L/2} \mp \frac{(\sqrt{3}-3)\mu}{12}\frac{Q_{xyy}}{2c_s}\Big|_{y=\pm L/2}, \\
P_{yy}\Big|_{y=\pm L/2} &= \frac{P_{yy}+\rho c_s^2}{2}\Big|_{y=\pm L/2} \pm \frac{(\sqrt{3}-1)\mu}{4}j_y\,c_s\Big|_{y=\pm L/2} \pm \frac{\mu}{3}\frac{Q_{yyy}-3c_s^2 j_y}{2c_s}\Big|_{y=\pm L/2},
\end{aligned}
\tag{4.67}
$$

$$
\begin{aligned}
Q_{xxx}\Big|_{y=\pm L/2} &= \frac{Q_{xxx}+3\rho c_s^2\,U_{\rm wall}}{2}\Big|_{y=\pm L/2} \pm \frac{\mu}{2\sqrt{2}}\frac{R_{xxxy}-3c_s^2P_{xy}}{\sqrt{6}\,c_s}\Big|_{y=\pm L/2} \mp \frac{(\sqrt{3}-1)\mu}{4}\frac{\psi}{6c_s^3}\Big|_{y=\pm L/2}, \\
Q_{yxx}\Big|_{y=\pm L/2} &= \frac{Q_{yxx}}{2}\Big|_{y=\pm L/2} \mp \frac{\mu c_s}{4\sqrt{3}}(c_s^2+U_{\rm wall}^2) \pm \frac{\mu}{4\sqrt{3}}\,P_{xx}c_s\Big|_{y=\pm L/2} \mp \frac{(\sqrt{3}-3)\mu}{12}\frac{R_{xxyy}}{2c_s}\Big|_{y=\pm L/2}, \\
Q_{xyy}\Big|_{y=\pm L/2} &= \frac{Q_{xyy}+\rho c_s^2\,U_{\rm wall}}{2}\Big|_{y=\pm L/2} \pm \frac{(\sqrt{3}-1)\,\mu}{4\sqrt{3}}\,P_{xy}c_s\Big|_{y=\pm L/2} \pm \frac{\mu}{\sqrt{6}}\frac{R_{xyyy}}{\sqrt{6}\,c_s}\Big|_{y=\pm L/2}, \\
Q_{yyy}\Big|_{y=\pm L/2} &= \frac{Q_{yyy}}{2}\Big|_{y=\pm L/2} \mp \frac{\mu}{4}\rho\,c_s^3\Big|_{y=\pm L/2} \pm \frac{\mu}{2}\,P_{yy}c_s\Big|_{y=\pm L/2},
\end{aligned}
\tag{4.68}
$$

$$
\begin{aligned}
R_{yxxx}\Big|_{y=\pm L/2} &= \frac{R_{yxxx}}{2}\Big|_{y=\pm L/2} \mp \frac{3\mu}{4\sqrt{3}} U_{\text{wall}} c_s^3 \pm \frac{\mu}{4\sqrt{3}} Q_{xxx} c_s\Big|_{y=\pm L/2} \pm \frac{(\sqrt{3}-1)\mu}{4} \frac{L_{xxxyy}}{\sqrt{12} c_s^3}\Big|_{y=\pm L/2}, \\
R_{xxyy}\Big|_{y=\pm L/2} &= \frac{R_{xxyy} + \rho c_s^2 (c_s^2 + U_{\text{wall}}^2)}{2}\Big|_{y=\pm L/2} \pm \frac{(3-\sqrt{3})\,\mu}{12}\, Q_{yxx}\Big|_{y=\pm L/2} c_s \pm \frac{\mu}{\sqrt{12}} \frac{L_{xxyyy}}{\sqrt{12}\, c_s}\Big|_{y=\pm L/2}, \\
R_{xyyy}\Big|_{y=\pm L/2} &= \frac{R_{xyyy}}{2}\Big|_{y=\pm L/2} \mp \frac{\mu}{4} U_{\text{wall}} c_s^3 \pm \frac{(\sqrt{3}-1)\mu}{4\sqrt{3}} j_x\, c_s^3\Big|_{y=\pm L/2} \pm \frac{\mu}{4}\, Q_{xyy} c_s\Big|_{y=\pm L/2},
\end{aligned}
\tag{4.69}
$$

$$
\begin{aligned}
L_{yyxxx}\Big|_{y=\pm L/2} &= \frac{L_{yyxxx} + \rho c_s^4\, U_{\text{wall}}}{2}\Big|_{y=\pm L/2} \pm \frac{(\sqrt{3}-1)\mu}{4\sqrt{3}} R_{yxxx} c_s\Big|_{y=\pm L/2} \pm \frac{(\sqrt{3}-3)\mu}{4} \frac{\psi}{6 c_s^3}\Big|_{y=\pm L/2}, \\
L_{xxyyy}\Big|_{y=\pm L/2} &= \frac{L_{xxyyy}}{2}\Big|_{y=\pm L/2} \mp \frac{\mu}{2} \rho U_{\text{wall}}^2 c_s^3 \pm \frac{(3-\sqrt{3})\,\mu}{12}\, R_{xxyy} c_s\Big|_{y=\pm L/2} \pm \frac{\sqrt{3}\mu}{\sqrt{2}} Q_{yxx}\, c_s^3\Big|_{y=\pm L/2}, \\
\psi\Big|_{y=\pm L/2} &= \frac{\psi}{2}\Big|_{y=\pm L/2} \mp \frac{3\sqrt{3}\mu}{4} \rho U_{\text{wall}} c_s^5 \pm \frac{\sqrt{3}\mu}{\sqrt{2}} Q_{xyy}\, c_s^3\Big|_{y=\pm L/2} \pm \frac{\mu}{2}\, L_{xxyyy} c_s\Big|_{y=\pm L/2}.
\end{aligned}
\tag{4.70}
$$

4.5.2 Shear Stress

For shear stress, from Eq.(4.57) we have

$$
P_{xy}\Big|_{y=L/2} = \frac{-\sqrt{3}\,\left(Q_{xyy} - j_x\, c_s^2\right)\Big|_{y=L/2} + \left(1+\sqrt{3}\right)\,\left(Q_{xyy} - \rho\, U_1\, c_s^2\right)\Big|_{y=L/2}}{(a+b)\; c_s}, \tag{4.71}
$$

and

$$P_{xy}\Big|_{y=-L/2} = -\frac{-\sqrt{3}\ (Q_{xyy} - j_x\, c_s^2)\Big|_{y=-L/2} + \left(1+\sqrt{3}\right)\ (Q_{xyy} - \rho\, U_2\, c_s^2)\Big|_{y=-L/2}}{(a+b)\ c_s}. \tag{4.72}$$

By substituting results of P_{xy} and Q_{xyy} from (4.45) and j_x from (4.46) to equation (4.71) and (4.72), we get:

$$P_{xy}(y) = \rho g y + \frac{\sqrt{3}\, A_4\, \sinh\left(\frac{L}{2\,\tau\,\sqrt{3\eta}\,c_s}\right)}{(a+b)\, c_s + \left(1+\sqrt{3}\right)\ \frac{L}{2\,\tau}} - \frac{c_s^2\,\rho}{\frac{(a+b)}{\left(1+\sqrt{3}\right)} c_s + \frac{L}{2\,\tau}}\ \frac{\Delta U}{2}, \tag{4.73}$$

and

$$\begin{aligned} j_x =& \rho\, \frac{U_1+U_2}{2} + \frac{\rho g\, L}{2\, c_s}\frac{a+b}{(1+\sqrt{3})} - \frac{\rho g}{2\nu}\left(y^2 - \frac{L^2}{4}\right) + \frac{2\,\rho\, g\,\tau}{1+\sqrt{3}} + \\ & \frac{A_3}{c_s^2}\ \cosh\left(\frac{y}{\tau\,\sqrt{3\eta}\,c_s}\right) - \frac{A_3\,\sqrt{3}}{c_s^2(1+\sqrt{3})}\ \cosh\left(\frac{L}{2\,\tau\,\sqrt{3\eta}\,c_s}\right) + \\ & \frac{A_4}{c_s^2}\ \sinh\left(\frac{y}{\tau\,\sqrt{3\eta}\,c_s}\right) - \frac{2\,\sqrt{3}\,\frac{A_4}{c_s^2}\ \sinh\left(\frac{L}{2\,\tau\,\sqrt{3\eta}\,c_s}\right)}{2\ (a+b)\ \tau\, c_s + \left(1+\sqrt{3}\right)\ L}\, y + \frac{1}{\frac{a+b}{1+\sqrt{3}}\,\tau\, c_s + \frac{L}{2}}\ \frac{\rho\,\Delta\, U}{2}\, y. \end{aligned} \tag{4.74}$$

with $\Delta U = U_1 - U_2$.

Furthermore, from Eq.(4.57), we have

$$\begin{aligned} (j_x - \rho U_1)\big|_{y=+L/2} &= \frac{-R_{xyyy}\big|_{y=+L/2} + c_s^2(a^2+ab+b^2)P_{xy}\big|_{y=+L/2}}{ab(a+b)\, c_s^3}, \\ (j_x - \rho U_2)\big|_{y=-L/2} &= \frac{R_{xyyy}\big|_{y=-L/2} - c_s^2(a^2+ab+b^2)P_{xy}\big|_{y=-L/2}}{ab(a+b)\, c_s^3}. \end{aligned} \tag{4.75}$$

However, we also have

$$R_{xyyy} = R^{(0)}_{xyyy} + R^{(1)}_{xyyy} = 3c_s^2 P_{xy} + 3c_s^2 \tau\eta\partial_y(c_s^2 j_x - Q_{xyy}). \tag{4.76}$$

Substituting it into the earlier equation we have:

$$\begin{aligned}
(j_x - \rho U_1)\big|_{y=+L/2} &= \frac{-3c_s^2\tau\eta\partial_y(c_s^2\, j_x - Q_{xyy})\big|_{y=+L/2} + c_s^2(a^2+ab+b^2-3)P_{xy}\big|_{y=+L/2}}{ab(a+b)\, c_s^3}, \\
(j_x - \rho U_2)\big|_{y=-L/2} &= \frac{3c_s^2\tau\eta\partial_y(c_s^2\, j_x - Q_{xyy})\big|_{y=-L/2} - c_s^2(a^2+ab+b^2-3)P_{xy}\big|_{y=-L/2}}{ab(a+b)\, c_s^3}.
\end{aligned} \tag{4.77}$$

Recall,

$$\tau\, c_s\, \sqrt{3\eta}\, \partial_y(c_s^2\, j_x - Q_{xyy}) = A_3 \sinh\left(\frac{y}{\tau\sqrt{3\eta}c_s}\right) + A_4 \cosh\left(\frac{y}{\tau\sqrt{3\eta}c_s}\right). \tag{4.78}$$

Thus we have,

$$\begin{aligned}
(j_x\, c_s^2 - \rho\, c_s^2\, U_1)\big|_{y=+L/2} = \frac{1}{ab(a+b)}\Bigg(&-\sqrt{3\eta}\left(A_3 \sinh\left(\frac{L}{2\tau\sqrt{3\eta}c_s}\right) + A_4 \cosh\left(\frac{L}{2\tau\sqrt{3\eta}c_s}\right)\right) + \\
&c_s(a^2+ab+b^2-3)P_{xy}\big|_{y=+L/2}\Bigg), \\
(j_x\, c_s^2 - \rho\, c_s^2\, U_2)\big|_{y=-L/2} = \frac{1}{ab(a+b)}\Bigg(&\sqrt{3\eta}\left(-A_3 \sinh\left(\frac{L}{2\tau\sqrt{3\eta}c_s}\right) + A_4 \cosh\left(\frac{L}{2\tau\sqrt{3\eta}c_s}\right)\right) - \\
&c_s(a^2+ab+b^2-3)P_{xy}\big|_{y=-L/2}\Bigg).
\end{aligned} \tag{4.79}$$

or,

$$c_s^2\left(j_x\big|_{y=L/2}+j_x\big|_{y=-L/2}\right)-\rho\,c_s^2\,(U_1+U_2)=\frac{-2\sqrt{\eta}\,A_3\sinh\left(\frac{1}{2\sqrt{\eta}\mathrm{Kn}}\right)+\rho\,g\,L\,c_s\,(1+\sqrt{3})}{(a+b)},$$

$$c_s^2\left(j_x\big|_{y=L/2}-j_x\big|_{y=-L/2}\right)-\rho\,c_s^2\,(U_1-U_2)=\frac{-2\sqrt{\eta}\,A_4\cosh\left(\frac{1}{2\sqrt{\eta}\,\mathrm{Kn}}\right)}{(a+b)}+\frac{2\,A_4\,\sinh\left(\frac{1}{2\sqrt{\eta}\,\mathrm{Kn}}\right)-\rho\,c_s^2\,\Delta\,U\frac{(a+b)^2}{6}}{\frac{4}{a+b}\mathrm{Kn}+1}\frac{2\,\mathrm{Kn}}{a+b}.\tag{4.80}$$

where Knudsen number is defined as

$$\mathrm{Kn}=\frac{\sqrt{3}\,\tau c_s}{L}.\tag{4.81}$$

Using Eq.(4.74)

$$c_s^2\left(j_x\big|_{y=L/2}+j_x\big|_{y=-L/2}-\rho\,(U_1+U_2)\right)=\frac{2}{(1+\sqrt{3})}\,A_3\,\cosh\left(\frac{1}{2\,\mathrm{Kn}\,\sqrt{\eta}}\right)+\rho g L\frac{a+b}{(1+\sqrt{3})}c_s+\frac{4\,\rho\,g\,\tau c_s^2}{1+\sqrt{3}},$$

$$c_s^2\left(j_x\big|_{y=L/2}-j_x\big|_{y=-L/2}-\rho\,(U_1-U_2)\right)=-\frac{2\mathrm{Kn}}{\mathrm{Kn}+\frac{a+b}{4}}\,\rho\,c_s^2\frac{\Delta U}{2}+2\left(A_4\,\sinh\left(\frac{1}{2\,\mathrm{Kn}\,\sqrt{\eta}}\right)\frac{\frac{4}{a+b}\mathrm{Kn}+\frac{1}{1+\sqrt{3}}}{\frac{4}{a+b}\mathrm{Kn}+1}\right),\tag{4.82}$$

which gives

$$
\begin{aligned}
A_3 &= -\frac{\rho\, g\, L\, c_s\, \left(1+\mathrm{Kn}\,\frac{2\mu}{a\,b}\right)}{\mu\,\cosh\left(\frac{1}{2\,\mathrm{Kn}\,\sqrt{\eta}}\right)+\frac{\mu^2}{2\,a\,b}\,\sqrt{\eta}\,\sinh\left(\frac{1}{2\,\mathrm{Kn}\,\sqrt{\eta}}\right)},\\
A_4 &= \frac{\rho\, c_s^2\,\Delta\, U}{\left(\mu+\frac{\mu^2}{4\,\mathrm{Kn}}\right)\sqrt{\eta}\,\cosh\left(\frac{1}{2\,\sqrt{\eta}\,\mathrm{Kn}}\right)+\sinh\left(\frac{1}{2\,\mathrm{Kn}\,\sqrt{\eta}}\right)\left(\frac{\mu^2}{2}+\frac{ab\,\mu}{2\,\mathrm{Kn}}\right)},
\end{aligned}
\tag{4.83}
$$

where $\mu = a + b$.

So using Eq.(4.73), we have:

$$
\frac{P_{xy}(y)}{\rho c_s^2} = \frac{g}{c_s^2}\,y - \frac{\Delta\, U}{L}\,\frac{\tau}{\Theta},
\tag{4.84}
$$

where:

$$
\Theta = 1 + 4\,\mathrm{Kn}\,\frac{\sqrt{\eta}\,\cosh\left(\frac{1}{2\,\sqrt{\eta}\,\mathrm{Kn}}\right)+\frac{\mu}{2}\,\sinh\left(\frac{1}{2\,\mathrm{Kn}\,\sqrt{\eta}}\right)}{\mu\,\sqrt{\eta}\,\cosh\left(\frac{1}{2\,\sqrt{\eta}\,\mathrm{Kn}}\right)+\sinh\left(\frac{1}{2\,\mathrm{Kn}\,\sqrt{\eta}}\right)2\,ab}.
\tag{4.85}
$$

Using Eq.(4.74), we have

$$
\begin{aligned}
u_x = \frac{U_1+U_2}{2} + \frac{y}{\Theta}\,\frac{\Delta\, U}{L} + \frac{g\, L}{c_s}\,\frac{a\,b}{\mu} - \frac{g}{2\nu}\left(y^2-\frac{L^2}{4}\right) + \frac{2\,g\,\tau}{1+\sqrt{3}} + \\
\frac{\Delta\, U}{\left(\mu+\frac{\mu^2}{4\,\mathrm{Kn}}\right)\sqrt{\eta}\,\cosh\left(\frac{1}{2\,\sqrt{\eta}\,\mathrm{Kn}}\right)+\sinh\left(\frac{1}{2\,\mathrm{Kn}\,\sqrt{\eta}}\right)\left(\frac{\mu^2}{2}+\frac{ab\,\mu}{2\,\mathrm{Kn}}\right)}\,\sinh\left(\frac{y}{L\,\mathrm{Kn}\,\sqrt{\eta}}\right) - \\
\frac{\frac{g\,L}{c_s}\left(1+\mathrm{Kn}\,\frac{2\mu}{a\,b}\right)}{\mu\,\cosh\left(\frac{1}{2\,\mathrm{Kn}\,\sqrt{\eta}}\right)+\frac{\mu^2}{2\,a\,b}\,\sqrt{\eta}\,\sinh\left(\frac{1}{2\,\mathrm{Kn}\,\sqrt{\eta}}\right)}\left(\cosh\left(\frac{y}{L\,\mathrm{Kn}\,\sqrt{\eta}}\right)-\frac{6}{\mu^2}\,\cosh\left(\frac{1}{2\,\mathrm{Kn}\,\sqrt{\eta}}\right)\right).
\end{aligned}
\tag{4.86}
$$

4.6 Shear Stress

4.6.1 Comments on limit of stress

In the case of $g = 0$, we have

$$\frac{P_{xy}(y)}{\rho c_s^2} = -\frac{\Delta U}{L}\frac{\tau}{\Theta}, \tag{4.87}$$

where Θ is already defined in (4.85). At very large Knudsen number, we have

$$-\frac{P_{xy}^{\infty}(y)}{\rho\,\Delta U\,c_s} = \lim_{\mathrm{Kn}\to\infty}\frac{1}{\sqrt{3}}\frac{\mathrm{Kn}}{\Theta} = \frac{\mu}{4\sqrt{3}}. \tag{4.88}$$

Adjusting the speed of sound, c_s to the definition used in Willis [40], we have:

$$-\frac{P_{xy}^{\infty}(y)}{\rho\,\Delta U\sqrt{\frac{k_B T_0}{2\pi m}}} = \frac{\mu\sqrt{2\pi}}{4\sqrt{3}} = \frac{\mu}{2}\sqrt{\frac{\pi}{6}} \approx 1.113. \tag{4.89}$$

Note that this limit is independent from the choice of η, which suggests that the hydrodynamic limit is actually inherent in the choice of the model.

4.6.2 Analysis on non-dimensional velocity gradient on the centerline

Again recall,

$$\frac{P_{xy}(y)}{\rho c_s^2} = -\frac{\Delta U}{L}\frac{\tau}{\Theta}. \tag{4.90}$$

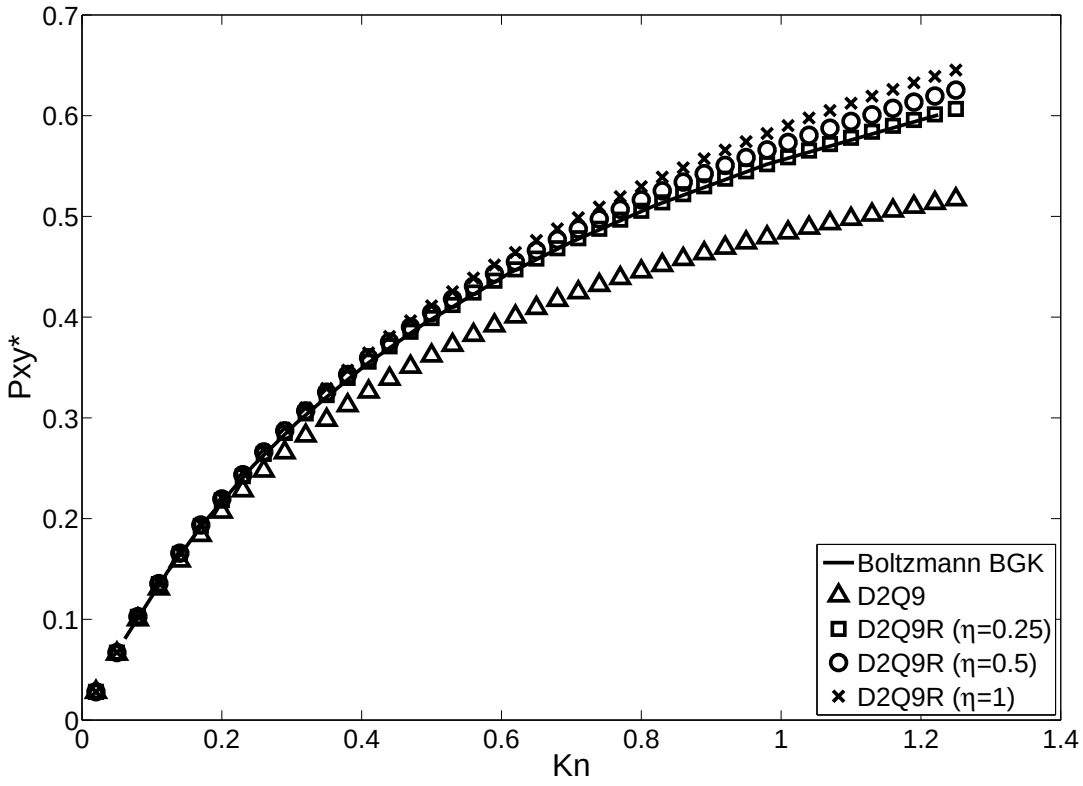

Figure 4.3: Shear stress versus Knudsen numbers for the Couette flow. Normalized function $P^*_{xy} = \frac{P_{xy}}{P^\infty_{xy}}$ is plotted, where P^∞_{xy} is the shear stress at Kn $\to \infty$ of the Boltzmann-BGK model.

The shear stress in the present model is purely Newtonian and satisfies a relation:

$$P_{xy} = -\rho\,\nu\,\frac{\partial u_x}{\partial y}, \tag{4.91}$$

However, what is non-trivial is the velocity gradient itself. The Navier-Stokes equation with no-slip boundary condition predicts that the velocity gradient is independent of the Knudsen number. However, we know from the numerical solutions of the linearized Bolztmann equation and DSMC simulations that this is not the case. A comparison

with $D2Q9$ model is possible by introducing a non-dimensional velocity gradient W at the center-line as

$$W = 1 - (U_2 - U_1) \left. \frac{\partial u_x}{\partial (y/L)} \right|_{y=0}, \tag{4.92}$$

which can be evaluated for the present model as,

$$W = 1 - \frac{1}{\Theta} = \frac{\Theta - 1}{\Theta}. \tag{4.93}$$

For $D2Q9$, we have:

$$W = \frac{2\,\mathrm{Kn}}{(2\,\mathrm{Kn} + 1)}, \tag{4.94}$$

and for $D2Q16$, we have:

$$W = \frac{4\,\mathrm{Kn}\,\frac{\sqrt{\eta}\,\cosh\left(\frac{1}{2\sqrt{\eta}\,\mathrm{Kn}}\right) + \frac{\mu}{2}\sinh\left(\frac{1}{2\,\mathrm{Kn}\sqrt{\eta}}\right)}{\mu\sqrt{\eta}\,\cosh\left(\frac{1}{2\sqrt{\eta}\,\mathrm{Kn}}\right) + \sinh\left(\frac{1}{2\,\mathrm{Kn}\sqrt{\eta}}\right) 2\,ab}}{1 + 4\,\mathrm{Kn}\,\frac{\sqrt{\eta}\,\cosh\left(\frac{1}{2\sqrt{\eta}\,\mathrm{Kn}}\right) + \frac{\mu}{2}\sinh\left(\frac{1}{2\,\mathrm{Kn}\sqrt{\eta}}\right)}{\mu\sqrt{\eta}\,\cosh\left(\frac{1}{2\sqrt{\eta}\,\mathrm{Kn}}\right) + \sinh\left(\frac{1}{2\,\mathrm{Kn}\sqrt{\eta}}\right) 2\,ab}}. \tag{4.95}$$

In Table 4.2, the $D2Q9$ model and $D2Q16$ model are compared against data for the linearized Boltzmann-BGK equation [40]. It can be seen from Table 4.2 that for $D2Q9$ in the slip-flow regime error with respect to the Boltzmann-BGK equation is around 20%,

while for the transitional flow it is around 30%. For $D2Q16$ model with $\eta = 1$, error in the slip-flow regime is less than 6%, while for the transitional flow is less than 15%. Clearly we can see that $D2Q16$ gives much better agreement with Boltzmann-BGK at slip-flow regime as well as at transitional flow regime. The significant reduction in error therefore supports the claim of convergence of LBM solution towards the continuous Boltzmann equation solution.

Table 4.1: Value of deviation of non-dimensional velocity gradient from Navier-Stokes value for the $D2Q9$ and $D2Q9R$ model with varying η.

Kn	Boltzmann-BGK	$D2Q9$	$D2Q9R$ ($\eta = 1$)	$D2Q9R$ ($\eta = 0.5$)	$D2Q9R$ ($\eta = 0.25$)
0.06124	0.09134	0.10911	0.08681	0.08886	0.09131
0.12247	0.1648	0.19675	0.15974	0.16321	0.16733
0.17496	0.2136	0.25922	0.21350	0.21791	0.22305
0.24495	0.2664	0.32881	0.27497	0.28054	0.28669
0.30619	0.3041	0.37979	0.32089	0.32748	0.33439
0.61327	0.4290	0.55087	0.48002	0.49046	0.50079
0.81649	0.4821	0.62020	0.54742	0.55876	0.57067
1.22474	0.5556	0.71010	0.63890	0.64994	0.66314

Table 4.2: Percentage error of the value of deviation of non-dimensional velocity gradient from Navier-Stokes value for the $D2Q9$ and $D2Q9$ renormalized model with varying η relative to Boltzmann-BGK value.

Kn	$D2Q9$	$D2Q9R$ ($\eta = 1$)	$D2Q9R$ ($\eta = 0.5$)	$D2Q9R$ ($\eta = 0.25$)
0.06124	19.45	4.95	2.71	0.03
0.12247	19.39	3.07	0.97	1.54
0.17496	21.36	0.05	2.02	4.42
0.24495	23.43	3.22	5.31	7.62
0.30619	24.89	5.52	7.69	9.96
0.61327	28.41	11.89	14.33	16.73
0.81649	28.64	13.55	15.90	18.37
1.22474	27.81	14.99	16.98	19.36

4.7 Slip Model

4.7.1 Velocity profile

Solving (4.45) and (4.46), we find the solution for the x-component of the velocity $u_x = j_x/\rho$:

$$u_x = \frac{U_1+U_2}{2} + \frac{y}{\Theta}\frac{\Delta U}{L} + \frac{g\,L^2}{2\tau\,c_s^2}\left[-\left(\frac{y}{L}-\frac{1}{2}\right)\left(\frac{y}{L}+\frac{1}{2}\right) + \frac{2}{\mu}\mathrm{Kn} + \frac{4}{3+3\sqrt{3}}\mathrm{Kn}^2\right] + \frac{\Delta U}{\left(\mu+\frac{\mu^2}{4\,\mathrm{Kn}}\right)\sqrt{\eta}\,\cosh\left(\frac{1}{2\sqrt{\eta}\,\mathrm{Kn}}\right)+\sinh\left(\frac{1}{2\,\mathrm{Kn}\sqrt{\eta}}\right)\left(\frac{\mu^2}{2}+\frac{ab\,\mu}{2\,\mathrm{Kn}}\right)}\sinh\left(\frac{y}{L\,\mathrm{Kn}\sqrt{\eta}}\right) + \frac{g\,L^2}{2\tau\,c_s^2}\left[-\frac{\frac{2}{\sqrt{3}}\mathrm{Kn}\left(1+\mathrm{Kn}\,\frac{2\mu}{\sqrt{3}}\right)\left(\cosh\left(\frac{y}{L\,\mathrm{Kn}\sqrt{\eta}}\right)-\frac{6}{\mu^2}\,\cosh\left(\frac{1}{2\,\mathrm{Kn}\sqrt{\eta}}\right)\right)}{\mu\,\cosh\left(\frac{1}{2\,\mathrm{Kn}\sqrt{\eta}}\right)+\frac{\mu^2}{2\,a\,b}\sqrt{\eta}\,\sinh\left(\frac{1}{2\,\mathrm{Kn}\sqrt{\eta}}\right)}\right]. \tag{4.96}$$

Note the similarity with the result obtained earlier from $D2Q9$ model, but with the additional hyperbolic function.

4.7.2 Flow Rate

Another important characteristics of the slip models is the ability to predicting a non-monotonic dependence of the mass flow rate in the Poiseuille flow on the Knudsen number (so-called Knudsen minimum problem). The flow rate Q is defined as

$$Q = \int_{y=-L/2}^{y=L/2} u_x\,dy. \tag{4.97}$$

Assuming Poiseuille flow condition $U_1 = U_2 = 0$ in the general solution (4.96), and taking into account the relation between the Knudsen number and shear viscosity,

$$\nu = \mathrm{Kn}\frac{c_\mathrm{s} L}{\sqrt{3}}, \tag{4.98}$$

we find the flow rate for the current model as follows:

$$\begin{aligned} Q = {} & \frac{\sqrt{3} g L^2}{2\, c_\mathrm{s}} \left(\frac{1}{6\,\mathrm{Kn}} + \frac{2}{\mu} + \frac{4}{3+3\sqrt{3}}\,\mathrm{Kn} \right) - \\ & \frac{\sqrt{3} g L^2}{2\, c_\mathrm{s}} \left(\frac{\frac{2}{\sqrt{3}} \left(1 + \mathrm{Kn}\,\frac{2\mu}{\sqrt{3}}\right) \left(2\mathrm{Kn}\sqrt{\eta}\,\sinh\left(\frac{1}{2\,\mathrm{Kn}\,\sqrt{\eta}}\right) - \frac{6}{\mu^2}\,\cosh\left(\frac{1}{2\,\mathrm{Kn}\,\sqrt{\eta}}\right)\right)}{\mu\,\cosh\left(\frac{1}{2\,\mathrm{Kn}\,\sqrt{\eta}}\right) + \frac{\mu^2}{2\,a\,b}\,\sqrt{\eta}\,\sinh\left(\frac{1}{2\,\mathrm{Kn}\,\sqrt{\eta}}\right)} \right). \end{aligned} \tag{4.99}$$

In the continuum limit (i.e. $\mathrm{Kn} \to 0$), we can see that the solution asymptotically approaches the Navier-Stokes solution,

$$Q_\mathrm{NS} = \frac{\sqrt{3} g L^2}{12\, c_\mathrm{s}} \frac{1}{\mathrm{Kn}}. \tag{4.100}$$

By defining $\hat{Q} = \frac{2 c_s}{\sqrt{2} g L^2}\, Q$ and $\hat{\mathrm{Kn}} = \sqrt{\frac{2}{3}}\,\mathrm{Kn}$, we obtain:

$$\begin{aligned} Q = {} & \frac{1}{6\hat{\mathrm{Kn}}} + \frac{\sqrt{6}}{\mu} + \frac{6}{3+3\sqrt{3}}\,\hat{\mathrm{Kn}} - \\ & \frac{\sqrt{2}\,\left(1 + \sqrt{2}\mu\,\hat{\mathrm{Kn}}\right)\left(\sqrt{6}\hat{\mathrm{Kn}}\sqrt{\eta}\,\sinh\left(\frac{1}{\hat{\mathrm{Kn}}\sqrt{6\eta}}\right) - \frac{6}{\mu^2}\,\cosh\left(\frac{1}{\hat{\mathrm{Kn}}\sqrt{6\eta}}\right)\right)}{\mu\,\cosh\left(\frac{1}{\hat{\mathrm{Kn}}\sqrt{6\eta}}\right) + \frac{\mu^2}{2\,a\,b}\,\sqrt{\eta}\,\sinh\left(\frac{1}{\hat{\mathrm{Kn}}\sqrt{6\eta}}\right)}. \end{aligned} \tag{4.101}$$

which on the limit of $\hat{\mathrm{Kn}} \to 0$ (ignoring terms higher than $\mathcal{O}(\mathrm{Kn})$), with $\eta = 1$, gives

us:

$$\begin{aligned}\lim_{\hat{\mathrm{Kn}}\to 0}\hat{Q} &= \frac{1}{6\hat{\mathrm{Kn}}}+\sqrt{\frac{9}{2}+\sqrt{3}-6\sqrt{3+\sqrt{3}}}+2\left(4+\sqrt{3}-\sqrt{6(3+\sqrt{3})}\right)\hat{\mathrm{Kn}},\\ \lim_{\hat{\mathrm{Kn}}\to 0}\hat{Q} &= \frac{1}{6\hat{\mathrm{Kn}}}+0.9506+0.8072\hat{\mathrm{Kn}}.\end{aligned} \tag{4.102}$$

On the other hand, limit of $\hat{\mathrm{Kn}}\to\infty$, with constant η, gives us:

$$\lim_{\hat{\mathrm{Kn}}\to\infty}\hat{Q}=\frac{\sqrt{27+\sqrt{3}}}{6}\approx 0.893371. \tag{4.103}$$

Thus, for any constant η, the expansion is no longer growing linearly in Kn as $\mathrm{Kn}\to\infty$, but in fact it is constant and approaching the number 0.89. Choice of η (as long as it is independent from Kn) will not affect the limit of the Q at infinite Knudsen number. We may observe a local Knudsen minima at certain range of η, however, the global minimum will only exist at limit Kn number approaching infinity. Thus, despite its ability to describe physically relevant Knudsen layers in the velocity profile, this model failed to capture the Knudsen paradox in the global sense as at infinite-Kn we have a finite Q.

4.8 Higher Order Moments

4.8.1 Third and Fourth Order Moments

In the present model, none of the third order moment (which are related to the energy flux) have independent dynamics. They are slaved by the dynamics of the lower-order

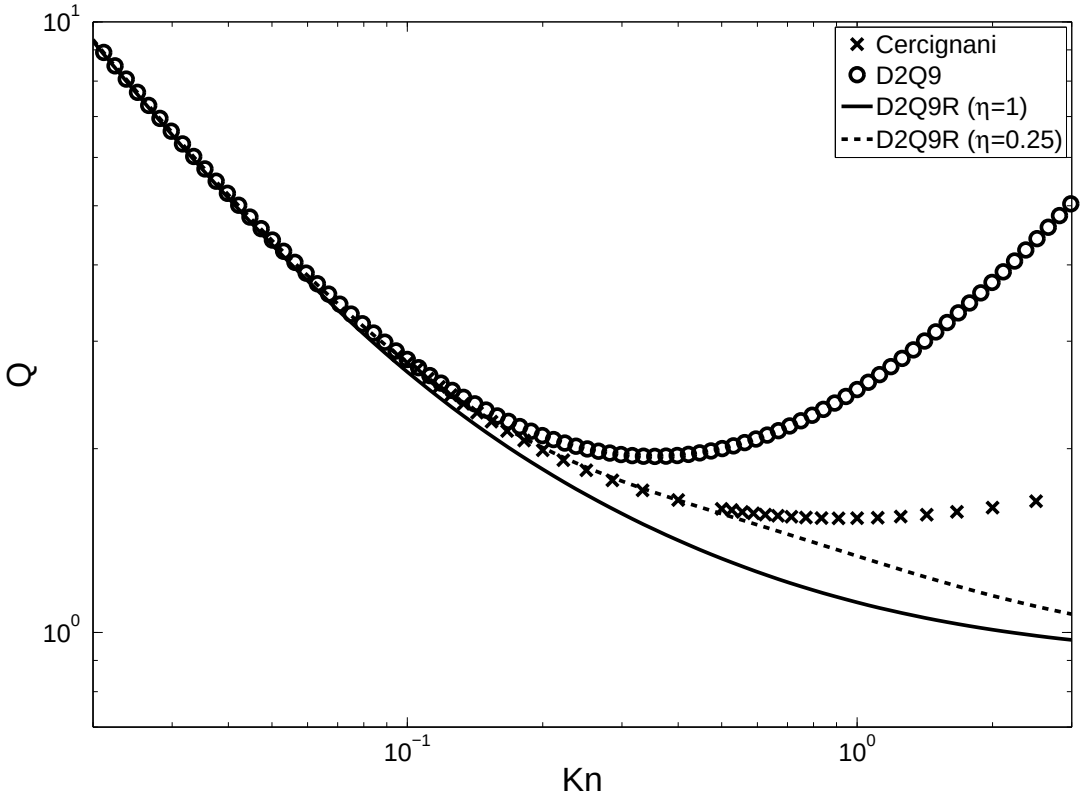

Figure 4.4: Normalized flow rate versus Knudsen numbers for the Poiseuille flow. Flow rate is normalized in such a way that $Q^*_{NS} = \frac{1}{6\mathrm{Kn}}$. $\eta = 0.25$ gives good agreement with Cercignani's data up to $\mathrm{Kn} \approx 1$

.

moments. This is not surprising as the dynamics considered here is essentially isothermal. In particular, we have already seen that one of third order moment Q_{xyy} (4.45) is such that

$$Q_{xyy} = c_s^2 \, (j_x - 2\rho \, g \, \tau), \tag{4.104}$$

that is, the longitudinal energy flux Q^{neq}_{xyy} reads,

$$Q^{\mathrm{neq}}_{xyy} = -2 \, c_s^2 \, \rho \, g \, \tau. \tag{4.105}$$

On the other hand, for the transversal energy flux, we have while using (3.27),

$$Q_{yxx}^{\mathrm{neq}} = -\tau\, \partial_y R_{xxyy}. \tag{4.106}$$

Furthermore, we now have,

$$R_{xxyy}^{\mathrm{neq}} = 3\, c_s^2\, \mathcal{N}^{\mathrm{neq}} + \tau\, \left(\phi_6 - 3\, c_s^2\, \phi_1\right), \tag{4.107}$$

which means that the transversal energy flux is completely determined from the knowledge of the non-equilibrium part of the normal stress difference.

4.9 Discussion

In this study, we introduce the $D2Q16$ model and the renormalization of the model to a more compact $D2Q9$-like form. We thus manage to obtain a modified $D2Q9$ moment chain which has the same dynamics as the $D2Q16$. Consequently, this methodology allows a simulation using the velocity set from $D2Q9$ system while obtaining the result of higher LB model (in this case $D2Q16$).

The velocity profile for $D2Q16$ model is quite similar to the result obtained from $D2Q9$ LB model earlier, but we observe an additional hyperbolic function, which is characteristic of a Knudsen layer. However, the Knudsen minima effect does not appear at a finite Knudsen number as expected. Rather, the flowrate keep decreasing as the Knudsen number increase and asymptotically approaches a constant number (≈ 0.89)

at a very large Knudsen number. Also, for any constant η, the expansion is no longer growing linearly in Kn as Kn $\to \infty$. Choice of η (as long as it is independent from Kn) will not affect the limit of the Q at infinite Knudsen number. Thus, despite its ability to describe physically relevant Knudsen layers in the velocity profile, this model failed to properly capture the Knudsen paradox.

In the next Chapter, we are trying to recover both Knudsen layer and Knudsen paradox effect by trying to group the velocities into shells based on their symmetrical properties. From these building blocks, we then introduce additional degree of freedom whereby the energy level of each shells are independent to each other. However, the additional degree of freedom should still be consistent with the equilibrium constraints. The resultant LB model is expected to not only to recover both Knudsen layer and Knudsen minima, but also reached sixth order accuracy and Galilean Invariance.

Chapter 5

Higher Order Galilean Invariant Lattice Boltzmann Method

5.1 Introduction

Galilean invariant hydrodynamics for the one-dimensional LB model is possible with the minimum of 4 velocities, provided they are chosen using the route of Gauss-Hermite quadrature [12]. Recently it was shown that a rational number approximation of the model allows an on-lattice model with the same accuracy [22]. This agrees with the usual understanding that the Gauss-Hermite quadrature is optimal in one-dimension [11, 12]. A remarkable result was obtained in Ref [23, 21], where it was shown that in three dimension it is possible to construct an on-lattice model with the Galilean invariant hydrodynamics with a velocity set of just 41 members . On the other hand,

[1]Parts of this chapter were published in Physical Review E.

taking tensor products of the one-dimensional Gauss-Hermite quadrature velocity set requires a velocity set of 64 members [12]. This result demonstrated that in the multi-dimensional case, taking the tensor multiplication of the Gauss-Hermite quadrature is sub-optimal. Indeed, a similar result is already known for lower order LB models too. In the case of lower order models (accurate up to the third order in Mach number), while the Gauss-Hermite route requires 27 velocity model [12] in three dimensions, two subsets of this velocity set with either 15 or 19 are sufficient to construct models with same accuracy in hydrodynamic limit. This particular observation that the Gauss-Hermite quadrature route is sub-optimal for the construction of the LB models, is the starting point for the current work.

We suggests an alternative framework to create discrete velocity set that is optimal, or at least better than existing scheme with the same number of discrete velocities. In this framework, the entropic formulation of the LB method can be naturally extended to obtain a discrete velocity set with a given accuracy. Here, we will derive a 27-velocity LB model with the Galilean invariant hydrodynamic limit. This is a huge improvement over the Gauss-Hermite quadrature or its rational approximation. The current method of constructing the LB models can be extended to arbitrary accuracy, as it is quite general in nature. Although the present framework can be understood as an efficient generalization of the traditional Gauss-Hermite quadrature, the optimality of the new quadrature yet to be proven. However, we believe that the efficiency of the current quadrature will be very useful for other numerical methods other than the LB model too, which uses multi-dimensional Gauss-Hermite quadrature.

This chapter is organized as follows: In section 5.2 a brief review of the LB method is presented. In section 5.3, a new construction framework for deriving the entropic LB models with arbitrary accuracy and the relevant H-function is presented. In section 5.4, a 27-velocity LB model with the sixth order accuracy is derived using the new framework. In section 5.5, an appropriate equilibrium distribution for the discrete velocity model is derived. In section 5.6, the moment representation of the kinetic equation is presented. In section 5.7, the hydrodynamic limit of the discrete velocity model is derived to show that the Galilean invariant hydrodynamics is recovered. In section 5.8, the formal solution for the case of the unidirectional stationary flow is presented and the diffusive boundary condition is used to obtain an explicit solution for the pressure driven and the Couette flow. These results are analyzed further in the section 5.9 and 5.10. An illustrative numerical example has been presented in section 5.11

5.2 Lattice Boltzmann method

Discrete velocity models are often used in the kinetic theory of gases to describe the propagation of shock waves [44]. Motivated by the search for the computationally effective microscopic schemes for the hydrodynamics, the concept of discrete kinetic modeling was revived in Ref [45]. In this pioneer work, it was shown that indeed a simple discrete kinetic model on lattice can describe the Navier-Stokes hydrodynamics in appropriate limits. The key new idea was to provide a reduced description of the

molecular motion, sufficient to describe the hydrodynamics at desired length scales, by considering pseudo-particle dynamics, where particles are constrained to move along some fixed discrete direction only. This concept was refined further in Ref [4, 1, 5] to obtain the LB model, a viable hydrodynamic simulation tool for the Navier-Stokes equations. In its typical formulation, one works with a set of discrete populations $f = \{f_i\}$ corresponding to the predefined discrete velocities $\mathbf{c}_i$ $(i = 1, \cdots, N)$ to represent the system. For this set of discrete populations, the evolution equation is often written in the BGK-form [37] as

$$f_i\left(\mathbf{x} + \mathbf{c}\,\Delta t, t + \Delta t\right) = f_i\left(\mathbf{x}, t\right) + 2\,\beta\,\left(f_i^{\mathrm{eq}}\left(f\left(\mathbf{x}, t\right)\right) - f_i\left(\mathbf{x}, t\right)\right), \tag{5.1}$$

where β denotes the discrete relaxation time and f_i^{eq}, a functional of f, is chosen in such a way that the correct hydrodynamic limit is recovered.

In the last few years, a lot of attention was paid on the construction of the appropriate equilibrium distribution in the discrete case. It was shown that it is possible to construct discrete analog of the Maxwell-Boltzmann distribution by proper choice of the H-function (a necessity to ensure thermodynamic consistency) [30, 31, 29, 28, 27, 10, 12]. As this extension, broadly known as the entropic LB method, is a generalization of the usual LB method, we will not distinguish between the two formulations in the present discussion but present the result for entropic formulations only.

Another crucial ingredient in LB modeling is the choice of the set of discrete velocities itself. An important progress was made in Ref [24, 25, 11], where it was shown that

the LB method is an approximate technique for solving the Boltzmann BGK equation in the low Mach number limit. These works showed that it is sufficient to consider the discrete velocity BGK model

$$\partial_t f_i + c_{i\alpha}\partial_\alpha f_i = -\frac{1}{\tau}\left(f_i - f_i^{eq}(f)\right), \tag{5.2}$$

where τ is the relaxation time and the set of discrete velocities are chosen as the root of Hermite polynomials and a low Mach number expansion of the Maxwell-Boltzmann distribution evaluated at the node of quadrature is used as discrete equilibrium f_i^{eq}. However, the problem with this approach was that one cannot ensure positivity of the f_i^{eq}. In order to fix this deficiency, the framework was later generalized to get the entropic LB method [10, 12], where it was shown that it is sufficient to consider the discretize the continuous H-function using the Gauss-Hermite quadrature as

$$H = \sum_{i=1}^{N} f_i \left(\ln\left(\frac{f_i}{w_i}\right) - 1\right), \tag{5.3}$$

with w_i as weights associated with quadrature and f_i^{eq} as minimum of this H-function under the constraint of the local conservation. For example in the case of isothermal hydrodynamics, we have conservation law for the mass density ρ and the momentum density J_α defined as

$$\rho = \sum_{i=1}^{N} f_i, \qquad J_\alpha = \sum_{i=1}^{N} f_i c_{i\alpha}. \tag{5.4}$$

So, in this case the equilibrium can be obtained as minimizer of the H-function (Eq.5.3) under the constraint of the fixed mass and the momentum density (Eq.5.4). An explicit solution of this minimization problem for the commonly used lattices of the LB method is presented in Ref [10]. This approach was generalized further in Ref [22], where it was shown that the rational number approximation of the model allows an on-lattice model with the same accuracy albeit with increased number of discrete velocities. Later, in Ref [23, 21], it was shown that in the multi-dimensional case number of discrete velocities can be drastically reduced by considering only a subset of the set of discrete velocities generated via the tensor product of the desired one dimensional set. These results suggest that the route of three dimensional lattices as a tensor product of one dimensional lattices is far from being optimal. Although it is possible to construct a reduced set by pruning of tensor product lattice [23, 21], it is not obvious that this route is optimal. In the subsequent sections, we will demonstrate that it is possible to create a desired velocity set entirely from multi-dimensional considerations and such a route leads to a discrete velocity set with much reduced number of discrete velocities.

5.3 Entropic Quadrature Method

In this section, we propose a set of ansatz needed to construct a discrete velocity set equipped with H-function directly in multi-dimensional case. These ansatz should be understood as culmination of the set of the rules developed to derive the entropic LB method [46, 30, 31, 29, 27, 28, 12, 10, 22, 23, 21, 47]. Before discussing these ansatz, it

is important to define a few higher order moments similar to Grad type moment system [26]. We now define relevant second, third and fourth order moment as

$$\begin{aligned}
\sigma_{\alpha\beta} &= \sum_{i=1}^{N} f_i \left(c_{i\alpha} c_{i\beta} - \frac{k_{\mathrm{B}}\, T_0}{m} \delta_{\alpha\beta} \right), \\
\hat{Q}_{\alpha\beta\gamma} &= \sum_{i=1}^{N} f_i \left\{ c_{i\alpha} c_{i\beta} c_{i\gamma} - \frac{k_{\mathrm{B}}\, T_0}{m} \left(\delta_{\alpha\beta} c_{i\gamma} + \delta_{\alpha\gamma} c_{i\beta\gamma} + \delta_{\beta} c_{i\alpha} \right) \right\}, \\
\hat{R}_{\alpha\beta\gamma\theta} &= \sum_{i=1}^{N} f_i \Bigg\{ c_{i\alpha} c_{i\beta} c_{i\gamma} c_{i\theta} + \left(\frac{k_{\mathrm{B}}\, T_0}{m} \right)^2 \left(\delta_{\alpha\beta}\delta_{\gamma\theta} + \delta_{\theta\alpha}\delta_{\gamma\beta} + \delta_{\theta\beta}\delta_{\gamma\alpha} \right) \\
&\quad - \frac{k_{\mathrm{B}}\, T_0}{m} \left(c_{i\alpha} c_{i\beta} \delta_{\gamma\theta} + c_{i\alpha} c_{i\theta} \delta_{\gamma\beta} + c_{i\alpha} c_{i\gamma} \delta_{\beta\theta} + c_{i\beta} c_{i\theta} \delta_{\gamma\alpha} + c_{i\beta} c_{i\gamma} \delta_{\theta\alpha} + c_{i\gamma} c_{i\theta} \delta_{\beta\alpha} \right) \Bigg\}.
\end{aligned} \tag{5.5}$$

It is often convenient to work with reduced fourth order moment defined as

$$\hat{R}_{\alpha\beta} = \sum_{i=1}^{N} f_i \left\{ c_i^2 \left(c_{i\alpha} c_{i\beta} - \frac{k_{\mathrm{B}}\, T_0}{m} \delta_{\alpha\beta} \right) + 5 \left(\frac{k_{\mathrm{B}}\, T_0}{m} \right)^2 \delta_{\alpha\beta} - \frac{7\, k_{\mathrm{B}}\, T_0}{m} c_{i\alpha} c_{i\beta} \right\}. \tag{5.6}$$

Finally, we present the necessary set of ansatz as:

1. **Condition on Equilibrium Moments:** Ideally, we would like that the equilibrium values of the second order moment $\sigma_{\alpha\beta}$, third order moment $Q_{\alpha\beta\gamma}$ and contracted fourth order moment $\hat{R}_{\alpha\beta}$ are the same as those obtained from the Maxwell-Boltzmann distribution, i.e.,

$$\sigma^{\mathrm{MB}}_{\alpha\beta} = \frac{1}{\rho}\, j_\alpha\, j_\beta, \qquad \hat{Q}^{\mathrm{MB}}_{\alpha\beta\gamma} = \frac{1}{\rho^2}\, j_\alpha\, j_\beta\, j_\gamma, \qquad \hat{R}^{\mathrm{MB}}_{\alpha\beta} = \frac{1}{\rho^2}\, j_\alpha\, j_\beta\, j^2. \tag{5.7}$$

However, typically in a discrete velocity model, the equilibrium distributions will

satisfy such conditions in an asymptotic sense only. So, we would like that these conditions are satisfied at least up to the fourth order in Mach number, i.e., $\mathcal{O}(u^4)$. This is sufficient to recover the Galilean invariant hydrodynamics [23].

2. **Discrete H-function:** It is sufficient to consider the discrete H-function of the Kullback form:

$$H = \sum_{i=1}^{N} f_i \left(\ln \left(\frac{f_i}{w_i} \right) - 1 \right), \qquad w_i > 0. \tag{5.8}$$

Here, the weights w_i are unknown positive definite numbers. The formal expression for the equilibrium distribution is

$$f_i^{eq} = w_i \, \exp\left(\alpha + \beta_\theta c_{i\theta}\right), \tag{5.9}$$

where α and β_θ are Lagrange multipliers associated with the mass and momentum conservation. We need to determine these weights such that the equilibrium distribution has desired higher order moments (See Eq. 5.7). Indeed these two ansatz were used earlier in Ref [22, 23] to construct on lattice higher order discrete Boltzmann equation.

3. **Constraints on weights:**We claim that in order to saftisfy first two ansatz (Eqs.5.7 and 5.8), it is sufficient that apart from positivity constraint ($w_i > 0$)

weights also obey following set of constraints on the even moments

$$\begin{aligned}
\sum_{i=1}^{N} w_i &= 1, \\
\sum_{i=1}^{N} w_i c_{i\alpha} c_{i\beta} &= \left(\frac{k_{\mathrm{B}}\, T_0}{m}\right) \delta_{\alpha\beta}, \\
\sum_{i=1}^{N} w_i c_{i\alpha} c_{i\beta} c_{i\gamma} c_{i\zeta} &= \left(\frac{k_{\mathrm{B}}\, T_0}{m}\right)^2 \Delta_{\alpha\beta\gamma\zeta}, \\
\sum_{i=1}^{N} w_i c_{i\alpha} c_{i\beta} c_{i\gamma} c_{i\zeta} c_{\zeta} c_{\theta} &= \left(\frac{k_{\mathrm{B}}\, T_0}{m}\right)^3 \Delta_{\alpha\beta\gamma\zeta\eta\theta},
\end{aligned} \tag{5.10}$$

where symbol Δ is used to denote symmetrized tensor generated from the Kronecker-delta. In particular

$$\begin{aligned}
\Delta_{\alpha\beta\gamma\zeta} &= \delta_{\alpha\beta}\delta_{\gamma\zeta} + \delta_{\alpha\gamma}\delta_{\beta\zeta} + \delta_{\alpha\zeta}\delta_{\beta\gamma}, \\
\Delta_{\alpha\beta\gamma\zeta\eta\theta} &= \delta_{\alpha\beta}\delta_{\gamma\zeta}\delta_{\eta\theta} + \delta_{\alpha\beta}\delta_{\gamma\eta}\delta_{\zeta\theta} + \delta_{\alpha\beta}\delta_{\gamma\theta}\delta_{\zeta\eta} + \delta_{\alpha\gamma}\delta_{\beta\zeta}\delta_{\eta\theta} + \delta_{\alpha\gamma}\delta_{\beta\eta}\delta_{\zeta\theta} + \delta_{\alpha\gamma}\delta_{\beta\theta}\delta_{\zeta\eta} + \\
&\quad \delta_{\alpha\zeta}\delta_{\beta\gamma}\delta_{\eta\theta} + \delta_{\alpha\zeta}\delta_{\beta\eta}\delta_{\gamma\theta} + \delta_{\alpha\zeta}\delta_{\beta\theta}\delta_{\gamma\eta} + \delta_{\alpha\eta}\delta_{\beta\gamma}\delta_{\zeta\theta} + \delta_{\alpha\eta}\delta_{\beta\zeta}\delta_{\gamma\theta} + \delta_{\alpha\eta}\delta_{\beta\theta}\delta_{\gamma\zeta} + \\
&\quad \delta_{\alpha\theta}\delta_{\beta\gamma}\delta_{\zeta\eta} + \delta_{\alpha\theta}\delta_{\beta\zeta}\delta_{\gamma\eta} + \delta_{\alpha\theta}\delta_{\beta\eta}\delta_{\gamma\zeta}.
\end{aligned} \tag{5.11}$$

The set of conditions on the odd moments are

$$\begin{aligned}
\sum_{i=1}^{N} w_i c_{i\alpha} &= 0, \\
\sum_{i=1}^{N} w_i c_{i\alpha} c_{i\beta} c_{i\gamma} &= 0, \\
\sum_{i=1}^{N} w_i c_{i\alpha} c_{i\beta} c_{i\gamma} c_{i\zeta} c_{\zeta} &= 0, \\
\sum_{i=1}^{N} w_i c_{i\alpha} c_{i\beta} c_{i\gamma} c_{i\zeta} c_{\zeta} c_{i\theta} c_{\kappa} &= 0.
\end{aligned} \tag{5.12}$$

As stated earlier, the condition on the equilibrium moments are satisfied up to the accuracy of $\mathcal{O}(u^4)$ only. In fact it can be easily proven that this ansatz is just a direct consequence of the previous two ansatz. The equivalence of the first two constraints with the third one is one of the central results of the present work. The practical consequence of this ansatz is that the problem of finding reliable entropic LB model is simplified to solving a set of algebraic equation coupled with positivity constraint. We defer the proof of this equivalence to later sections and propose a few more ansatz which will allow an analytically solvable set of algebraic equations.

4. **Energy Dependent Weights:** Any meaningful set of discrete velocities is composed by choosing discrete velocities with different energy $E \equiv c_x^2 + c_y^2 + c_z^2$. Thus a convenient notation of energy shell was introduced in the Ref [29]. We assume that the weights, w_i are just a function of energy E. In fact, all existing LB models satisfy this criteria.

5. **Symmetry Group of the Lattice:** For any discrete velocity set $\mathcal{C}$, we must have

   - **Closure under Inversion:** if a discrete velocity $\mathbf{c}_i \equiv (c_{ix}, c_{iy}, c_{iz})$ is an element of the set i.e. $\mathbf{c}_i \in \mathcal{C}$, then $-\mathbf{c}_i \in \mathcal{C}$. This closure, coupled with ansatz 4, trivially ensures that Eq.(5.12) is satisfied.

   - **Closure under Reflection:** If a discrete velocity $\mathbf{c}_i \equiv (c_{ix}, c_{iy}, c_{iz})$ is an element of the set i.e. $\mathbf{c}_i \in \mathcal{C}$, then all possible reflection of it are also a member of the set (i.e. $(\pm c_{ix}, \pm c_{iy}, \pm c_{iz}) \in \mathcal{C}$). The first condition is just a special case of the second one. Thus, any discrete velocity set constructed in this way will satisfy Eq. (5.12) trivially. Furthermore, as this condition ensures that there is no preference on a specific direction, so for any natural number n

$$\begin{aligned} \sum_{i=1}^{N} c_{ix}^{2n} = \sum_{i=1}^{N} c_{iy}^{2n} = \sum_{i=1}^{N} c_{iz}^{2n}, \\ \sum_{i=1}^{N} c_{ix}^{2n} c_{iy}^{2m} = \sum_{i=1}^{N} c_{ix}^{2n} c_{iz}^{2m} = \sum_{i=1}^{N} c_{iy}^{2n} c_{iz}^{2m}. \end{aligned} \tag{5.13}$$

   This means in order to satisfy conditions on even moments (Eq. 5.10), it is

sufficient to satisfy 7 scalar equations:

$$\sum_{i=1}^{N} w_i = 1, \qquad \sum_{i=1}^{N} w_i c_{ix}^2 = \frac{k_{\mathrm{B}}\, T_0}{m}\,, \qquad \sum_{i=1}^{N} w_i c_{ix}^4 = 3\left(\frac{k_{\mathrm{B}}\, T_0}{m}\right)^2,$$
$$\sum_{i=1}^{N} w_i c_{ix}^2\, c_{iy}^2 = \left(\frac{k_{\mathrm{B}}\, T_0}{m}\right)^2, \quad \sum_{i=1}^{N} w_i c_{ix}^6 = 15\left(\frac{k_{\mathrm{B}}\, T_0}{m}\right)^3, \quad (5.14)$$
$$\sum_{i=1}^{N} w_i c_{ix}^2\, c_{iy}^4 = 3\left(\frac{k_{\mathrm{B}}\, T_0}{m}\right)^3, \qquad \sum_{i=1}^{N} w_i c_{ix}^2\, c_{iy}^2 c_{iz}^3 = \left(\frac{k_{\mathrm{B}}\, T_0}{m}\right)^3.$$

We therefore need at least seven degree of freedom in the model to obtain the sixth order accuracy.

5.4 Construction of Velocity Set

Ansatz 5 mentioned in the previous section is trivially satisfied if we sample the discrete velocities from the cubic Bravais lattices. Thus, apart from the zero energy vector ($\mathbf{c} = \{0, 0, 0\}$) other simple choices is to generate energy shell is to sample discrete velocities from either of the three simple cubic lattices ,i.e., Simple Cubic (SC) , Face-Centered Cubic (FCC), or Body-Centered Cubic(BCC) struture [48]. Here, we remind the reader that we need to satisfy seven non-linear algebraic equations along with inequalities $w_i > 0$. As any energy shell has two degree of freedoms (magnitude of the energy and weight associated with the shell), apart from zero energy shell, we need to have at least three more energy shells.

The energy shells are chosen via a trial-and-error procedure. Only available guideline is that one would like to have as few as possible energy shells and within the energy

shell the number of the discrete velocities as few as possible. The optimal choice is to choose three energy shells from the SC structure. However, that set is inadmissible as weights are negative for that choice. However, it is possible to satisfy all equations with positive values of the weights if we chose each of the three energy shells from different structure simultaneously (one each from SC, FCC, and BCC structure, see Fig.5.1). Thus, instead of assuming that the magnitude of energy are in ratio of $1:2:3$, we put it as $a^2:2b^2:3d^2$, where a, b and d are the distortion parameters.

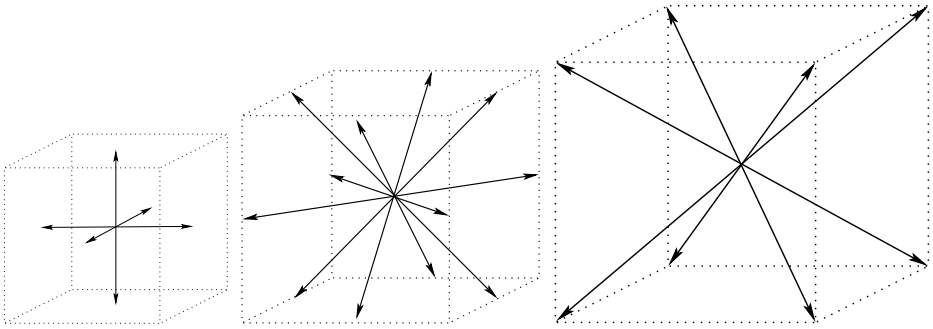

Figure 5.1: Admissible energy shells: Notice that unlike typical $D3Q27$ lattice Boltzmann model we are not assuming that magitude of energy are in ratio $1:2:3$.

In this case, Eq.(5.14) can be simplified to

$$\begin{aligned}
w_0 + 8w_a + 12w_b + 8w_d &= 1, \\
2a^2 w_a + 8b^2 w_b + 8d^2 w_d &= \left(\frac{k_\mathrm{B}\, T_0}{m}\right), \\
2a^4 w_a + 8b^4 w_b + 8d^4 w_d &= 3\left(\frac{k_\mathrm{B}\, T_0}{m}\right)^2, \\
4b^4 w_b + 8d^4 w_d &= \left(\frac{k_\mathrm{B}\, T_0}{m}\right)^2, \\
2a^6 w_a + 8b^6 w_b + 8d^6 w_d &= 15\left(\frac{k_\mathrm{B}\, T_0}{m}\right)^3, \\
4b^6 w_b + 8d^6 w_d &= 3\left(\frac{k_\mathrm{B}\, T_0}{m}\right)^3, \\
8d^6 w_d &= \left(\frac{k_\mathrm{B}\, T_0}{m}\right)^3,
\end{aligned} \tag{5.15}$$

where w_0, w_a, w_b, and w_d are weights corresponding to shell with energy zero, a^2, $2b^2$, and $3d^2$, respectively. Solving for this, we get two valid solutions (which satisfy $w_i > 0$):

$$\begin{aligned}
a &= \sqrt{\frac{15-\sqrt{15}}{2}}, & b &= \sqrt{6+\sqrt{15}}, & c &= \sqrt{9-2\sqrt{15}}, \\
w_0 &= \frac{8(90-\sqrt{15})}{2205}, & w_a &= \frac{270+46\sqrt{15}}{15435}, \\
w_b &= \frac{162-41\sqrt{15}}{6174}, & w_c &= \frac{783+202\sqrt{15}}{24696},
\end{aligned} \tag{5.16}$$

and,

$$a = \sqrt{\frac{15+\sqrt{15}}{2}}, \qquad b = \sqrt{6-\sqrt{15}}, \qquad c = \sqrt{9+2\sqrt{15}},$$
$$w_0 = \frac{8(90+\sqrt{15})}{2205}, \qquad w_a = \frac{270-46\sqrt{15}}{15435}, \tag{5.17}$$
$$w_b = \frac{162+41\sqrt{15}}{6174}, \qquad w_c = \frac{783-202\sqrt{15}}{24696}.$$

By just comparing the weights and energy level, there is no clear preference among these two solutions. Therefore, we will choose to work with the first choice. The solution for the second model will be easily obtained via the same process. At this juncture, it is pertinent to compare the current choice of 27 velocity model with the usual Hermite based $D3Q27$ model (see for example [10]). In the usual $D3Q27$ model, the three energy shell are sampled from the same cube, so energy of the shells are in the ratio $1:2:3$. As fixation of the energy ratio will reduce the available degrees of freedom, it is clear that usual $D3Q27$ model fails to satisfy all the seven conditions. However, in the current case no such restriction is imposed, so we have managed to satisfy all seven conditions on the moment of the weights (Eq.5.14). However, the price to pay is that the discrete velocity set is no longer space-filling. Thus compared to usual $D3Q27$ model implementation of the advection will be non-trivial.

5.5 Equilibrium Distribution

In this section, we shall present the explicit expression for the equilibrium distribution (Eq. 5.9). For algebraic convenience we rewrite the formal expression of the equilibrium

distribution as

$$f_i^{eq} = w_i \, \rho \, A \, \exp\left(\beta_\theta c_{i\theta}\right), \tag{5.18}$$

where $A = \rho^{-1} \exp\alpha > 0$. Our task here is to find the Lagrange multipliers in terms of conserved moments ρ and u_θ using Eq. (5.4). For this non-linear problem, the explicit solution is not available. However, we know that at zero velocity ($u_\theta = 0$), the solution to Lagrange multipliers are

$$A = 1, \qquad \beta_\theta = 0. \tag{5.19}$$

Since LB method works in subsonic region where Ma (Mach number) is considerably small, we can take the Mach number (velocity) to be the smallness parameter, and work out a pertubative scheme around the zero velocity. So we introduce a formal smallness parameter ϵ and write

$$\begin{aligned} A &= 1 + \epsilon A^{(1)} + \epsilon^2 A^{(2)} + \epsilon^3 A^{(3)} + \epsilon^4 A^{(4)} + \epsilon^5 A^{(5)} + \epsilon^6 A^{(6)} + \cdots \\ \beta_\theta &= \epsilon B_\theta^{(1)} + \epsilon^2 B_\theta^{(2)} + \epsilon^3 B_\theta^{(3)} + \epsilon^4 B_\theta^{(4)} + \epsilon^5 B_\theta^{(5)} + \epsilon^6 B_\theta^{(6)} + \cdots \end{aligned} \tag{5.20}$$

when substituted to (5.18) gives:

$$f_i^{eq} = w_i\,\rho\left[1+\epsilon\left(A^{(1)}+B_\theta^{(1)}c_{i\theta}\right)+\epsilon^2\left(A^{(2)}+B_\theta^{(2)}c_{i\theta}+B_\kappa^{(1)}c_{i\kappa}\left(A^{(1)}+B_\theta^{(1)}c_{i\theta}\right)\right)+\right.$$
$$\epsilon^3\left\{A^{(3)}+\frac{1}{6}\,B_\theta^{(1)}B_\kappa^{(1)}B_\eta^{(1)}c_{i\theta}c_{i\kappa}c_{i\eta}+\frac{1}{2}\,\left(2\,B_\theta^{(1)}B_\kappa^{(1)}\,A^{(1)}+B_\theta^{(2)}B_\kappa^{(1)}+B_\theta^{(1)}B_\kappa^{(2)}\right)c_{i\theta}c_{i\kappa}\right.$$
$$\left.\left.+\left(B_\theta^{(3)}+A^{(2)}\,B_\theta^{(1)}+A^{(1)}\,B_\theta^{(2)}\right)c_{i\theta}\right\}+\cdots\right]. \tag{5.21}$$

Coupled with

$$\sum_{i=1}^{N} f_i^{eq}=\rho, \qquad\qquad \sum_{i=1}^{N} f_i^{eq}c_{i\theta}=\epsilon\,\rho\,u_\theta, \tag{5.22}$$

we now have a set of linear equations to be solved at each order of ϵ.

We have at $\mathrm{O}(\epsilon^0)$:

$$\sum_{i=1}^{N} w_i=1, \qquad\qquad \sum_{i=1}^{N} w_i\,c_{i\theta}=0. \tag{5.23}$$

Notice that ansatz 1, implies that at $\mathrm{O}(\epsilon^0)$ we we must have

$$\sigma_{\alpha\beta}^{\mathrm{eq}}=0, \qquad \hat{Q}_{\alpha\beta\gamma}^{\mathrm{eq}}=0, \qquad \hat{R}_{\alpha\beta}^{\mathrm{eq}}=0, \tag{5.24}$$

which is trivially satisfied if ansatz 3 (Eq. 5.10 and 5.12) is true.

Solving order by order, we get, up to sixth order of ϵ (at $\epsilon = 1$):

$$\begin{aligned} A &= 1 - \frac{u^2}{\left(\frac{k_{\mathrm{B}}\, T_0}{m}\right)} + \frac{u^4}{\left(\frac{k_{\mathrm{B}}\, T_0}{m}\right)^2} - \frac{u^6}{\left(\frac{k_{\mathrm{B}}\, T_0}{m}\right)^3} + \mathcal{O}(u^8), \\ \beta_\theta &= \frac{u_\theta}{\left(\frac{k_{\mathrm{B}}\, T_0}{m}\right)} + \mathcal{O}(u^7). \end{aligned} \tag{5.25}$$

Finally the higher order moment can be computed to obtain

$$\begin{aligned} \sigma^{\mathrm{eq}}_{\alpha\beta} - \sigma^{\mathrm{MB}}_{\alpha\beta} &= \mathcal{O}(u^6), \\ \hat{Q}^{\mathrm{eq}}_{\alpha\beta\gamma} - \hat{Q}^{\mathrm{MB}}_{\alpha\beta\gamma} &= \mathcal{O}(u^5), \\ \hat{R}^{\mathrm{eq}}_{\alpha\beta} - \hat{R}^{\mathrm{MB}}_{\alpha\beta} &= \mathcal{O}(u^4). \end{aligned} \tag{5.26}$$

Thus, we can see that we do recover the desired moments up to the order $\mathcal{O}(u^4)$, which also shows that it is sufficient that discrete velocity models satisfy the ansatz 2 and 3.

5.6 Moment Chain and Resemblance to Grad's Method

In order to compare the present model with a typical Grad's moment system, it would be convenient to write the moment chain for the present kinetic equation (5.2). As, we have 27 discrete velocities, we can have only 27 independent moments. The set of 27 independent moments are

$$M = \left\{ \rho, j_\alpha, \sigma_{\alpha\beta}, \hat{Q}_{\alpha\beta\gamma}, \hat{R}_{\alpha\beta}, \psi \right\}, \tag{5.27}$$

where

$$\psi = \sum_{i=1}^{N} f_i \left(c_i^6 - 21 c_i^4 \left(\frac{k_{\mathrm{B}}\, T_0}{m} \right) + 105 c_i^2 \left(\frac{k_{\mathrm{B}}\, T_0}{m} \right)^2 - 105 \left(\frac{k_{\mathrm{B}}\, T_0}{m} \right)^3 \right), \tag{5.28}$$

is a scalar created from contracted sixth order moment. Although fifth order moments are not independent variables, it would be convenient to define the fifth order moment

$$\hat{N}_{\alpha\beta\gamma} = \sum_i f_i \Bigg\{ \left(c_i^2 - 7\, \frac{k_{\mathrm{B}}\, T_0}{m} \right) c_{i\alpha} c_{i\beta} c_{i\gamma} - \left(c_i^2 \frac{k_{\mathrm{B}}\, T_0}{m} - 5 \left(\frac{k_{\mathrm{B}}\, T_0}{m} \right)^2 \right) (\delta_{\alpha\beta} c_{i\gamma} + \delta_{\alpha\gamma} c_{i\beta} + \delta_{\beta\gamma} c_{i\alpha}) \Bigg\}, \tag{5.29}$$

for presenting the moment system.

As we are dealing with a discrete velocity model system, one can always write the closed form of the moment chain. Once we have decided the choice of independent moment, we can write the moment system. In the present case, they give rise to a closed chain of 27 equation, as we have 27 discrete velocities. The first four are the usual conservation laws for mass and momentum

$$\partial_t \rho + \partial_\alpha J_\alpha = 0, \qquad \partial_t J_\alpha + \partial_\beta \left(\sigma_{\alpha\beta} + \rho\, \frac{k_B T_0}{m} \delta_{\alpha\beta} \right) = 0. \tag{5.30}$$

Here it needs to be reminded that the energy conservation is absent in an isothermal discrete velocity model. The evolution equation for the second and third order moments

$\sigma_{\alpha\beta}$ and $\hat{Q}_{\alpha\beta\gamma}$ are

$$\begin{aligned}
\partial_t \sigma_{\alpha\beta} + \partial_\gamma \hat{Q}_{\alpha\beta\gamma} + \frac{k_B T_0}{m} \left(\partial_\alpha J_\beta + \partial_\beta J_\alpha\right) &= \frac{1}{\tau}\left(\frac{J_\alpha J_\beta}{\rho} - \sigma_{\alpha\beta}\right), \\
\partial_t \hat{Q}_{\alpha\beta\gamma} + \partial_\theta \hat{R}_{\alpha\beta\gamma\theta} + \frac{k_\mathrm{B}\, T_0}{m}\left(\partial_\gamma \sigma_{\alpha\beta} + \partial_\beta \sigma_{\alpha\gamma} + \partial_\alpha \sigma_{\beta\gamma}\right) &= \frac{1}{\tau}\left(\frac{J_\alpha J_\beta J_\gamma}{\rho} - \hat{Q}_{\alpha\beta\gamma}\right).
\end{aligned} \tag{5.31}$$

For the first 20 moments, there is no difference in the present system (Eqs. 5.30 and 5.31) and the Grad's 20-moment system. In the Grad's 20-moment system, one would prescribe the closure for the fourth order moment $\hat{R}_{\alpha\beta\gamma\theta}$. However, in the present set we have the evolution equation for the contracted fourth order moment $\hat{R}_{\alpha\beta}$ as

$$\partial_t \hat{R}_{\alpha\beta} + \partial_\gamma \hat{N}_{\alpha\beta\gamma} + \frac{k_\mathrm{B}\, T_0}{m}\left(\partial_\alpha\, \hat{q}_\beta + \partial_\beta\, \hat{q}_\alpha\right) = -\frac{1}{\tau}\hat{R}_{\alpha\beta}, \tag{5.32}$$

with

$$\begin{aligned}
\hat{N}_{\alpha\beta\gamma} = {} & \left(20 - 6\sqrt{15}\right)\hat{Q}_{\alpha\beta\gamma} + \left(9 - 3\sqrt{15}\right)\left(q_\alpha \delta_{\beta\gamma} + q_\beta \delta_{\alpha\gamma} + q_\gamma \delta_{\alpha\beta}\right) + \left(-15 + 8\sqrt{15}\right) q_\eta \delta_{\alpha\beta\gamma\eta} + \\
& \left(\frac{95 - 67\sqrt{15}}{2}\right)\hat{Q}_{\eta\theta\kappa}\, \delta_{\alpha\beta\gamma\eta\theta\kappa} + \left(\frac{-15 + 8\sqrt{15}}{3}\right)\hat{Q}_{\eta\theta\kappa}\, \square_{\alpha\beta\gamma\eta\theta\kappa},
\end{aligned} \tag{5.33}$$

where

$$\begin{aligned}
\square_{\alpha\beta\gamma\eta\theta\kappa} = {} & \big(\delta_{\alpha\beta}\delta_{\gamma\eta\theta\kappa} + \delta_{\alpha\gamma}\delta_{\beta\eta\theta\kappa} + \delta_{\alpha\eta}\delta_{\beta\gamma\theta\kappa} + \delta_{\alpha\theta}\delta_{\beta\gamma\eta\kappa} + \delta_{\alpha\kappa}\delta_{\beta\gamma\eta\theta} + \\
& \delta_{\beta\gamma}\delta_{\alpha\eta\theta\kappa} + \delta_{\beta\eta}\delta_{\alpha\gamma\theta\kappa} + \delta_{\beta\theta}\delta_{\alpha\gamma\eta\kappa} + \delta_{\beta\kappa}\delta_{\alpha\gamma\eta\theta} + \delta_{\gamma\eta}\delta_{\alpha\beta\theta\kappa} + \\
& \delta_{\gamma\theta}\delta_{\alpha\beta\eta\kappa} + \delta_{\gamma\kappa}\delta_{\alpha\beta\eta\theta} + \delta_{\eta\theta}\delta_{\alpha\beta\gamma\kappa} + \delta_{\eta\kappa}\delta_{\alpha\beta\gamma\theta} + \delta_{\theta\kappa}\delta_{\alpha\beta\gamma\eta}\big).
\end{aligned} \tag{5.34}$$

This is also not unusual in Grad's moment type approach. Since Grad's 20-moment system is a superset of Grad's 13-moment system, one could create a 26-moment system with $\hat{R}_{\alpha\beta}$ as independent variables, which will give rise to the same equation as Eq.(5.32) and one would prescribe the closure for $\hat{N}_{\alpha\beta\gamma}$ (which may differ from Eq.5.33) and $\hat{R}_{\alpha\beta\gamma\theta}$ based on the 26-moment expansion of the distribution function. However, in present approach we have the evolution equation for the sixth order moment ψ as

$$\partial_t \psi + \partial_\alpha S_\alpha = \frac{1}{\tau}(\psi^{\mathrm{eq}} - \psi), \tag{5.35}$$

where

$$\begin{aligned}
\psi^{\mathrm{eq}} &= \frac{3}{2}\left(65 - 9\sqrt{15}\right)\frac{J_\alpha J_\alpha}{\rho}, \\
S_\alpha &= 3\left(65 - 9\sqrt{15}\right)\, J_\alpha + \frac{3}{2}\left(783 - 181\sqrt{15}\right)\hat{q}_\alpha - \frac{1}{2}\left(1665 - 398\sqrt{15}\right)\hat{Q}_{\beta\gamma\eta}\,\delta_{\alpha\beta\gamma\eta}.
\end{aligned} \tag{5.36}$$

Lastly, the closures for $\hat{R}_{\alpha\beta\gamma\theta}$ is defined as follows:

$$\begin{aligned}
\hat{R}_{\alpha\beta\gamma\eta} = &\left(\frac{135 + 23\sqrt{15}}{10290}\,\psi - \frac{81 + 4\sqrt{15}}{98}\,\sigma\right)(\Delta_{\alpha\beta\gamma\eta} - 5\delta_{\alpha\beta\gamma\eta}) + \\
&\hat{R}\left(\frac{36 + 29\sqrt{15}}{98}\,\delta_{\alpha\beta\gamma\eta} - \frac{20 + 27\sqrt{15}}{196}\,\Delta_{\alpha\beta\gamma\eta}\right) + \\
&\left(\frac{5 - 2\sqrt{15}}{35}\right)\left(\hat{R}_{\alpha\beta}\delta_{\gamma\eta} + \hat{R}_{\alpha\gamma}\delta_{\beta\eta} + \hat{R}_{\alpha\eta}\delta_{\beta\gamma} + \hat{R}_{\beta\gamma}\delta_{\alpha\eta} + \hat{R}_{\beta\eta}\delta_{\alpha\gamma} + \hat{R}_{\gamma\eta}\delta_{\alpha\beta}\right) + \\
&\hat{R}_{\theta\kappa}\left(\frac{1}{10}\sqrt{15}\,\Box_{\alpha\beta\gamma\eta\theta\kappa} + \frac{1}{20}\sqrt{15}\,\Delta_{\alpha\beta\gamma\eta\theta\kappa} - \frac{19}{10}\sqrt{15}\,\delta_{\alpha\beta\gamma\eta\theta\kappa}\right).
\end{aligned} \tag{5.37}$$

The moment system described above (Eqs. 5.30, 5.31,5.32, 5.33, 5.32, 5.35, and 5.37) is equivalent to the original kinetic equation. Indeed, a very similar set of equations will be obtained if Grad's 26-moment system is extended with the sixth order moment ψ as an independent variable. What is very different from the usual Grad's moment system is the choice of the variable itself. It is not really obvious why Grad's 26-moment system should be extended by just one higher order moment. Typically, when Grad's system is extended, usually one includes next higher order moment (or some meaningful contraction of it) into the list of variables. In the present context, the choice of the 27th variable as ψ (which is a sixth order rather than fifth order moment) emerged automatically from the choice of the lattice itself. Such unusual extensions of the Grad's moment system is a typical feature of the LB type equations [13], although significance of such extension is not yet clear. All one can say at this juncture is that, such unusual extensions of the Grad's system leads to boundary condition in a natural way via discrete equivalent of diffusive boundary conditions [9].

5.7 Hydrodynamic Limit

It is expected that discrete kinetic equation, in the hydrodynamic limit, which is limit of Kundsen number going to zero, will lead to Navier-Stokes type equation. The usual procedure to obtain the transport coefficients and the hydrodynamic equation is to do the Chapman-Enskog expansion of the kinetic equation [42]. In this procedure, one writes the distribution function f and its time derivative in the powers of Knudsen

number Kn. In the present context, it means we have

$$\begin{aligned} f &= f^{\text{eq}} + \tau f^{(0)} + \tau^2 f^{(2)} + \cdots \\ \partial_t &= \partial_t^{(0)} + \tau \partial_t^{(1)} + \tau^2 \partial_t^{(2)} + \cdots \end{aligned} \tag{5.38}$$

The hydrodynamic variables are not expanded and in order to define time-derivatives consistency condition is used, which means that the derivatives of all other variables are evaluated using chain rules via time derivatives of the conserved quantities. Thus, we have

$$\sigma_{\alpha\beta}^{(0)} = \frac{J_\alpha J_\beta}{\rho}, \qquad \hat{Q}_{\alpha\beta\gamma}^{(0)} = \frac{J_\alpha J_\beta J_\gamma}{\rho^2}. \tag{5.39}$$

Using Eq.(5.30), we define time derivatives as

$$\begin{aligned} \partial_t^{(0)} \rho &= -\partial_\alpha J_\alpha, \\ \partial_t^{(0)} J_\alpha &= -\partial_\beta \left(\frac{J_\alpha J_\beta}{\rho} + \rho \frac{k_B T_0}{m} \delta_{\alpha\beta} \right). \end{aligned} \tag{5.40}$$

Using chain rule, we have

$$\begin{aligned} \partial_t^{(0)} \sigma_{\alpha\beta}^{(0)} &= \left(\partial_t^{(0)} \rho \right) \left(\frac{\partial \sigma_{\alpha\beta}^{\text{eq}}}{\partial \rho} \right) + \left(\partial_t^{(0)} j_\gamma \right) \left(\frac{\partial \sigma_{\alpha\beta}^{\text{eq}}}{\partial j_\gamma} \right) \\ &= -\frac{J_\alpha J_\beta}{\rho^2} \partial_\alpha J_\alpha - \left(\frac{J_\alpha}{\rho} \delta_{\beta\gamma} + \frac{J_\beta}{\rho} \delta_{\alpha\gamma} \right) \partial_\beta \left(\frac{J_\alpha J_\beta}{\rho} + \rho \frac{k_B T_0}{m} \delta_{\alpha\beta} \right). \end{aligned} \tag{5.41}$$

Also, using Eq.(5.31), we have

$$\partial_t^{(0)}\sigma_{\alpha\beta}^{(0)} + \partial_\gamma \hat{Q}_{\alpha\beta\gamma}^{(0)} + \frac{k_B T_0}{m}\left(\partial_\alpha J_\beta + \partial_\beta J_\alpha\right) = -\sigma_{\alpha\beta}^{(1)}, \tag{5.42}$$

which can be simplified using Eq.(5.41) to obtain

$$\sigma_{\alpha\beta}^{(1)} = -\rho\frac{k_\mathrm{B}\, T_0}{m}\left(\partial_\alpha \frac{j_\beta}{\rho} + \partial_\beta \frac{j_\alpha}{\rho}\right). \tag{5.43}$$

Thus in hydrodynamic limit, we do recover the Navier-Stokes equation:

$$\partial_t J_\alpha + \partial_\beta\left(\frac{J_\alpha J_\beta}{\rho} + \rho\,\frac{k_B T_0}{m}\delta_{\alpha\beta}\right) = \partial_\beta\left(\mu\,\left(\partial_\alpha \frac{j_\beta}{\rho} + \partial_\beta \frac{j_\alpha}{\rho}\right)\right), \tag{5.44}$$

where viscosity coefficient is $\mu = \tau\,\rho\,k_\mathrm{B}\,T_0/m$.

The important thing to notice here is that only $\sigma_{\alpha\beta}^{\mathrm{eq}}$ and $\hat{Q}_{\alpha\beta\gamma}^{\mathrm{eq}}$ appear in the first order expansion. So, it is sufficient that the equilibrium values of those match with those obtained from Maxwell-Boltzmann distribution. Thus, it confirms that our ansatz one was correct.

5.8 Unidirectional Flow: Stationary Solution

In order to verify the usefulness of the modified D3Q27, presented in this work, we chose to illustrate the stationary solution of the model for pressure driven and Couette flow. We wish to compare the solution obtained with the current model with that obtained

from the Boltzmann BGK solution. We have chosen this set-up as Couette flow was earlier analyzed in detail using the LB equation (see for example [13]). It is known from there that Knudsen layer is predicted only by D2Q16 model, which in three dimension means a model with 64 discrete velocities. Thus, it is a good set up to compare the effectiveness of the current model.

5.8.1 Setup description and outline of solution

We consider the fluid to be enclosed by two parallel plates normal to z direction and separated by a distance of L. The bottom plate at $z = -L/2$ moves unidirectionally with the velocity $\{U_1, 0, 0\}$ while the top place at $z = L/2$ moves with velocity $\{U_2, 0, 0\}$. It is assumed that tube is infinitely long in x direction and constant pressure gradient is imposed in the x direction. We aim at finding the steady state solution to the kinetic equation in this particular setup.

Integration of the steady state moment system is done under three assumptions:

- The flow is unidirectional, where all the fields except density depends only on the z coordinate.
- No mass flow through the walls.
- For low Mach number flows, the non-linearities can be ignored and it is sufficient to consider the linearized moment system.

As the result, we find the inner solution for all the moments. This inner solution is a parametric family that depends on yet undetermined constants of integrations.

Figure 5.2: The cross section of channel geometry where the fluid is enclosed in the z-direction by two parallel plates with forcing only applied in the x-direction. The y-direction is perpendicular to this page and it is assumed that the fluid is periodic in this direction.

In order to find the constants of integrations, we need to include the boundary condition, which is available in population representation. Thus, we either should transform the inner solution obtained earlier (in terms of moments) to population, or to find the moment representation at the boundary (where the relevant populations are taken from the boundary, and the rest from the inner population). Note that this solution is still dependent on the same constants of integrations. Matching this solution with the inner solution will give us the value of integration constant, and thus solving the entire problem. Here, solving for J_x will be prioritized. The same strategy is already used and elaborated in details in [49].

5.8.2 Inner solution to the unidirectional stationary moment system

In this part, we start with the assumption that the flow is in a steady state and is unidirectional (all the fields depend only on the z coordinate due to the nature of the setup, which is infinite in x and y direction) with the exception of ρ, which only depends on x and not z. The continuity equation in this limit simplifies to $\partial_z J_z = 0$, which because of the boundary condition (no mass leak from the wall) reduces to

$$J_z = 0. \tag{5.45}$$

The momentum conservation equation in the x-direction simplifies as

$$\sigma_{xz} = -\frac{dp_0}{dx} z + k_1, \tag{5.46}$$

where $p_0 = \rho\ (k_B T_0/m)$. Here we assume that the pressure drop, dp_0/dx, is a constant. Now, we will try to formally solve for J_x related moments with the usual quadratic

equilibrium. The equations are listed below:

$$
\begin{aligned}
\partial_z \hat{Q}_{xzz} + \frac{k_B T_0}{m}\,\partial_z J_x = -\frac{1}{\tau}\,\sigma_{xz} \qquad &\Rightarrow \qquad \frac{k_B T_0}{m}\,J_x = -\hat{Q}_{xzz} + \frac{1}{2\tau}\frac{dp_0}{dx}z^2 - \frac{k_1}{\tau}z + k_2,\\
\partial_z \hat{R}_{xzzz} + 2\,\frac{k_{\mathrm{B}}\,T_0}{m}\,\partial_z \sigma_{xz} = -\frac{1}{\tau}\,\hat{Q}_{xzz},&\\
\partial_z \hat{R}_{xxxz} = -\frac{1}{\tau}\,\hat{Q}_{xxx} \qquad &\Rightarrow \qquad \hat{Q}_{xxx} = \hat{Q}_{xzz} - 2\,\frac{k_{\mathrm{B}}\,T_0}{m}\,\frac{dp_0}{dx}\tau,\\
\partial_z \hat{R}_{xzyy} = -\frac{1}{\tau}\,\hat{Q}_{xyy} \qquad &\Rightarrow \qquad \hat{Q}_{xyy} = \frac{1}{6}\left(3-\sqrt{15}\right)\hat{Q}_{xxx},\\
\partial_z \hat{R}_{xz} + 2\,\frac{k_{\mathrm{B}}\,T_0}{m}\,\partial_z \sigma_{xz} = -\frac{1}{\tau}\,\hat{q}_x \qquad &\Rightarrow \qquad \hat{q}_x = \frac{1}{6}(15-\sqrt{15})\hat{Q}_{xzz} - \frac{1}{3}\left(9-\sqrt{15}\right)\,\frac{k_{\mathrm{B}}\,T_0}{m}\,\frac{dp_0}{dx}\tau,\\
\partial_z \hat{N}_{xzz} + \frac{k_{\mathrm{B}}\,T_0}{m}\,\partial_z\,\hat{q}_x = -\frac{1}{\tau}\hat{R}_{xz}.&
\end{aligned}
\tag{5.47}
$$

Simplifying the last equation, we have

$$
\begin{aligned}
\partial_z \hat{N}_{xzz} + \frac{k_{\mathrm{B}}\,T_0}{m}\,\partial_z\,\hat{q}_x &= -\frac{1}{\tau}\hat{R}_{xz},\\
\frac{k_{\mathrm{B}}\,T_0}{m}\,\partial_z\left[\left(14-\sqrt{15}\right)\hat{Q}_{xzz} + \left(9-3\sqrt{15}\right)\hat{Q}_{xyy} + \left(4-\sqrt{\frac{5}{3}}\right)\hat{Q}_{xxx}\right] + \frac{k_{\mathrm{B}}\,T_0}{m}\,\partial_z\,\hat{q}_x &= -\frac{1}{\tau}\hat{R}_{xz},\\
\frac{k_{\mathrm{B}}\,T_0}{m}\,\partial_z\left[\left(15-\sqrt{15}\right)\hat{Q}_{xzz} + \left(10-3\sqrt{15}\right)\hat{Q}_{xyy} + \left(5-\sqrt{\frac{5}{3}}\right)\hat{Q}_{xxx}\right] &= -\frac{1}{\tau}\hat{R}_{xz},\\
\frac{1}{2}\left(65-9\sqrt{15}\right)\,\frac{k_{\mathrm{B}}\,T_0}{m}\,\partial_z\hat{Q}_{xzz} &= -\frac{1}{\tau}\hat{R}_{xz}.
\end{aligned}
\tag{5.48}
$$

So we need to solve

$$
\begin{aligned}
\frac{1}{2}\left(65-9\sqrt{15}\right)\,\frac{k_{\mathrm{B}}\,T_0}{m}\,\partial_z\hat{Q}_{xzz} &= -\frac{1}{\tau}\hat{R}_{xz},\\
\partial_z \hat{R}_{xzzz} + 2\,\frac{k_{\mathrm{B}}\,T_0}{m}\,\partial_z\sigma_{xz} &= -\frac{1}{\tau}\,\hat{Q}_{xzz},
\end{aligned}
\tag{5.49}
$$

which gives us

$$\begin{aligned}\hat{Q}_{xzz} &= 2\,\frac{k_{\mathrm{B}}\,T_0}{m}\,\frac{dp_0}{dx}\tau - A_1\sinh\left(\frac{z}{\eta\,\mathrm{Kn}\,L}\right) - A_2\cosh\left(\frac{z}{\eta\,\mathrm{Kn}\,L}\right),\\ \hat{R}_{xz} &= \frac{35\sqrt{12-\sqrt{15}}}{15+\sqrt{15}}\left[A_1\cosh\left(\frac{z}{\eta\,\mathrm{Kn}\,L}\right) + A_2\sinh\left(\frac{z}{\eta\,\mathrm{Kn}\,L}\right)\right]\sqrt{\frac{k_{\mathrm{B}}\,T_0}{m}},\end{aligned} \tag{5.50}$$

where

$$\mathrm{Kn} = \frac{\tau}{L}\sqrt{\frac{3\,k_{\mathrm{B}}\,T_0}{m}}, \qquad\qquad \eta = \sqrt{4-\sqrt{\frac{5}{3}}}. \tag{5.51}$$

Substituting the expression for $\hat{Q}_{xzz}$ given in (5.50) into the first equation in (5.47), we have explicit form of J_x as

$$J_x = -2\,\frac{dp_0}{dx}\tau + \frac{m}{k_{\mathrm{B}}\,T_0}\left(A_1\sinh\left(\frac{z}{\eta\,\mathrm{Kn}\,L}\right) + A_2\cosh\left(\frac{z}{\eta\,\mathrm{Kn}\,L}\right) + \frac{1}{2\tau}\,\frac{dp_0}{dx}z^2 - \frac{k_1}{\tau}z + k_2\right). \tag{5.52}$$

Here, we obtained a family of moments that is dependent on four integration constants (k_1, k_2, A_1, A_2). To determine these, we need to specify boundary conditions at the walls. Note that this is an advantage of LB hierarchy, since it is well known for other moments method (such as Grad's systems), that it is not possible to provide self-consistent boundary conditions for the moments [26]. In our case, this is possible because the boundary conditions for the LB kinetic equations are formulated in terms of populations rather than in terms of moments [9].

5.8.3 Diffusive wall boundary condition

Boundary conditions for discrete velocity models are formulated in terms of distribution function. Thus, in order to apply boundary conditions, it is more convenient to come back from the moment representation to the distribution representation. For the present system, we apply the classical Maxwell's diffusive wall boundary condition. In this condition, particles that reach the wall are redistributed in a way consistent with the mass-balance and normal-flux condition,

$$f_i|_{\mathbf{c}\cdot\mathbf{n}>0} = \frac{\sum_{\mathbf{c}_j\cdot\mathbf{n}<0} |(\mathbf{c}_j\cdot\mathbf{n})| f_j}{\sum_{\mathbf{c}_j\cdot\mathbf{n}<0} |(\mathbf{c}_j\cdot\mathbf{n})| f_j^{eq}(\rho,\mathbf{U}_{\text{wall}})} f_i^{eq}(\rho,\mathbf{U}_{\text{wall}}), \tag{5.53}$$

where $\mathbf{n}$ is the inner normal at the wall, and $\mathbf{U}_{wall}$ is the wall velocity. This boundary condition redistributes the populations that reach the wall according to the equilibrium distribution of the population that leaves the wall.

Since the solution for the moments must be continuous, we should have the inner solution same as the result obtained from the boundary condition, where f_i is taken from (5.53) whenever $\mathbf{c}\cdot\mathbf{n} > 0$ and taken from the Grad representation f_i, if otherwise. With such definition of f_i, we can have the following boundary condition (given in Eqs. 5.54 and 5.55) by taking the moment of f_i with respect to $c_{ix}c_{iz}^2$ and $c_{ix}c_{iy}^2c_{iz}^2$, on the top and bottom wall, respectively.

At the top wall ($z = L/2$), we have:

$$\begin{aligned}
\left(\frac{k_{\mathrm{B}}\,T_0}{m}\right)^{3/2}(J_x-\rho U_2) &= \frac{2w_b(2b^7-7b^5)+4w_d(3d^7-7d^5)}{5(8-\sqrt{15})}\,\hat{R}_{xz}+ \\
&\quad \left(\frac{k_{\mathrm{B}}\,T_0}{m}\right)\left(2w_b b^5+4w_d d^5\right)\,\sigma_{xz}-\sqrt{\frac{k_{\mathrm{B}}\,T_0}{m}}\,\hat{Q}_{xzz}, \\
\left(\frac{k_{\mathrm{B}}\,T_0}{m}\right)^{3/2}(J_x-\rho U_2) &= \frac{4w_d(3d^9-7d^7)}{5(8-\sqrt{15})}\,\hat{R}_{xz}+\left(\frac{k_{\mathrm{B}}\,T_0}{m}\right)4w_d d^7\,\sigma_{xz}- \\
&\quad \sqrt{\frac{k_{\mathrm{B}}\,T_0}{m}}\left(\left(4w_d(d^8-3d^6)\right)\hat{Q}_{xxx}+\left(4w_d(d^8-d^6)\right)(\hat{Q}_{xyy}+\hat{Q}_{xzz})\right).
\end{aligned} \tag{5.54}$$

While at the bottom wall ($z = -L/2$), we have:

$$\begin{aligned}
\left(\frac{k_{\mathrm{B}}\,T_0}{m}\right)^{3/2}(J_x-\rho U_1) &= -\frac{2w_b(2b^7-7b^5)+4w_d(3d^7-7d^5)}{5(8-\sqrt{15})}\,\hat{R}_{xz}- \\
&\quad \left(\frac{k_{\mathrm{B}}\,T_0}{m}\right)\left(2w_b b^5+4w_d d^5\right)\,\sigma_{xz}-\sqrt{\frac{k_{\mathrm{B}}\,T_0}{m}}\,\hat{Q}_{xzz}, \\
\left(\frac{k_{\mathrm{B}}\,T_0}{m}\right)^{3/2}(J_x-\rho U_1) &= -\frac{4w_d(3d^9-7d^7)}{5(8-\sqrt{15})}\,\hat{R}_{xz}-\left(\frac{k_{\mathrm{B}}\,T_0}{m}\right)4w_d d^7\,\sigma_{xz}- \\
&\quad \sqrt{\frac{k_{\mathrm{B}}\,T_0}{m}}\left(\left(4w_d(d^8-3d^6)\right)\hat{Q}_{xxx}+\left(4w_d(d^8-d^6)\right)(\hat{Q}_{xyy}+\hat{Q}_{xzz})\right).
\end{aligned} \tag{5.55}$$

Since we have 4 equations and 4 unknowns, the system can be solved unambiguously. Substituting the inner solution to (5.54) and (5.55) and solving for the unknowns give

rise to the following solutions:

$$k_1 = \frac{2.76662 \coth\left(\frac{1}{2\eta \mathrm{Kn}}\right) + 2.88642}{(4.79193 + 7.1253\mathrm{Kn}) \coth\left(\frac{1}{2\eta \mathrm{Kn}}\right) + (4.99943 + 8.82956\mathrm{Kn})} \rho(U_1 - U_2)\,\mathrm{Kn} \sqrt{\frac{k_\mathrm{B}\, T_0}{m}},$$

$$A_1 = \frac{\rho(U_1 - U_2)\,\mathrm{Kn}}{(4.79193 + 7.1253\mathrm{Kn}) \cosh\left(\frac{1}{2\eta \mathrm{Kn}}\right) + (4.99943 + 8.82956\mathrm{Kn}) \sinh\left(\frac{1}{2\eta \mathrm{Kn}}\right)} \frac{k_\mathrm{B}\, T_0}{m}, \tag{5.56}$$

$$k_2 = \frac{\rho(U_1 + U_2)}{2} \frac{k_\mathrm{B}\, T_0}{m} - L \frac{dp_0}{dx} \left(\frac{\sqrt{3}}{8\mathrm{Kn}} + 0.764749 - \frac{(3.39265 + 28.5339\mathrm{Kn})}{29.2802 \coth\left(\frac{1}{2\eta \mathrm{Kn}}\right) + 28.0649} \right) \sqrt{\frac{k_\mathrm{B}\, T_0}{m}},$$

$$A_2 = \frac{5.07205 + 42.6586\mathrm{Kn}}{29.2802 \cosh\left(\frac{1}{2\eta \mathrm{Kn}}\right) + 28.0649 \sinh\left(\frac{1}{2\eta \mathrm{Kn}}\right)} L \frac{dp_0}{dx} \sqrt{\frac{k_\mathrm{B}\, T_0}{m}}. \tag{5.57}$$

5.9 Couette Flow

The shear stress is the quantity of interest in the Couette flow. We define dimensionless shear stress consistent with the Ref [40] as

$$\sigma^*_{xz} = -\frac{\sigma_{xz}}{\rho(U_2 - U_1)} \sqrt{\frac{2\pi\, m}{k_\mathrm{B}\, T_0}}. \tag{5.58}$$

For the current model with the first basis, we have dimensionless shear stress as

$$\sigma^*_{xz} = \frac{\left(6.93489 \coth\left(\frac{0.303784}{\mathrm{Kn}}\right) + 7.23518\right)\,\mathrm{Kn}}{(4.79193 + 7.1253\mathrm{Kn}) \coth\left(\frac{0.303784}{\mathrm{Kn}}\right) + (4.99943 + 8.82956\mathrm{Kn})}, \tag{5.59}$$

and a similar computation for the second basis gives

$$\sigma^*_{xz} = \frac{\left(18.1766 \coth\left(\frac{0.217371}{\mathrm{Kn}}\right) + 6.95667\right)\ \mathrm{Kn}}{(12.5598 + 21.9968\mathrm{Kn}) \coth\left(\frac{0.217371}{\mathrm{Kn}}\right) + (4.80697 + 8.96816\mathrm{Kn})}. \tag{5.60}$$

The convergence of the discrete Boltzmann equation towards its continuous counterpart

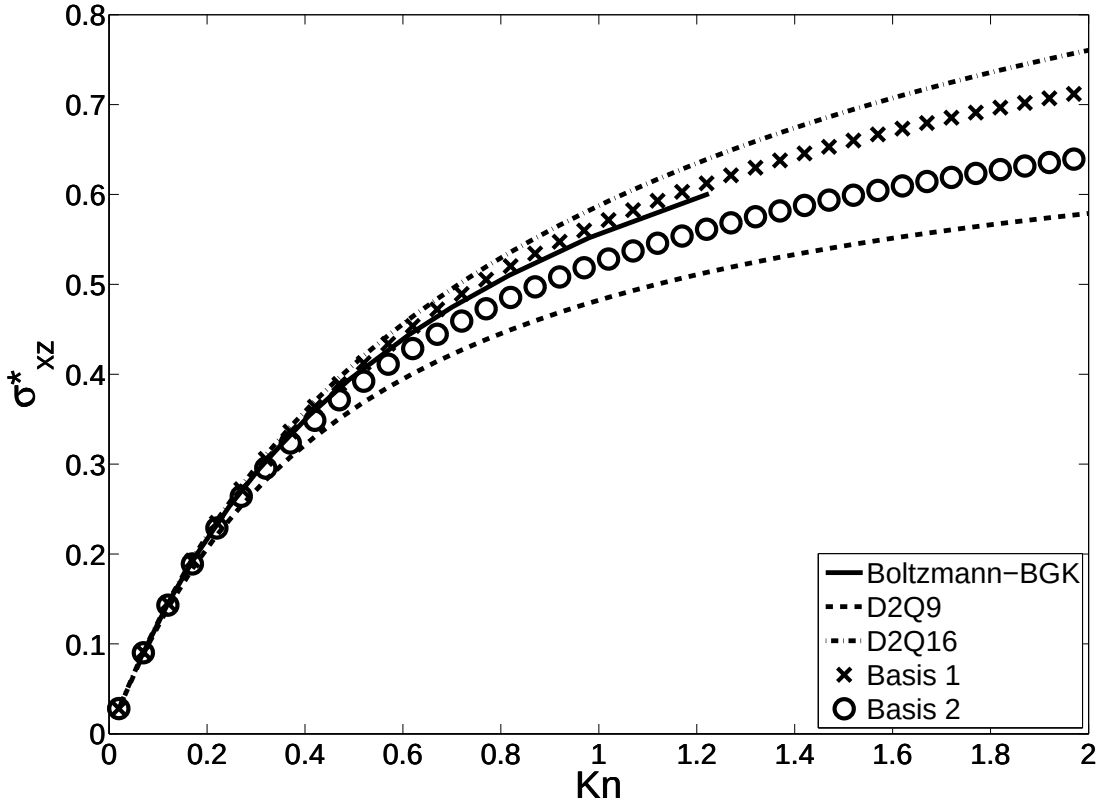

Figure 5.3: Shear stress profile for Couette flow

can also be analyzed via solution at $\mathrm{Kn} \to \infty$. For example, we know that the infinite Knudsen limit of the dimensionless shear stress $\nu^{\infty}_{\mathrm{eff}}$ for the Boltzmann-BGK equation is equal to unity. The comparison is tabulated in table 5.1. From the table, it is evident that the current model with the first basis is converging much faster to the Boltzmann

equation compared to any other approximation. Furthermore, the quality of result also suggest that the model with first basis performs much better compared to the second one.

Table 5.1: Comparison of effective shear viscosity at Kn $\to \infty$ between the Boltzmann-BGK model and various LB models.

Model	$\nu_{\text{eff}}^{\infty}$
Boltzmann-BGK	1
$D2Q9$	0.723
$D2Q16$	1.113
Current Model 1	0.973
Current Model 2	0.826

Yet another useful quantity which shows non-trivial behavior in high Knudsen number cases is non-dimensional centerline velocity gradient W, defined as

$$\begin{aligned} W &= 1 - \frac{1}{U_2 - U_1}\left(\frac{du_x}{dz/L}\right)_{z=0} \\ &= 1 + \frac{m}{k_{\text{B}}\,T_0}\left(\frac{A_1}{\eta \text{Kn}} - \frac{k_1}{\text{Kn}}\sqrt{\frac{3k_{\text{B}}\,T_0}{m}}\right). \end{aligned} \tag{5.61}$$

The result and its relative error are tabulated in table 5.2. From the table, it is evident that the current model with the first basis is converging much faster to the Boltzmann equation compared to any other approximation. Furthermore, the quality of result also suggest that the model with first basis performs much better compared to the second one.

Table 5.2: Deviation of non-dimensional velocity gradient from Navier-Stokes value for the Boltzmann-BGK kinetic equations, the $D2Q9$ model and the two new proposed models. Percentage error of the value of deviation is relative to Boltzmann-BGK value.

Kn	Values				Error (%)		
	Boltzmann-BGK	$D2Q9$	Model 1	Model 2	$D2Q9$	Model 1	Model 2
0.06124	0.09134	0.10911	0.09152	0.09973	19.450	0.1971	9.185
0.12247	0.1648	0.1968	0.1749	0.1860	19.387	5.775	12.864
0.17496	0.2136	0.2592	0.2384	0.2480	21.358	10.403	16.104
0.24495	0.2664	0.3288	0.3096	0.3165	23.427	13.953	18.806
0.30619	0.3041	0.3798	0.3611	0.3663	24.890	15.785	20.454
0.61237	0.4290	0.5509	0.5301	0.5332	28.408	19.071	24.289
0.81650	0.4821	0.6202	0.5986	0.6024	28.646	19.462	24.953
1.22474	0.5556	0.7101	0.6880	0.6930	27.808	19.244	24.730

5.10 Knudsen Paradox

It is well known that the for the pressure driven flow, so called "Knudsen paradox" behavior where the flow rate shows a minima as a function of the Knudsen number. In the present section, we compare the result from the present discrete velocity model with the continuous Boltzmann-BGK equation as well as existing Hermite based latttice Boltzmann models. For pressure driven flows, we can set $U_1 = U_2 = 0$ in the general solution Eq.(5.52). In this set-up the quantity of interest is the dimensionless flow rate Q defined as

$$Q = -\frac{1}{L^2}\left(\frac{dp_0}{dx}\right)^{-1}\sqrt{\frac{2k_{\mathrm{B}}\,T_0}{m}}\int_{z=-L/2}^{z=L/2} J_x\,dz. \tag{5.62}$$

In order to compare present result with the existing result in the literature, we follow the convention in the literature and redefined Knudsen number $\hat{\mathrm{K}}\mathrm{n}$ such that $\hat{\mathrm{K}}\mathrm{n} = \mathrm{Kn}\sqrt{2/3}$. From the Boltzmann BGK equation, we know that in this particular setup,

the dimensionless flow rate defined in Eq.(5.62) theoretically should have a minima at $\hat{\text{Kn}} \approx 1$ [36].

For the first basis, using Eq.(5.52) we have dimensionless flow rate as

$$Q = \frac{1}{6\hat{\text{Kn}}} + 1.08152 + 2\,\hat{\text{Kn}} - \frac{4.79793 + 57.8374\hat{\text{Kn}} + 174.303\hat{\text{Kn}}^2}{29.2802\coth\left(\frac{0.248039}{\hat{\text{Kn}}}\right) + 28.0649}. \tag{5.63}$$

It can be shown that this profile indeed exhibit Knudsen paradox with the Knudsen minima occuring at $\text{Kn} \approx 0.5886$. Similarly for second basis, we have:

$$Q = \frac{1}{6\hat{\text{Kn}}} + 1.14248 + 2\,\hat{\text{Kn}} - \frac{89.5403 + 2562.31\hat{\text{Kn}} + 14596.1\hat{\text{Kn}}^2}{1295.28\coth\left(\frac{0.177483}{\hat{\text{Kn}}}\right) + 1279.29}. \tag{5.64}$$

with the flat profile, which has no minima and distinct value in the limit of Knudsen number going to infinity. Thus, similar to $D2Q16$ model, the second model present in the present case do not exhibit Kndusen paradox behavior.

We can see that the first term of the flow rate (order of $\hat{\text{Kn}}^{-1}$) basically represents the Navier-Stokes limit. We also compared the result with the Cercignani quadratic approximation using the slip flow model that also used in comparing $D2Q9$ model in [49], which in our notation gives:

$$Q = \frac{1}{6\hat{\text{Kn}}} + 1.01617 + 1.5324\,\hat{\text{Kn}}. \tag{5.65}$$

Finally, we would like to comment on the other possible models of microflow. Recently, Grad moment method was modified to obtain the so called $R13$ equation [50, 51],

for which boundary condition was developed in Ref [52] . In recent year, it has been shown that $R13$ with proper boundary condition gives as good result as LB for microflows [52]. The $R13$ approach gives the expression of the flow rate Q as

$$Q = \frac{1}{6\hat{\mathrm{Kn}}} + 0.97108 + 1.1333\,\hat{\mathrm{Kn}} - \frac{0.0848528\left(1 + 3.53553\hat{\mathrm{Kn}}\right)^2}{0.931695\coth\left(\frac{0.527046}{\hat{\mathrm{Kn}}}\right) + 1}. \tag{5.66}$$

From Fig. 5.4, it is visible that our current approach with the first basis gives an almost exact agreement with the result of R13. Further, it behaves much better than $D2Q16$ model used in literature as the present model can capture boundary layer as well as Knudsen minima.

5.11 Numerical illustration

In this section, numerical result corresponding to the Couette flow simulations has been illustrated for on-lattice and off-lattice representations with $D3Q27$ velocity model. The numerical setup has been explained earlier in Section 5.8. In the computational domain the moving walls are considered to be located at $z = 0$ and $z = L$. Here, two representative Knudsen numbers (Kn = 0.5 and 1.0) are considered and an isothermal equilibrium distribution function given by Eq. (5.18) is used. The flow Mach number is kept constant (Ma = 0.075) in these simulation runs. A diffusive wall boundary condition given by Eq. (5.53) is used for walls in z-direction and a periodic boundary condition is employed in x-direction. The computational procedure is described as

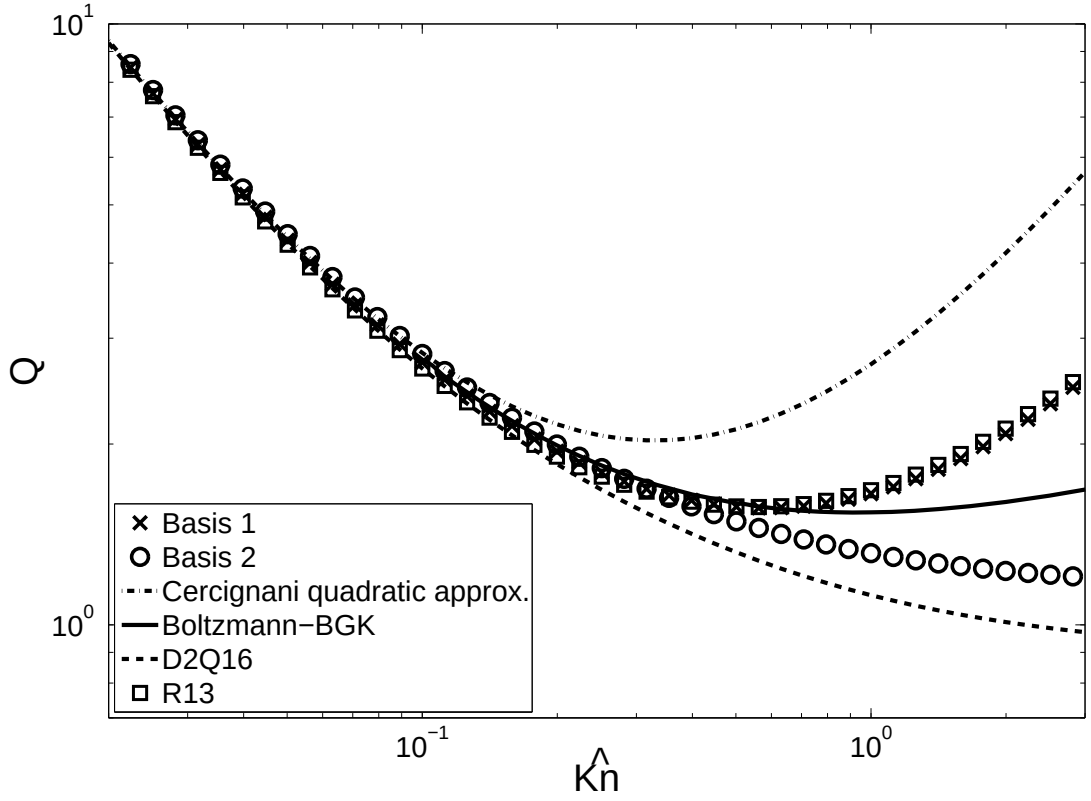

Figure 5.4: Flow rate Q as a function of the resized Knudsen number $\hat{\text{Kn}}$ for Poiseuille flow

follows.

- A formal solution for Eq. (5.2) may be written as,

$$f_i\left(\mathbf{x}+\mathbf{c}\Delta t, \mathbf{c}, t+\Delta t\right) = f_i\left(\mathbf{x}, \mathbf{c}, t\right) + \int_0^{\Delta t} \Omega_i\left(f_i\left(\mathbf{x}+\mathbf{c}s, \mathbf{c}, t+s\right)\right) ds. \qquad (5.67)$$

where, $\Omega_i = 1/\tau\left(f_i^{eq} - f_i\right)$ is the usual BGK collision kernel. Further, a short-time solution may be written by evaluating the collision term using the trapezoidal

rule (assuming linear interpolation)

$$f_i\left(\mathbf{x}+\mathbf{c}\Delta t,\mathbf{c},t+\Delta t\right)=f_i\left(\mathbf{x},\mathbf{c},t\right)+\frac{\Delta t}{2}\left[\Omega_i\left(f_i\left(\mathbf{x},\mathbf{c},t\right)\right)+\Omega_i\left(f_i\left(\mathbf{x}+\mathbf{c}\Delta t,\mathbf{c},t+\Delta t\right)\right)\right]+\mathcal{O}(\Delta t^3). \tag{5.68}$$

- Firstly, in order to create an efficient explicit numerical scheme we transform the distribution functions, f_i, in terms of g_i using the following,

$$g_i\left(\mathbf{x},\mathbf{c},t\right)=f_i\left(\mathbf{x},\mathbf{c},t\right)-\frac{\Delta t}{2\tau}\left(f_i^{eq}\left(\mathbf{x},\mathbf{c},t\right)-f_i\left(\mathbf{x},\mathbf{c},t\right)\right), \tag{5.69}$$

and hence the corresponding LB evolution equation using the above transformation is,

$$g_i\left(\mathbf{x}+\mathbf{c}\,\Delta t,t+\Delta t\right)=g_i\left(\mathbf{x},t\right)+2\,\beta\,\left(g_i^{\mathrm{eq}}\left(g\left(\mathbf{x},t\right)\right)-g_i\left(\mathbf{x},t\right)\right), \tag{5.70}$$

where, $\beta=\Delta t/(2\tau+\Delta t)$.

- The Eq. (5.70) may be written as consisting of two-steps, namely, local-collision and streaming. The post-collision distribution functions ($g_i^{\star}$) may be found as,

$$g_i^{\star}\left(\mathbf{x},t\right)=g_i\left(\mathbf{x},t\right)+2\,\beta\,\left(g_i^{\mathrm{eq}}\left(\mathbf{x},t\right)-g_i\left(\mathbf{x},t\right)\right), \tag{5.71}$$

and thus computed $g_i^{\star}$'s may then be streamed for the usual on-lattice represen-

tation as,

$$g_i\left(\mathbf{x}, t+\Delta t\right) = g_i^{\star}\left(\mathbf{x}-\mathbf{c}\,\Delta t, t\right). \tag{5.72}$$

- Further, the grid-spacing, $\delta x = \delta y = \delta z$ and the time-step, $\Delta t = \delta x/b$ is chosen.

- In an off-lattice simulation, the usual streaming procedure (Eq. (5.72)) is performed for the distribution functions corresponding to the energy shell, b. Hence, a convection term contribution needs to be computed for the energy shells apart from b. This contribution is evaluated after calculating the post-collision distribution functions using Eq. (5.71) as,

$$\begin{aligned} g_i\left(\mathbf{x}, t+\Delta t\right) &\approx g_i^{\star}\left(\mathbf{x}, t\right) - \frac{\partial g_i^{\star}}{\partial x_\alpha} c_{i\alpha}\Delta t \\ &\approx g_i^{\star}\left(\mathbf{x}, t\right) + \frac{\mp g_i^{\star}\left(\mathbf{x} \mp c_{i\alpha}\Delta t, t\right) \pm g_i^{\star}\left(\mathbf{x}, t\right)}{\delta x} |c_{i\alpha}|\Delta t. \end{aligned} \tag{5.73}$$

Here, a quasi two-dimensional approximation has been made. This is because, the illustrative example under consideration is an unidirectional. The approximation implies $\partial g_i/\partial y = 0$ and hence no convection in y-direction. The gradients of the distribution functions are evaluated using a first-order upwind scheme. The scheme is stable and sufficiently accurate. Further, we found that the use of central-difference scheme is unstable. Here, we do acknowledge the fact that for a full three-dimensional simulations, estimation of the gradients of g_i's is an involved task.

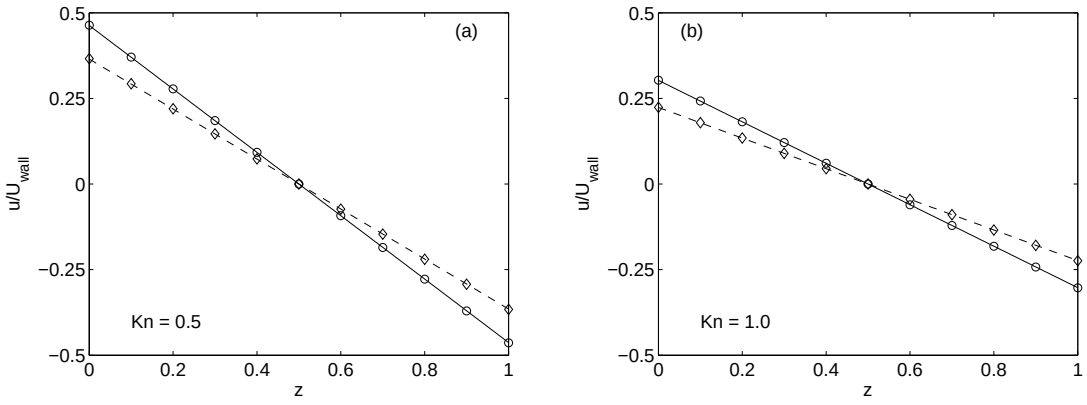

Figure 5.5: Comparison of the analytical solution (symbols; $\diamond$: on-lattice, $\circ$: off-lattice representation) with the numerical data (dotted line: on-lattice, solid line: off-lattice). (a) Kn = 0.5; (b) Kn = 1.0.

A computational mesh comprises a total of $(16 \times 1 \times 128)$ number of lattice points. In Fig. 5.5, the x-directional velocity (u) normalized with respect to the positive x-directional wall velocity (U_{wall}) has been plotted versus the z co-ordinate. From Fig. 5.5 a very good comparison of the numerical results (shown using lines) with the analytical solution (shown using symbols) obtained from Section 5.9) may be clearly seen. Further, a slope of the curve predicted using the off-lattice representation is observed to be larger than that of on-lattice model. From this numerical exercise, we conclude that an off-lattice LB ($D3Q27$) is easily implementable with a good accuracy for finite Knudsen flows.

5.12 Discussion

In this Chapter, we have presented a novel model that contains both Knudsen layer and Knudsen minima, with rather minimal number of discrete velocities for three di-

mensional system. In particular, we have studied the velocity profile and shear stress profile under the action of external force.

The presented scheme has high efficiency for realistic applications due to the minimal number of discrete velocities and its Galilean invariance. The advantage of the current model is that not only it captures the Knudsen layer effect which does not exist in $D2Q9$ model, it also has a Knudsen minima which does not exist in $D2Q16$ model. Therefore, it combines the advantages of $D2Q9$ and $D2Q16$ at the same time.

Thus to conclude, we have presented a novel model which can predict both Knudsen layer effect and Knudsen paradox, with rather minimal number of discrete velocities for three dimensional system with built-in Galilean invariance.

Chapter 6

Conclusions and Future Work

6.1 Conclusions

The analysis of standard Lattice Boltzmann Method hierarchy, in particular $D2Q9$ and $D2Q16$ methods are presented in this thesis. A renormalization method is introduced to reduce the velocity set in the system while keeping the physics and accuracy level of the higher-order model. An alternate framework to create discrete velocity set is suggested, and it is shown that in this framework the entropic formulation of the LB method can be naturally extended to obtain a discrete velocity set with a given accuracy. As an example, a 27-velocity LB model with the Galilean invariant hydrodynamic limit is derived. As compared to existing model, the advantage of the current model is that it not only captures the Knudsen layer effect which does not exist in $D2Q9$ model, it also has a Knudsen minimum which does not exist in $D2Q16$ model. Therefore, it combines the advantages of $D2Q9$ and $D2Q16$ at the same time. We have obtained a novel model

which can predict both Knudsen layer effect and Knudsen paradox, with rather minimal number of discrete velocities for three dimensional system. The presented scheme has high efficiency for realistic applications due to the minimal number of discrete velocities. It gives an edge for quantitative computation in engineering application, given some modification for computational purpose (due to the fact that it is off-lattice), and may even be suitable for simulating mixtures.

6.2 Future Work

The extensive computations such as turbulence study are proposed for further research work. Simulations on channel flow, bounded flow and flow around the sphere may provide us with more insight on the stability and robustness of the Higher Order Galilean Invariant Lattice Boltzmann Model. Additionally, simulating Kida flow and Taylor Green vortex flow may give insight of the performance of the new model at high Reynolds number.

Bounded flow is very common in real life application, and the interaction of the fluid with boundary wall is inevitable for a lot of realistic setup. It is crucial in bounded system to have a model with correct representation of the boundary condition, so that the simulation results are accurate, physically consistent and realistic. Practicality of Higher Order Galilean Invariant Lattice Boltzmann Model also should be tested with the simulation of flow around the sphere. Reproducing Von-Karman Street effect using the model can be a challenging task due to possible interference from the artificial

diffusion, but this can be minimized if the off-lattice streaming step is properly approximated in the simulation.

Further analysis of the model in curvelinear coordinate system (in particular, cylindrical coordinate system) may provide us with more insight, especially if an explicit analytical solution for the velocity profile is available in cases such as pipe flow. The current work also can be extended in the future to the case of two component mixture, where the proposed model are likely to perform more efficiently given the minimal number of velocities.

6.2.1 Irregular Lattice Population Transformation

One major drawback of the Higher Order Galilean Invariant Lattice Boltzmann Model is its off-lattice structure, which numerically complicate the streaming step and the implementation of boundary condition. It may be possible to tackle this particular problem using irregular lattice population transformation, which has the same basic idea as the renormalization method.

As an example, a unidirectional distortion on 2-D lattice system is depicted in Fig. 6.1 (in this case we assume for simplicity that the wall is parallel to one of the lattice grid axis). From the figure, we can see that the last layer of lattice (layer C) is exactly coincide with wall, but the spacing to the next layer (layer B) is different compared to the regular spacing. The lattice at layer B will have asymmetric neighboring point, which in this case will not allow the normal streaming procedure to the top layer (layer C).

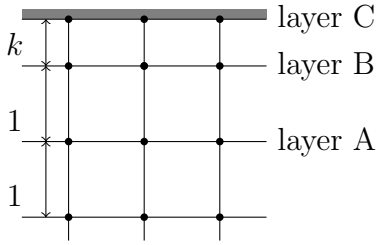

Figure 6.1: Unidirectional Homogenized Distortion in 2-D system

As we already know from the theory of Lattice Boltzmann Method, a continuous distribution function $f(\mathbf{x}, \mathbf{c}, t)$ is represented by a number of discrete distribution functions (which correspond to each discrete velocities in the set) $f(\mathbf{x}, \mathbf{c}_i, t)$ (or simply $f_i(\mathbf{x}, t)$). By choosing different discrete velocities, $\mathbf{c}_i$, we can modify distribution function at each point such that the left hand side of the Boltzmann-BGK evolution equation becomes a free-streaming process to each neighboring lattice when discretized. The correctional term of the transformation shall be taken care of by the collisional term after streaming process complete.

Let us denote f as the normal population and $\hat{f}$ as the distorted one. As we can

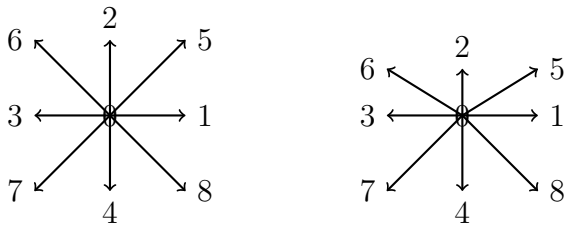

Figure 6.2: Comparison of discrete velocities between normal population f (left) and distorted population $\hat{f}$ (right).

see from Fig. 6.2, the distorted population fits into the layer B profile of neighboring

lattice, and from which one can deduce that in the absence of collisional term, the free streaming will take place.

In this approach, we shall assume the moments of both systems (normal and distorted) are the same, i.e.

$$\begin{aligned} \mathcal{M} &= \Psi \cdot f, \\ \mathcal{M} &= \Gamma \cdot \hat{f}, \end{aligned} \tag{6.1}$$

where $\mathcal{M}$ denotes the moment space. Now we can write

$$f = \left(\Psi^{-1}\Gamma\right) \cdot \hat{f}, \tag{6.2}$$

and now the evolution equation can be written as

$$\begin{aligned} \partial_t \left(\Psi^{-1}\Gamma\right) f + \partial_\alpha \left(D_{c_\alpha} \Psi^{-1}\Gamma\right) f &= -\frac{1}{\tau}\left(\left(\Psi^{-1}\Gamma\right) f - \left(\Psi^{-1}\Gamma\right) f^{\mathrm{eq}}\right), \\ \partial_t \hat{f} + \partial_\alpha \left(\Gamma^{-1}\Psi D_{c_\alpha} \Psi^{-1}\Gamma\right) \hat{f} &= -\frac{1}{\tau}\left(\hat{f} - \left(\Psi^{-1}\Gamma\right) f^{\mathrm{eq}}\right), \end{aligned} \tag{6.3}$$

where D_{c_α} is diagonal matrix with c_α as the diagonal element.

The final equation reads

$$\partial_t \hat{f} + \partial_\alpha \hat{c}_\alpha \hat{f} = -\frac{1}{\tau}\left(\hat{f} - \left(\Psi^{-1}\Gamma\right) f^{\mathrm{eq}}\right) - \partial_\alpha \left(\Gamma^{-1}\Psi D_{c_\alpha} \Psi^{-1}\Gamma - D_{\hat{c}_\alpha}\right) \hat{f}. \tag{6.4}$$

The equation can be separated into two part: the left hand side is the advection step that usually applied in the simulation, while the right hand side appears as a slightly

modified collision step with additional 'forcing' term. Thus, streaming will be done as per normal, with correctional term appears at the collision step, as an additional forcing.

6.2.2 Even Higher Order Galilean Invariant LB Method

Extended version of Higher Order Galilean Invariant LB Method, which may contain probably up to 41 discrete velocities will be considered as well. This may be achieved from pruning either $D3Q64$ or $D3Q125$ Models. It is also expected that the model might represent a thermal model. Other than that, there is a possibility of extended version of Higher Order Galilean Invariant LB Method may contain a consistent binary collision model. This may lead to a possible Monte-Carlo scheme with high efficiency, where the collision step is mainly done by swapping populations under certain conditions.

Appendix A

$D2Q9$ Model Appendix

A.1 Populations representation in terms of moments

We can explicitly represent populations f_i in terms of moments:

$$
\begin{aligned}
f_0 &= \rho - \frac{P_{xx}}{3c_s^2} - \frac{P_{yy}}{3c_s^2} + \frac{R_{xxyy}}{9c_s^4},\\
f_1 &= \frac{j_x}{2\sqrt{3}\,c_s} + \frac{P_{xx}}{6c_s^2} - \frac{Q_{xyy}}{6\sqrt{3}\,c_s^3} - \frac{R_{xxyy}}{18c_s^4},\\
f_2 &= \frac{j_y}{2\sqrt{3}\,c_s} + \frac{P_{yy}}{6c_s^2} - \frac{Q_{yxx}}{6\sqrt{3}\,c_s^3} - \frac{R_{xxyy}}{18c_s^4},\\
f_3 &= -\frac{j_x}{2\sqrt{3}\,c_s} + \frac{P_{xx}}{6c_s^2} + \frac{Q_{xyy}}{6\sqrt{3}\,c_s^3} - \frac{R_{xxyy}}{18c_s^4},\\
f_4 &= -\frac{j_y}{2\sqrt{3}\,c_s} + \frac{P_{yy}}{6c_s^2} + \frac{Q_{yxx}}{6\sqrt{3}\,c_s^3} - \frac{R_{xxyy}}{18c_s^4},\\
f_5 &= \frac{P_{xy}}{12c_s^2} + \frac{Q_{xyy}}{12\sqrt{3}\,c_s^3} + \frac{Q_{yxx}}{12\sqrt{3}\,c_s^3} + \frac{R_{xxyy}}{36c_s^4},\\
f_6 &= -\frac{P_{xy}}{12c_s^2} - \frac{Q_{xyy}}{12\sqrt{3}\,c_s^3} + \frac{Q_{yxx}}{12\sqrt{3}\,c_s^3} + \frac{R_{xxyy}}{36c_s^4},\\
f_7 &= \frac{P_{xy}}{12c_s^2} - \frac{Q_{xyy}}{12\sqrt{3}\,c_s^3} - \frac{Q_{yxx}}{12\sqrt{3}\,c_s^3} + \frac{R_{xxyy}}{36c_s^4},\\
f_8 &= -\frac{P_{xy}}{12c_s^2} + \frac{Q_{xyy}}{12\sqrt{3}\,c_s^3} - \frac{Q_{yxx}}{12\sqrt{3}\,c_s^3} + \frac{R_{xxyy}}{36c_s^4}.
\end{aligned}
\tag{A.1}
$$

These expressions can be used to obtain:

$$
\begin{aligned}
f_5 - f_6 &= \frac{P_{xy}}{6\,c_s^2} + \frac{Q_{xyy}}{6\sqrt{3}\,c_s^3},\\
f_5 + f_6 &= \frac{Q_{yxx}}{6\sqrt{3}\,c_s^3} + \frac{R_{xxyy}}{18c_s^4},\\
f_7 + f_8 &= -\frac{Q_{yxx}}{6\sqrt{3}\,c_s^3} + \frac{R_{xxyy}}{18\,c_s^4},\\
f_7 - f_8 &= \frac{P_{xy}}{6\,c_s^2} - \frac{Q_{xyy}}{6\,\sqrt{3}\,c_s^3}.
\end{aligned}
\tag{A.2}
$$

These expressions can be used to write the boundary conditions in terms of the moments. From the boundary condition we have:

$$\begin{aligned}
(f_5 + f_6)\big|_{y=-L/2} &= \frac{\rho}{18} + \frac{\rho\, U_1^2}{18\, c_s^2}, \\
(f_7 + f_8)\big|_{y=L/2} &= \frac{\rho}{18} + \frac{\rho\, U_2^2}{18\, c_s^2}, \\
(f_5 - f_6)\big|_{y=-L/2} &= \frac{\rho\, U_1}{6\sqrt{3}\, c_{\mathrm{s}}}, \\
(f_7 - f_8)\big|_{y=L/2} &= -\frac{\rho\, U_2}{6\sqrt{3}\, c_{\mathrm{s}}}.
\end{aligned} \tag{A.3}$$

Finally, using (A.2), we get:

$$\begin{aligned}
\Big(Q_{xyy} + \sqrt{3} c_{\mathrm{s}}\, P_{xy}\Big)\big|_{y=-L/2} &= \rho c_{\mathrm{s}}^2\, U_1, \\
\Big(Q_{xyy} - \sqrt{3} c_{\mathrm{s}}\, P_{xy}\Big)\big|_{y=L/2} &= \rho c_{\mathrm{s}}^2\, U_2, \\
X_1|_{y=-L/2} &= \rho c_{\mathrm{s}}^2\, \left(U_1^2 - u_x^2\right)\big|_{y=-L/2}, \\
X_2|_{y=L/2} &= \rho c_{\mathrm{s}}^2\, \left(U_2^2 - u_x^2\right)\big|_{y=L/2}.
\end{aligned} \tag{A.4}$$

A.2 Identities for the Boundary Condition

First, we group the velocity set into three subsets: velocity vectors with positive y velocity, negative y velocity and zero y velocity. In order to find out contribution to

moments by individual subsets, following identities for $D2Q9$ model will be required:

$$\begin{aligned}
&\sum_{c_{iy}<0} w_i = \frac{1}{6}, \quad \sum_{c_{iy}<0} w_i c_{ix} = 0, \quad \sum_{c_{iy}<0} w_i c_{iy} = -\frac{1}{6}\, c, \\
&\sum_{c_{iy}>0} w_i = \frac{1}{6}, \quad \sum_{c_{iy}>0} w_i c_{ix} = 0, \quad \sum_{c_{iy}>0} w_i c_{iy} = \frac{1}{6}\, c,
\end{aligned}$$

$$\begin{aligned}
&\sum_{c_{iy}<0} w_i c_{ix}^2 = \frac{1}{18}\, c^2, \quad \sum_{c_{iy}<0} w_i c_{ix} c_{iy} = 0, \quad \sum_{c_{iy}<0} w_i c_{iy}^2 = \frac{1}{6}\, c^2, \\
&\sum_{c_{iy}>0} w_i c_{ix}^2 = \frac{1}{18}\, c^2, \quad \sum_{c_{iy}>0} w_i c_{ix} c_{iy} = 0, \quad \sum_{c_{iy}>0} w_i c_{iy}^2 = \frac{1}{6}\, c^2,
\end{aligned} \tag{A.5}$$

$$\begin{aligned}
&\sum_{c_{iy}<0} w_i c_{ix}^2 c_{iy} = -\frac{1}{18}\, c^3, \quad \sum_{c_{iy}<0} w_i c_{ix} c_{iy}^2 = 0, \quad \sum_{c_{iy}<0} w_i c_{ix}^2 c_{iy}^2 = \frac{1}{18}\, c^4, \\
&\sum_{c_{iy}>0} w_i c_{ix}^2 c_{iy} = \frac{1}{18}\, c^3, \quad \sum_{c_{iy}>0} w_i c_{ix} c_{iy}^2 = 0, \quad \sum_{c_{iy}>0} w_i c_{ix}^2 c_{iy}^2 = \frac{1}{18}\, c^4,
\end{aligned}$$

where $c = \sqrt{3} c_\mathrm{s}$.

A.3 Derivation of the Result of Distribution Function Summation

First of all, we calculate:

$$\begin{aligned}
\sum_{\mathbf{c}_i \cdot \mathbf{n}<0} w_i \left[\rho + \frac{j_\alpha c_{i\alpha}}{c_\mathrm{s}^2} \right] &= \sum_{\mathbf{c}_i \cdot \mathbf{n}<0} w_i \left[\rho + \frac{j_x c_{ix}}{c_\mathrm{s}^2} + \frac{j_y c_{iy}}{c_\mathrm{s}^2} \right] \\
&= \frac{\rho}{6} + 0 + 0 = \frac{\rho}{6},
\end{aligned} \tag{A.6}$$

since $\sum_{\mathbf{c}_i\cdot\mathbf{n}<0} w_i c_{ix} = 0$ and $j_y = 0$.

Next, term by term, by applying the identities from $(A.5)$ we have:

$$\begin{aligned}\sum_{\mathbf{c}_i\cdot\mathbf{n}<0} w_i \left[\frac{\mathcal{F}^{(2)}}{2c_{\mathrm{s}}^4}\right] &= \frac{1}{2c_{\mathrm{s}}^4}\sum_{\mathbf{c}_i\cdot\mathbf{n}<0} w_i \left[(P_{xx}-\rho c_{\mathrm{s}}^2)(c_{ix}^2-c_{\mathrm{s}}^2)+(P_{yy}-\rho c_{\mathrm{s}}^2)(c_{iy}^2-c_{\mathrm{s}}^2)+2P_{xy}c_{ix}c_{iy}\right]\\ &= \frac{1}{2c_{\mathrm{s}}^4}\left[(P_{xx}-\rho c_{\mathrm{s}}^2)(\frac{1}{18}\,3c_{\mathrm{s}}^2-\frac{1}{6}\,c_{\mathrm{s}}^2)+(\rho c_{\mathrm{s}}^2-\rho c_{\mathrm{s}}^2)(\frac{1}{6}\,3c_{\mathrm{s}}^2-\frac{1}{6}\,c_{\mathrm{s}}^2)+0\right]=0,\end{aligned} \tag{A.7}$$

$$\begin{aligned}\sum_{\mathbf{c}_i\cdot\mathbf{n}<0} w_i \left[\frac{\mathcal{F}^{(3)}}{6c_{\mathrm{s}}^6}\right] &= \frac{1}{6c_{\mathrm{s}}^6}\sum_{\mathbf{c}_i\cdot\mathbf{n}<0} w_i \left[3(Q_{yxx}-j_y c_{\mathrm{s}}^2)(c_{ix}^2c_{iy}-c_{iy}c_{\mathrm{s}}^2)+3(Q_{xyy}-j_x c_{\mathrm{s}}^2)(c_{ix}c_{iy}^2-c_{ix}c_{\mathrm{s}}^2)\right]\\ &= \frac{1}{2c_{\mathrm{s}}^6}\left[(Q_{yxx}-j_y c_{\mathrm{s}}^2)(\mp\frac{1}{18}c^3-\mp\frac{1}{6}c\,c_{\mathrm{s}}^2)+(Q_{xyy}-j_x c_{\mathrm{s}}^2)(0-0)\right]\\ &= \frac{1}{2c_{\mathrm{s}}^6}\left[(Q_{yxx}-j_y c_{\mathrm{s}}^2)(\mp\frac{1}{18}\,3c_{\mathrm{s}}^2-\mp\frac{1}{6}\,c_{\mathrm{s}}^2)\,c+(Q_{xyy}-j_x c_{\mathrm{s}}^2)(0-0)\right]=0,\end{aligned} \tag{A.8}$$

$$\begin{aligned}\sum_{\mathbf{c}_i\cdot\mathbf{n}<0} w_i \left[\frac{\mathcal{F}^{(4)}}{4c_{\mathrm{s}}^8}\right] &= \frac{1}{4c_{\mathrm{s}}^8}\sum_{\mathbf{c}_i\cdot\mathbf{n}<0} w_i \left(R_{xxyy}-Pc_{\mathrm{s}}^2+\rho c_{\mathrm{s}}^4\right)\left(c_{ix}^2-c_{\mathrm{s}}^2\right)\left(c_{iy}^2-c_{\mathrm{s}}^2\right)\\ &= \frac{1}{4c_{\mathrm{s}}^8}\sum_{\mathbf{c}_i\cdot\mathbf{n}<0} w_i \left(R_{xxyy}-Pc_{\mathrm{s}}^2+\rho c_{\mathrm{s}}^4\right)\left(c_{ix}^2c_{iy}^2-(c_{ix}^2+c_{iy}^2)c_{\mathrm{s}}^2+c_{\mathrm{s}}^4\right)\\ &= \frac{1}{4c_{\mathrm{s}}^8}\left(R_{xxyy}-Pc_{\mathrm{s}}^2+\rho c_{\mathrm{s}}^4\right)\left(\frac{1}{18}\,c^4-\left(\frac{1}{18}\,c^2+\frac{1}{6}\,c^2\right)c_{\mathrm{s}}^2+\frac{1}{6}\,c_{\mathrm{s}}^4\right)\\ &= \frac{1}{4c_{\mathrm{s}}^8}\left(R_{xxyy}-Pc_{\mathrm{s}}^2+\rho c_{\mathrm{s}}^4\right)\left(\frac{1}{18}\,9c_{\mathrm{s}}^4-\left(\frac{4}{18}\,3c_{\mathrm{s}}^2\right)c_{\mathrm{s}}^2+\frac{1}{6}\,c_{\mathrm{s}}^4\right)=0,\end{aligned} \tag{A.9}$$

which complete the proof.

A.4 Moments of Forcings

For first type of forcing, we have:

$$
\begin{aligned}
\phi_1(\mathcal{F}^{(1)}) &= \left(2j_x - \frac{j_x^3}{\rho^2 c_{\mathrm{s}}^2}\right) g_x, \\
\phi_2(\mathcal{F}^{(1)}) &= j_y\, g_x + j_x\, g_y, \\
\phi_3(\mathcal{F}^{(1)}) &= \left(2j_y - \frac{j_y^3}{\rho^2 c_{\mathrm{s}}^2}\right) g_x, \\
\phi_4(\mathcal{F}^{(1)}) &= j_y \left(\frac{2\, j_x}{\rho} - \frac{j_x^3}{\rho^3\, c_s^2}\right) g_x + \left(\frac{j_x^2}{\rho}\left(1 - \frac{j_y^2}{\rho^2\, c_s^2}\right) + \rho c_{\mathrm{s}}^2\right) g_y, \\
\phi_5(\mathcal{F}^{(1)}) &= \left(\frac{j_y^2}{\rho}\left(1 - \frac{j_x^2}{\rho^2\, c_s^2}\right) + \rho c_{\mathrm{s}}^2\right) g_x + j_x \left(\frac{2\, j_y}{\rho} - \frac{j_y^3}{\rho^3\, c_s^2}\right) g_y, \\
\phi_6(\mathcal{F}^{(1)}) &= \left(2c_{\mathrm{s}}^2 - \frac{j^2}{\rho^2}\right)(j_x g_x + j_y g_y) + 3\, j_x\, g_x\, \frac{j_y^2}{\rho^2} + 3\, j_y\, g_y\, \frac{j_x^2}{\rho^2},
\end{aligned}
\tag{A.10}
$$

For second type of forcing, we have:

$$
\begin{aligned}
\phi_1(\mathcal{F}^{(2)}) &= 2\, j_x\, g_x, \\
\phi_2(\mathcal{F}^{(2)}) &= j_y\, g_x + j_x\, g_y, \\
\phi_3(\mathcal{F}^{(2)}) &= 2\, j_y\, g_y, \\
\phi_4(\mathcal{F}^{(2)}) &= \rho\, c_{\mathrm{s}}^2\, g_y, \\
\phi_5(\mathcal{F}^{(2)}) &= \rho\, c_{\mathrm{s}}^2\, g_x, \\
\phi_6(\mathcal{F}^{(2)}) &= 2\, c_{\mathrm{s}}^2\, (j_x g_x + j_y g_y)\,,
\end{aligned}
\tag{A.11}
$$

Appendix B

Forcing Moments of $D2Q16$ Model

For the forcing we use for $D2Q16$ model, we have:

$$\begin{aligned}
\phi_1(\mathcal{F}) &= 2\, j_x\, g_x, \\
\phi_2(\mathcal{F}) &= j_y\, g_x + j_x\, g_y, \\
\phi_3(\mathcal{F}) &= 2\, j_y\, g_y,
\end{aligned} \tag{B.1}$$

$$\begin{aligned}
\phi_4(\mathcal{F}) &= \rho\, c_{\mathrm{s}}^2\, g_y, \\
\phi_5(\mathcal{F}) &= \rho\, c_{\mathrm{s}}^2\, g_x,
\end{aligned} \tag{B.2}$$

$$
\begin{aligned}
\phi_6(\mathcal{F}) &= 2\, c_{\mathrm{s}}^2\ (j_x g_x + j_y g_y)\,, \\
\phi_7(\mathcal{F}) &= 3\rho\, c_{\mathrm{s}}^2\, g_x, \\
\phi_8(\mathcal{F}) &= 3\rho\, c_{\mathrm{s}}^2\, g_y, \\
\phi_9(\mathcal{F}) &= 3\, c_{\mathrm{s}}^2\ (j_x g_x + j_y g_y)\,, \\
\phi_{10}(\mathcal{F}) &= 3\, c_{\mathrm{s}}^2\ (j_x g_x + j_y g_y)\,,
\end{aligned}
\tag{B.3}
$$

$$
\begin{aligned}
\phi_{11}(\mathcal{F}) &= 3\rho\, c_{\mathrm{s}}^4\, g_x, \\
\phi_{12}(\mathcal{F}) &= 3\rho\, c_{\mathrm{s}}^4\, g_y, \\
\phi_{13}(\mathcal{F}) &= 9\, c_{\mathrm{s}}^4\ (j_x g_x + j_y g_y)\,,
\end{aligned}
\tag{B.4}
$$

Bibliography

[1] H. Chen, S. Chen, and W. Matthaeus. Recovery of the Navier-Stokes Equation Using a Lattice-Gas Boltzmann method. *Phys. Rev. A*, 45:R5339–R5342, 1992.

[2] H. Chen, S. Kandasamy, S. Orszag, R. Shock, S. Succi, and V. Yakhot. Extended-Boltzmann Kinetic Equation for Turbulent Flows. *Science*, 301:633–636, 2003.

[3] S. Chen and G.D̃. Doolen. Lattice Boltzmann Method for Fluid Flows. *Annu. Rev. Fluid Mech.*, 30:329, 1998.

[4] F. Higuera, S. Succi, and R Benzi. Lattice Gas-Dynamics with Enhanced Collisions. *Europhys. Lett.*, 9:345–349, 1989.

[5] Y. H. Qian, D. d'Humieres, and P. Lallemand. Lattice BGK Models for Navier-Stokes Equation. *Europhys. Lett.*, 17:479–484, 1992.

[6] S. Succi. *The Lattice Boltzmann Equation for Fluid Dynamics and Beyond*. Oxford University Press, Oxford, 2001.

[7] S. Succi, R Benzi, and M. Vergassola. The Lattice Boltzmann Equation – Theory and Applications. *Phys. Rep.*, 222:145–197, 1992.

[8] S Succi, I. V. Karlin, and H. Chen. Role of the H-theorem in Lattice Boltzmann hydrodynamics. *Rev. Mod. Phys.*, 74:1203, 2002.

[9] S. Ansumali and I. V. Karlin. Kinetic Boundary Condition for the Lattice Boltzmann Method. *Phys. Rev. E*, 66:026311, 2002.

[10] S. Ansumali, I. V. Karlin, and H. C. Öttinger. Minimal Entropic Kinetic Models for Simulating Hydrodynamics. *Europhys. Lett.*, 63:798–804, 2003.

[11] X. Shan and X. He. Discretization of the Velocity Space in the Solution of the Boltzmann Equation. *Phys. Rev. Lett.*, 80(1):65–68, 1998.

[12] S. Ansumali and I. V. Karlin. Consistent Lattice Boltzmann method. *Phys. Rev. Lett.*, 95(26):260605, 2005.

[13] S. Ansumali, I. V. Karlin, S. Arcidiacono, A. Abbas, and N. I. Prasianakis. Hydrodynamics beyond Navier-Stokes: Exact Solution to the Lattice Boltzmann Hierarchy. *Phys. Rev. Lett.*, 98(12):124502, 2007.

[14] J. Horbach and S. Succi. Lattice Boltzmann versus Molecular Dynamics Simulation of Nanoscale Hydrodynamic Flows. *Phys. Rev. Lett.*, 96:224503, 2006.

[15] B. Li and D. Kwok. Discrete Boltzmann Equation for Microfluidics. *Phys. Rev. Lett.*, 90:124502, 2003.

[16] X. D. Niu, C. Shu, and Y.T. Chew. Lattice Boltzmann BGK Model for simulation of micro flows. *Europhys. Lett.*, 67:600–606, 2004.

[17] V. Sofonea and R. Sekerka. Viscosity of Finite Difference Lattice Boltzmann models. *J. Comput. Phys.*, 207:639–659, 2005.

[18] S. Succi. Mesoscopic Modeling of Slip Motion at Fluid-Solid Interfaces with Heterogeneous Catalysis. *Phys. Rev. Lett.*, 89:064502, 2002.

[19] S. H. Kim, H. Pitsch, and I. D. Boyd. Lattice Boltzmann modeling of multicomponent diffusion in narrow channels. *Phys. Rev. E*, 79(1):016702, 2009.

[20] S. Ansumali. *Minimal kinetic modeling of hydrodynamics*. PhD thesis, ETH Zurich, Ref. No. 15534, 2004.

[21] S. S. Chikatamarla. *Hierarchy of lattice Boltzmann models for fluid mechanics*. PhD thesis, ETH Zurich, Ref. No. 17893, 2008.

[22] S. S. Chikatamarla and I. V. Karlin. Entropy and Galilean invariance of Lattice Boltzmann theories. *Phys. Rev. Lett.*, 97(19):190601, 2006.

[23] S. S. Chikatamarla and I. V. Karlin. Lattices for the Lattice Boltzmann method. *Phys. Rev. E*, 79:046701, 2009.

[24] X. He and L.S. Luo. A priori derivation of the lattice Boltzmann equation. *Phys. Rev. E*, 55(6):6333–6336, 1997.

[25] X. He and L.S. Luo. Theory of the lattice Boltzmann method: From the Boltzmann equation to the lattice Boltzmann equation. *Phys. Rev. E*, 56(6):6811–6817, 1997.

[26] H. Grad. On the kinetic theory of rarefied gases. *Comm. Pure Appl. Math*, 2(4):331–407, 1949.

[27] B.M̃. Boghosian, J. Love, P., P.Ṽ. Coveney, I. V. Karlin, S. Succi, and J. Yepez. Galilean-Invariant Lattice-Boltzmann Models with H-Theorem. *Phys. Rev. E.*, 68:025103, 2003.

[28] B. M. Boghosian, J Yepez, P. V. Coveney, and A. J. Wagner. Entropic Lattice Boltzmann Methods. *Proc. Roy. Soc. Lond. A*, 457:717–766, 2001.

[29] I. V. Karlin, A Ferrante, and H. C. Öttinger. Perfect Entropy Functions of the Lattice Boltzmann Method. *Europhys. Lett.*, 47:182–188, 1999.

[30] I. V. Karlin, A. N. Gorban, S. Succi, and V. Boffi. Maximum Entropy Principle for Lattice Kinetic Equations. *Phys. Rev. Lett.*, 81:6–9, 1998.

[31] A. J. Wagner. An H-Theorem for the Lattice Boltzmann Approach to Hydrodynamics. *Europhys. Lett.*, 44:144–149, 1998.

[32] AM Kogan. Derivation of Grad–type equations and study of their properties by the method of entropy maximization. *Prikl. Math. Mech*, 29(1):122–133, 1965.

[33] S. Arcidiacono, J. Mantzaras, S. Ansumali, IV Karlin, C. Frouzakis, and KB Boulouchos. Simulation of binary mixtures with the lattice Boltzman method. *Phys. Rev. E*, 74:056707, 2005.

[34] S. H. Kim, H. Pitsch, and I. D. Boyd. Accuracy of higher-order lattice Boltzmann methods for microscale flows with finite Knudsen numbers. *J. Comput. Phys.*, 227(19):8655–8671, 2008.

[35] R. L. Liboff. *Kinetic Theory.* Springer, New York, 2003.

[36] C. Cercignani. *Theory and Application of the Boltzmann Equation.* Scottish Academic Press, Edinburgh, 1975.

[37] P. L. Bhatnagar, E. P. Gross, and M. Krook. A Model for Collision Processes in Gases. I. Small Amplitude Processes in Charged and Neutral One-Component Systems. *Phys. Rev.*, 94:511–525, 1954.

[38] A. Beskok and G. E. Karniadakis. *Microflows: Fundamentals and Simulation.* Springer, Berlin, 2001.

[39] X. He, X. Shan, and G.D. Doolen. Discrete Boltzmann equation model for nonideal gases. *Phys. Rev. E*, 57(1):13–16, 1998.

[40] D. R. Willis. Comparison of kinetic theory analyses of linearized Couette flow. *Phys. Fluids*, 5(2):127–135, February 1962.

[41] X. He, S. Chen, and G. D. Doolen. A novel thermal model for the lattice Boltzmann method in incompressible limit. *J. Comput. Phys.*, 146(1):282, 1998.

[42] S. Chapman and T. G. Cowling. *The Mathematical Theory of Non-Uniform Gases.* Cambridge University Press, Cambridge, 1970.

[43] I. V. Karlin and S. Ansumali. Renormalization of the Lattice Boltzmann hierarchy. *Phys. Rev. E*, 76:025701, Aug 2007.

[44] J. E. Broadwell. Study of Rarefied Shear Flow by the Discrte Velocity Method. *J. Fluid Mech.*, 19:401–414, 1964.

[45] U. Frisch, B. Hasslacher, and Y. Pomeau. Lattice-gas Automata for the Navier-Stokes Equation. *Phys. Rev. Lett.*, 56:1505, 1986.

[46] Y.H̃. Qian and S.Ã. Orszag. Lattice BGK Models for the Navier-Stokes Equation: Nonlinear Deviation in Compressible Regimes. *Europhys. Lett.*, 21:255–259, 1993.

[47] B. Keating, G. Vahala, J. Yepez, M. Soe, and L. Vahala. Entropic Lattice Boltzmann representations required to recover Navier-Stokes flows. *Phys. Rev. E*, 75(3):036712, 2007.

[48] N.W. Ashcroft and N.D. Mermin. *Solid State Physics*. Singapore, 1976.

[49] W. P. Yudistiawan, S. Ansumali, and I. V. Karlin. Hydrodynamics beyond Navier-Stokes: Slip Flow Model. *Phys. Rev. E*, 78(1):016705, 2008.

[50] I. V. Karlin, A. N. Gorban, G. Dukek, and T. F. Nonnenmacher. Dynamic correction to moment approximations. *Phys. Rev. E*, 57(2):1668–1672, 1998.

[51] H. Struchtrup and M. Torrilhon. Regularization of Grad 13-moment equations: Derivation and linear analysis. *Phys. Fluids*, 15:2668, 2003.

[52] H. Struchtrup and M. Torrilhon. H-Theorem, Regularization, and Boundary Conditions for Linearized 13 Moment Equations. *Phys. Rev. Lett.*, 99(1):014502, 2007.

PUBLICATION LIST

Journal Papers

1. W.P. Yudistiawan, S.Ansumali, and I.V. Karlin, Hydrodynamics beyond Navier-Stokes: Renormalized Lattice Boltzmann, in preparation.

2. W.P. Yudistiawan, S.K. Kwak, D.V. Patil, and S. Ansumali, Higher-order Galilean-invariant lattice Boltzmann model for microflows: Single-component gas, *Physical Review E* 82:046701, 2010.

3. W.P. Yudistiawan, S. Ansumali, and I.V. Karlin, Hydrodynamics beyond Navier-Stokes: The slip flow model, *Physical Review E* 78:016705, 2008.

Conference Presentations

1. W.P. Yudistiawan, S.K. Kwak, and S. Ansumali, Higher order Galilean invariant lattice Boltzmann model, 18th Discrete Simulation of Fluid Dynamics, 2009, Beijing, China.

2. W.P. Yudistiawan, S.K. Kwak, and S. Ansumali, Higher order Galilean invariant lattice Boltzmann model, 6th International Conference for Mesoscopic Methods in Engineering and Science, 2009, Guangzhou, China.

3. E.P. Hu, Z.P. Lai, W.P. Yudistiawan, and S. Ansumali, An extended hydrodynamic model for gaseous mixture, 18th Discrete Simulation of Fluid Dynamics, 2009, Beijing, China.

4. E.P. Hu, Z.P. Lai, W.P. Yudistiawan, and S. Ansumali, An extended hydrodynamic model for gaseous mixture, 6th International Conference for Mesoscopic Methods in Engineering and Science, 2009, Guangzhou, China.

Conference Proceedings

1. A. Majumder, W. P. Yudistiawan, V. Kariwala, S. Ansumali and A. Rajendran. Lattice Boltzmann method for solving Population balance equations, in proceedings of 2nd International Conference on Chemical Engineering, Dhaka, Bangladesh, 2008.

2. A. Majumder, W. P. Yudistiawan, V. Kariwala, S. Ansumali and A. Rajendran. Lattice Boltzmann method for solving 1D Population balance equations, in proceedings of 15th Regional Symposium of Chemical Engineering, Kuala Lumpur, Malaysia, 2008.